

Development of Potent and Selective Tissue Transglutaminase (TG2) Inhibitors— their effect on TG2 function and application in pathological conditions

Eduard Badarau ^{a,†,§}, Zhuo Wang ^{a,†}, Dan L. Rathbone ^a, Andrea Costanzi ^a, Thomas Thibault ^a, Colin E Murdoch ^b, Said El Alaoui ^c, Milda Barkeviciute ^b, Martin Griffin ^{a*}

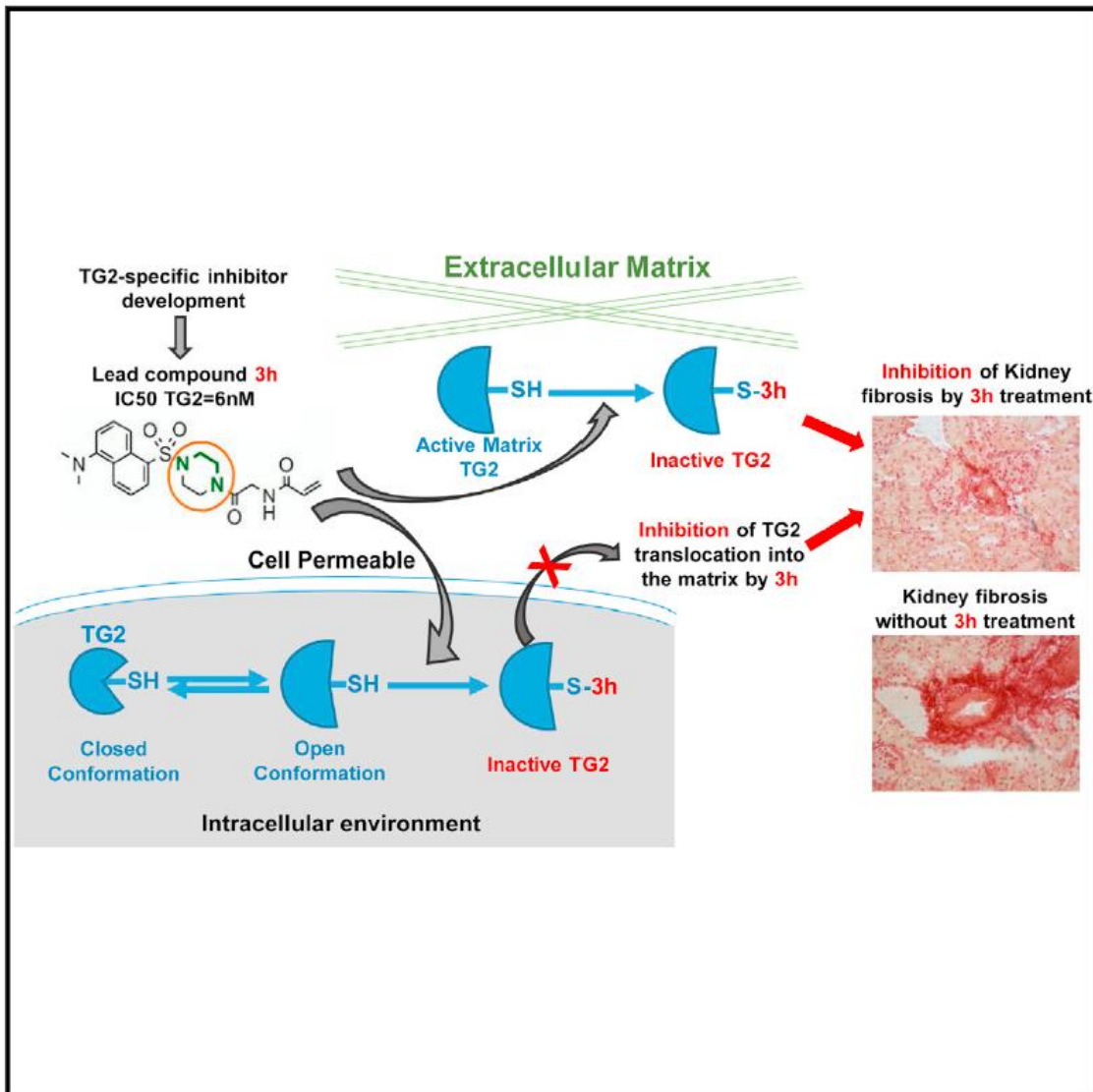
^a School of Life and Health Sciences, Aston University, Aston Triangle, Birmingham B4 7ET, United Kingdom; ^b Aston Medical Research Institute, Aston Medical School, Aston University, Aston Triangle, Birmingham B4 7ET, United Kingdom; ^c Covalab France, 11 avenue Albert Einstein, 69100 Villeurbanne, France

* Corresponding Author, Prof Martin Griffin. Email: M.Griffin@aston.ac.uk, School of Life and Health Sciences, Aston University, Aston Triangle, Birmingham B4 7ET, UK

† These authors contributed equally to this work.

§ Present Addresses, European Institute of Chemistry and Biology, 2 Rue Robert Escarpit, 33607 Pessac, FRANCE

Graphical Abstract



Summary

Potent-selective peptidomimetic inhibitors of tissue transglutaminase (TG2) were developed through a combination of protein-ligand docking and molecular dynamic techniques. Derivatives of these inhibitors were made with the aim of specific TG2 targeting to the intra- and extracellular space. A cell-permeable fluorescently labelled derivative enabled detection of in situ cellular TG2 activity in human umbilical cord endothelial cells and TG2-transduced NIH3T3 cells, which could be enhanced by treatment of cells with ionomycin. Reaction of TG2 with this fluorescent inhibitor in NIH3T3 cells resulted in loss of binding of TG2 to cell surface syndecan-4 and inhibition of translocation of the enzyme into the extracellular matrix, with a parallel reduction in fibronectin deposition. In human umbilical cord endothelial cells, this same fluorescent inhibitor also demonstrated a reduction in fibronectin deposition, cell motility, and cord formation in Matrigel. Use of the same inhibitor in a mouse model of hypertensive nephrosclerosis showed over a 40% reduction in collagen deposition.

In Brief

Badarau et al. design and develop high potency TG2-specific irreversible inhibitors that show reactivity with the intracellular active form of TG2, leading to inhibition of its translocation into the extracellular matrix. The compounds are effective in inhibiting in vitro angiogenesis and hypertensive nephrosclerosis in animal models.

Highlights

- Irreversible tissue transglutaminase (TG2) inhibitors of high selectivity and potency
- Target the Ca^{2+} activated form of TG2 in the intra- and/or extracellular space
- Reactive with intracellular TG2 and block its translocation into the matrix
- Effective in blocking hypertensive nephrosclerosis in animal models

SUMMARY

Potent-selective peptidomimetic inhibitors of tissue transglutaminase (TG2) were developed through a combination of protein-ligand docking and molecular dynamic techniques. Derivatives of these inhibitors were made with the aim of specific TG2 targeting to the intra- and extracellular space. A cell-permeable fluorescently labeled derivative enabled detection of in situ cellular TG2 activity in human umbilical cord endothelial cells and TG2-transduced NIH3T3 cells, which could be enhanced by treatment of cells with ionomycin. Reaction of TG2 with this fluorescent inhibitor in NIH3T3 cells resulted in loss of binding of TG2 to cell surface syndecan-4 and inhibition of translocation of the enzyme into the extracellular matrix, with a parallel reduction in fibronectin deposition.

In human umbilical cord endothelial cells, this same fluorescent inhibitor also demonstrated a reduction in fibronectin deposition, cell motility, and cord formation in Matrigel. Use of the same inhibitor in a mouse model of hypertensive nephrosclerosis showed over a 40% reduction in collagen deposition.

INTRODUCTION

Transglutaminases (TGs) belong to a family of protein crosslinking enzymes that catalyze an acyl transfer reaction between the γ -carboxamide group of peptide-bound glutamine and the ϵ -amino group of peptide-bound lysine (or a suitable primary amine) resulting in formation of a $\epsilon(\gamma$ -glutamyl)lysine isopeptide bond (Griffin et al., 2002). In mammals, eight catalytically active TGs, each Ca^{2+} -dependent, are found in this family, of which tissue transglutaminase (TG2) is probably the most ubiquitous in human tissues. The current challenges in studying the role of TG2 are to (1) develop inhibitors that target TG2 and not other members of the TG family (specificity); (2) investigate independently the intracellular and extracellular roles of the enzyme (cell permeability); (3) characterize the effect of specifically inhibiting TG2 crosslinking activity in physiological/ pathological conditions. TG2 is involved in a host of human diseases such as celiac disease, cancer, fibrosis, multiple sclerosis, and neurodegeneration (Wang and Griffin, 2012). As a consequence, TG2 has become a potential therapeutic target for the treatment of these pathological conditions (Badarau et al., 2013a). Moreover, since TG2 is found both in the intra- and extracellular space, both targeted specificity for TG2 itself and specific targeting to a particular subcellular space are needed. We recently described inhibitors aimed at targeting only the extracellular space (Badarau et al., 2013b; Griffin et al., 2008). These molecules incorporate two key polar groups in their structure in order to assure their high hydrophilic character: a carboxylate moiety and a charged warhead represented either by a dimethylsulfonium (Griffin et al., 2008) or by an imidazolium function (Badarau et al., 2013b). Despite their activities in the low micromolar range, these derivatives have great potential because of their high aqueous solubility and their excellent cellular toxicity profile. In fact, since their intracellular access is restrained, these inhibitors show very little toxicity in cells up to 750 μM over 72 hr (Wang and Griffin, 2013). They have also shown considerable success in proof-of-concept studies in animal models of kidney fibrosis over 120 days without any signs of toxicity but with significant improvements in kidney function (Huang et al., 2009; Johnson et al., 2007). However, the major drawback with these extracellular acting TG inhibitors is potency and specificity. Therefore, the first objective of our work was to design potent, highly specific TG2 inhibitors that could be used for targeting the intra- and/or extracellular space, were not toxic in cellular systems, and had the potential to be used in preclinical studies.

In the design of this new family of inhibitors, we were also very much aware that, once deposited into the extracellular matrix (ECM), TG2 is tightly associated with its potential substrates and is not easily accessible; and that the secretion and translocation of TG2 onto the cell surface and into the extracellular matrix ECM, which is independent of the conventional ER/Golgi pathway, requires the binding of TG2 to the cell surface heparan sulfate proteoglycan syndecan-4. Importantly, the binding of TG2 to this proteoglycan is highly favoured by its compact closed conformation (Wang et al., 2012; Lortat-Jacob et al., 2012). Hence, a further objective in this work was to assess whether suitably labeled irreversible TG2 specific inhibitors that can permeate the cell can also bind TG2 inside the cell thus both inhibiting enzyme activity and locking it into its open confirmation. This is particularly important when considering TG2 as a therapeutic target since TG2 in its open confirmation is likely to be blocked in its translocation to the cell surface and into the ECM because it is unable to bind effectively to cell surface heparan sulfates (Wang et al., 2012). Moreover, if it does manage to reach the ECM, e.g. from cell lysis, it reaches it in an inactive form. Such inhibitors are likely to have a broad spectrum of application in TG2-mediated human pathologic conditions in which TG2 is acting either inside or outside the cell.

RESULTS

In developing the TG2 inhibitors, the work was divided into two interlinked processes: *in silico* molecular modeling to first design and then synthesize the inhibitors and then a series of studies on their characterization. The latter included enzyme potency, specificity, cell permeability, solubility, and *in vitro* ADME (absorption, distribution, metabolism, excretion) characterization followed by an assessment of their potential application in biological systems using cell-based and *in vivo* preclinical models.

Generation of New Peptidomimetic TG2 Inhibitors

Molecular modelling was used to yield insights into the probable binding pattern of our previous peptidic water-soluble derivatives. The modelling approach was based on the Michaelis- Menten

complexes generated by docking of these compounds with the open conformation of TG2 (PDB: 2Q3Z). These were then subsequently “relaxed” by molecular dynamics conducted in explicit water at 300 K (see Supplemental Experimental Procedures).

The trajectories generated provided a rich source of information that helped in the development of the new TG2 inhibitors. One of the successfully exploited pathways relied on the observation that, during the dynamics trajectory, the water-soluble ligands tend to adopt a specific conformation in the central amino acid region. In fact, the dihedral N1-C2-C3-N4 emphasized in Figure 1A stabilized around 0° with a limited variation of $\pm 20^\circ$. This key observation was the starting point for the design of a new series of inhibitors.

In order to mimic the observed conformation for the central N1-C2-C3-N4 region, we next introduced a piperazine scaffold, as indicated in Figure 1B. The same three-atom linker was preserved between N4 and the carbonyl (vicinal to the warhead), however, in order to facilitate the subsequent chemical modifications, a new nitrogen atom was introduced. One of the first structures synthesized to validate this “restrained conformation” hypothesis exhibited the same activity range as the initial water soluble substrates (1a, Figure 1B). The irreversibility of the inhibitors was first confirmed by prior incubation of the compounds with recombinant purified human TG2 and then subsequent dilution prior to assay of the incubated enzyme as previously described (Griffin et al., 2008). An indication of the hydrophilic character of this derivative was observed experimentally during the isolation step by freeze-drying the aqueous layer after separation from the organic layer. In addition, an indication of its cellular toxicity profile was undertaken in human umbilical cord endothelial cells (HUVECs). As very little cellular toxicity was observed after 72 hr at concentrations up to 100 μ M (Figure S1), this new molecule (1a) represented the starting point for subsequent modifications. To rule out the effect of any potential TG2 and FXIII present in the serum from the cell culture medium, which could eliminate the effect of the compounds in the toxicity assay, the HUVECs were cultured in serum-free endothelial cell medium in the presence of compounds 3h, 1h, and 3e up to 72 hr, with no significant toxicity detected at the concentrations used (Figure S2).

Optimization of Inhibitor Potency

The first step of our modification strategy focused on the central amino acid region of the newly designed ligands. In order to evaluate the effect of steric hindrance that could be generated by additional substituents in this position, derivatives bearing new core amino acids were synthesized (Figure 1C, Schemes 1 and 2). As summarized in Table 1A, the activity was lost when using bulky substituents arising from phenylalanine (1l, 1k), the same but more moderate trend being observed for small substituents (1i, 1j). It should also be mentioned that the chirality of the stereogenic carbon atom seemed important, the analog in the L-Ala series (1i) being favored over its D isomer (1j).

Our attention next focused on the electrophilic warhead region. Different groups were tested in order to evaluate their influence on the binding process. As a possible means of targeting the extracellular space by limiting cell permeability, highly polar warheads were attached to the newly designed skeleton. As shown in Table 1B, the dialkylsulfonium moieties retained a good inhibition range (1a, 1q), while the imidazolium warhead induced a complete loss of activity (1s). It should be noted that, in our initial water-soluble peptidic inhibitors, the same imidazolium warhead maintained a good TG2 inhibition range (Badarau et al., 2013b), suggesting the binding patterns of the two classes of inhibitors are very different.

Our next approach was to design inhibitors containing lipophilic warheads, which were more likely to be cell permeable and could be used to target the intracellular space. As the catalytic CYS residue was revealed by the different available crystal structures of TG2 to be hosted in a narrow tunnel (PDB: 2Q3Z, Pinkas et al., 2007; PDB: 1KV3, Liu et al., 2002; PDB: 3LY6, Han et al., 2010), our choice was focused on terminal Michael acceptors such as acrylamides and vinylsulfonamides. Such warheads possess an additional carbon atom in the electrophilic region of the ligand, and it is likely that this will induce a different conformation of the warhead around the catalytic CYS residue compared with the sulfonium-based inhibitors. Table 1B shows that both of these new warheads preserved a good inhibition range (2a, 3a), the vinylsulfonamide having a more favourable effect on binding.

Other modifications were performed in the carbamate region (Table 1C). As this moiety was predicted by modelling to bind in the hydrophobic pocket of the binding site (as revealed by the crystal structure of the open-form conformation; (Pinkas et al., 2007), different-size aromatic carbamates were tested in

the first instance. In this case, the corresponding bromide precursors originally developed for inhibiting the serine proteases (Schoellmann and Shaw, 1963), and which have high reactivity with the enzymatic nucleophile, were also biologically evaluated. If for the dimethylsulfonium and acrylamide warheads the inhibition varies in the lower micromolar range, for the corresponding halomethylketones the potency was increased to the lower nanomolar range. However, their high cellular toxicity profile for the halide precursors, particularly the more reactive bromides, confirmed their limited pharmacological use.

A new set of inhibitors was prepared following the same hypothesis of targeting the hydrophobic pocket of the active site. An adamantyl moiety was chosen as the reference substituent and its distance from the piperazine ring was systematically varied in order to find an optimum for the interaction with the enzyme. The corresponding tert-butyl carbamate was also synthesized. The best median inhibitory concentration (IC₅₀) in the “lipophilic” series was obtained for the acrylamide warhead (3e), while in the “hydrophilic” series, the tert-butyl carbamate (1m) outperformed its analogs (Table 1C).

Design and Characterization of a Fluorescent Probe and Further Characterization of Lead Compounds

A dansyl fluorescent tag was attached to the central piperazine scaffold to fully exploit the biological potential of this new class of TG2-specific inhibitors, with the view to being able to pin point and visualize the presence of the inhibitors, most importantly the presence of the active enzyme located at a cellular level. Analogs in both water-soluble and lipophilic series were obtained and evaluated for their activity on a battery of TGs (Table 2A). Compound 3h had an excellent IC₅₀ of 6 nM for TG2, as well as a good toxicity profile when tested up to 100 μM (Figure 1E), and showed selectivity for TG2 when assayed against TG1, TG3, TG6, and Factor XIIIa (FXIIIa). A comparable TG selectivity profile was also shown for 1h with an IC₅₀ value of 380 nM, again with a good toxicity profile (Figure S1).

Measurement of the K_i and K_{inact} of 3h and 1h using the glutamate dehydrogenase coupled assay indicated high potency, particularly 3h, with a K_{inact} of 0.387 min⁻¹, a K_i of 1.31 mM, and a K_{inact}/K_i of 297,692 min⁻¹M⁻¹. This was comparable with the other high-potency non-dansylated inhibitor 3e (IC₅₀ 125 nM), which had a calculated K_{inact} of 0.275 min⁻¹, a K_i of 1.63 mM, and a K_{inact}/K_i of 171,875 min⁻¹M⁻¹. The other fluorescent inhibitor, 1h, in line with its lower IC₅₀ (380 nM), had a K_i of 57 mM, a K_{inact} of 0.337 min⁻¹ and a K_{inact}/K_i of 5,830 min⁻¹M⁻¹. Given the potential application of 3h and 1h in TG2 conformational studies, it was important to demonstrate that their reactivity was Ca²⁺ dependent. For this, recombinant human TG2 was incubated for 30 min at 4°C with either Ca²⁺ (1 mM) or GTP (1 mM), and then for a further 30 min in the presence of compound 3h (10 nM) or 1h (1 mM). Spin columns were then used to remove excess inhibitor. Evaluation of TG2 activity after removal of the excess inhibitor indicated that only the enzyme incubated with GTP was active (Figure 2A), thus confirming the requirement of Ca²⁺ for the inhibitors 3h and 1h to access the transamidating active site. To rule out potential off-target effects of the inhibitors, inhibition of the cysteine proteases Caspase 3 and 7 was undertaken. HUVECs were induced into apoptosis and the caspase activity measured in situ in the presence and absence of 3h and 1h. No inhibition of Caspase 3 or 7 was shown (Figure 2B). The same results were obtained for the inhibitors 1e and 3e, which carry the dimethylsulfonium and the acrylamide warheads, respectively.

Other potent compounds were also tested for their specificity toward TG2 compared with other TG family members. Biotinylated TG-specific glutamine-containing peptides specific for TG family members, including TG1, FXIIIa, TG3, and TG6, were used in these assays (CovTests; Perez Alea et al., 2009). Comparable IC₅₀ values of these inhibitors for TG2 were detected in both the CovTest and the biotin-cadaverine incorporation assay. All derivatives from this series proved selective over the TG1, TG3, and FXIIIa TGs with selectivity shown against TG6 for compounds 1e, 1f, and 3f although less selectivity was shown for TG6 with compound 3e (Table 2B). A moderate TG1 inhibition trend was observed for the halomethylamides. In the case of TG2, however, the inhibition activities are in the lower nanomolar range (>100-fold selectivity ratio). To rule out any non-specific reaction of the inhibitors with TG1, TG3, and FXIIIa, the dansylated probes 3h and 1h were incubated with these three isoforms in the presence of Ca²⁺ and with EDTA, enzymes were then separated by denaturing SDS gel electrophoresis and western blotted for the detection of the dansyl group, which showed negligible reactivity of the TG isoforms with either inhibitor (Figure S3).

Further Characterization of the TG2 Inhibitors Toxicity Studies

The toxicity profile of some of these new potent inhibitors was evaluated in HUVECs using the XTT-based assay as described previously (Wang and Griffin, 2013). The toxicity varied between 25 and 100 μM (Table S1 and Figure S1). As expected, in relation to their high reactivity, the halomethylketones (6n, 6o) were the most toxic compounds. The more hydrophilic inhibitors bearing the dimethylsulfonium warhead were well tolerated by the same cell lines with toxicity thresholds of $<100 \mu\text{M}$. Encouraging results were also obtained for the compounds designed to be more lipophilic, especially 3e, which has an inhibition activity for TG2 in the nanomolar range ($\text{IC}_{50} = 0.125 \pm 0.066 \text{ nM}$). Different toxicity profiles were observed between the acrylamide- and vinylsulfonamide-based derivatives (3e vs 2e), which might be explained in part by their different chemical reactivities.

Confirmation of Covalent Interaction and Targeting the Active Site Cys277 by 1h and 3h

The fluorescent inhibitor probes allowed us to demonstrate that these compounds were targeting the active site Cys277 in their covalent reactivity. Pure recombinant wild-type (wt) TG2 and its active site mutant Cys277Ser were incubated with the compound 1h in the presence of Ca^{2+} for 3 hr. As a positive control, the wt enzyme was incubated with the competitive amine substrate monodansylcadaverine (MDC), which becomes enzymatically incorporated into available g-glutamyl residues on neighboring TG2 molecules.

Following incubation, TG2 was separated on denaturing SDS-PAGE and western blotted using an anti-dansyl antibody (Figure 2C). Bands were seen in the positive control containing the MDC and in the wt enzyme where the active site Cys277 is intact, indicating covalent interaction of the inhibitor with TG2. In the Cys277Ser mutant, no incorporation of MDC was detected in a band that was indicative for TG2. Presence of the inhibitor was not detected with the Cys277Ser mutant, suggesting that fluorescent inhibitor 1h is specifically targeting the active site Cys277.

Cellular Permeability

The cellular permeability profile for a subset of compounds was investigated using the irreversible imidazolium-based inhibitor R283 (Freund et al., 1994), which is cell permeable, and the peptidic inhibitor R281, which is cell impermeable, as reference as described previously (Baumgartner et al., 2004). This assay is based on the ability of compounds to permeate the cell and inhibit intracellular TG2 activity after its activation by the elevation of intracellular Ca^{2+} using ionomycin. As initially designed, the assay confirmed that acrylamide-based inhibitors 3e, 3f and the fluorescent probe 3h penetrate the cell and inhibit intracellular TG2 activity, contrary to the charged compounds 1e and 1f (Figure 2D). As a means of validating the permeability assay used in these studies, the cell permeability of compounds 3h, 3e, and 1h was also determined in MDCKII-MDR1 cells. The assay was conducted in the presence of the efflux transporter inhibitor GF120918. Using this assay, the passive permeability (P_{exact}) of compounds 3h, 1h, and 3e was 649, 1.3, and 676 nm^2/s respectively, confirming that the acrylamide inhibitors 3h and 3e are cell permeable. In contrast, the positively charged 1h is cell impermeable. Measurement of the thermodynamic solubility of these same three compounds in PBS (pH 7.4) over 24 hr was 24 μM for 3h, 1594.6 μM for 1h, and 698 μM for 3e.

In Vitro ADME Properties of Compounds 3h, 1h, and 3e

Further characterization of lead compounds 3h, 1h and 3e by in vitro ADME assays are shown in Table S2. Microsomal stability assessed in human microsomes indicated that compounds 3h and 1h exhibited low and high stability, respectively, with compound 3e demonstrating moderate stability. In contrast in the cell health screen assessed in the hepatic cell line HepG2, no significant effect was observed for any of the compounds on mitochondrial potential, nuclear morphology, and membrane permeability. Importantly, no significant effect was observed for hERG liability with any of the compounds and their binding to human serum albumin and α -glycoprotein indicated that none of them had very high binding.

Assaying for the Presence of Potential Intracellular In Situ TG2 Activity/Open Conformation Using Dansyl Derivative 3h

The measured cell permeability of the fluorescent inhibitor 3h, which requires TG2 to be in its Ca^{2+} -bound open conformation prior to its irreversible binding, should enable the detection of TG2 in its open/relaxed conformation inside the cell when combined with fluorescent microscopy and/or co-immunoprecipitation (co-IP) studies. NIH3T3 cells transduced with wt TG2 were used to confirm whether the intracellular reaction of 3h with TG2 could take place. Figure 2E shows that inhibitor 3h permeates into NIH3T3 cells and reacts with intracellular TG2, which can be increased further in the presence of the Ca^{2+} ionophore ionomycin (Figure 2E). This is demonstrated by co-IP of the inhibitor/TG2 complex in the cytosolic fraction of cells using an anti-dansyl antibody and TG2 revealed

in this complex using an anti-TG2 antibody by western blotting. Importantly, the reactivity of 3h with intracellular TG2 was reduced by incubating in the presence of the cell-permeable inhibitor 3e (Figure 2E).

To confirm that the newly developed fluorescent inhibitors 3h or 1h only interact with TG2 in its open Ca^{2+} bound conformation and lock the enzyme into this conformation, wt recombinant TG2 pre-treated with Ca^{2+} or GTP was incubated with inhibitor 3h and then separated by native PAGE. As shown in Figure 2F, 3h and 1h in the presence of Ca^{2+} bind to TG2 and hold it in its open conformation, while the binding of GTP, which holds TG2 in its closed conformation, blocks the interaction of 3h or 1h with TG2 and gives rise to increased mobility.

HUVECs, which contain high levels of endogenous TG2, were also used to verify our observations in TG2-transduced NIH3T3 cells. Cells were incubated in the absence or presence of the Ca^{2+} ionophore ionomycin (positive control). Mouse endothelial cells isolated from TG2^{-/-} mice were used as the negative control together with HUVECs incubated with 3h in the presence of the cell-permeable non-dansylated inhibitor 3e. After fixation of the cells and removal of any excess inhibitor by washing, fluorescence microscopy revealed a faint intracellular dansyl signal in the HUVECs without ionomycin treatment, which was increased with ionomycin and reduced in the presence of inhibitor 3e. No dansyl signal was detected in the negative control mouse endothelial cells, which are null for TG2 after fixing and washing out any excess inhibitor (Figure 3A). Further confirmation that the dansyl inhibitor is targeting TG2 was obtained by co-IP of the dansyl-labeled proteins in the cell cytosol fractions of cell lysates and the detection of TG2 by western blotting. TG2 was found to be present in the HUVECs with or without ionomycin. The signal was reduced in the cells treated with the inhibitor 3e and, importantly, as found with immunofluorescent microscopy, totally absent in the TG2^{-/-} mouse endothelial cells (Figure 3B). Hence, in both TG2-transduced NIH3T3 cells and in HUVECs, TG2 appears to be present in the intracellular environment in an open conformation and able to react with inhibitor 3h, suggesting that the enzyme could be active if suitable substrates are available to it, or, dependent on its environment, is simply alternating between the open and closed conformation.

Effect of 3h on TG2 Interaction with Syndecan-4 and its Translocation to the Cell Surface and ECM

The interaction between TG2 and syndecan-4 has been reported to be not only essential for the externalization of the enzyme onto the cell surface and deposition into the ECM (Wang et al., 2012) but also for its pathological roles in fibrosis (Scarpellini et al., 2014). Previous work from us and others suggested the importance of TG2 crosslinking activity in pathological conditions such as fibrosis, angiogenesis, and multiple sclerosis. Therefore, we next studied the effect of inhibitor 3h on the binding of TG2 to syndecan-4 and its subsequent translocation into the ECM.

It has been reported that TG2 binding to syndecan-4 is favoured by the compact conformation (Wang et al., 2012) of the enzyme. It has been shown in Figure 2F that the inhibitor 3h locks TG2 into its open conformation, which would have a significant impact on the binding of the enzyme to syndecan-4. Therefore, we next studied the effect of 3h binding to TG2 on the enzyme's binding to cell surface heparan sulfates. Figure 3C shows that in NIH3T3 cells, previously used to show TG2 binding to cell surface syndecan-4, 3h significantly reduced the interaction between TG2 and cell surface syndecan-4 following co-IP of TG2 with anti-syndecan-4 antibody as previously documented (Wang et al., 2012). Importantly, in these same cells, binding of TG2 to 3h led to a dramatic reduction in the presence of the enzyme on the cell surface and in the ECM (Figure 3D), which paralleled a dramatic reduction in the deposition of fibronectin (FN) into the ECM (Figure 3D).

Effects of Fluorescent TG2 Inhibitor 3h on Endothelial Cell Function

In our previous report, using our first generation of peptidic TG inhibitors, we showed that extracellular TG2 could be a potential target in the treatment of VEGF-induced angiogenesis due to its ability to block the deposition of FN, which is one of the important ECM proteins required for matrix-bound VEGF signalling (Wang et al., 2013). Given the ability of compound 3h to react with both intracellular and extracellular HUVEC TG2, we tested the effects of compound 3h on different but related endothelial cell functions. Figure 4A shows that inhibitor 3h reduced the deposition of FN into the ECM by HUVECs, which agrees with its effect in NIH3T3 cells (Figure 3D). One further role of TG2 in endothelial cell angiogenesis is in cell migration during tubule formation (Wang et al., 2013), which is dependent on the crosslinking activity of the enzyme. Figures 4B and 4C demonstrate that compound 3h inhibited HUVEC migration in the wound healing assay and in Matrigel cord formation assays.

Potency of Inhibitor 3h in an In Vivo Model of Hypertensive Nephrosclerosis

As a further means of demonstrating the potential application of these new peptidomimetic inhibitors in human disease where TG2 has been shown to act extracellularly, we next looked at the effects of inhibitor 3h, which blocks both intracellular and extracellular TG2 activity, on angiotensin II (AngII)-induced hypertensive nephrosclerosis in mice. Before undertaking these studies, we first gained an approximate cell IC₅₀ for 3h by looking at the inhibition of FN deposition in HUVECs and in mouse endothelial cells, which in both cases gave an approximate IC₅₀ for 3h of 0.3 μ M in human HUVECs and 0.4 μ M in mouse endothelial cells (Figure S4).

AngII and 3h were delivered using a subcutaneously implanted osmotic minipump (Azlet) over 14 days. Mice receiving AngII alone together with inhibitor vehicle showed signs of increased collagen deposition around the arterioles and, in some cases, in the glomeruli and interstitial tubular space. In contrast, animals receiving AngII plus compound 3h showed significantly reduced (approx. 40%) collagen deposition in all these regions (Figure 5A) with around 45% reduction around the blood vessels (Figure 5B) in the kidneys of inhibitor-treated animals. No obvious signs of toxicity were observed in the animals after inhibitor treatment.

DISCUSSION

In this paper, we report a new series of small-molecule peptidomimetic inhibitors that are selective for TG2 activity. Importantly, we also demonstrate the biological impact of these inhibitors and demonstrate their potential application in both cell and animal models for the targeting of TG2 in diseases such as fibrosis and pathological angiogenesis.

Contrary to the classic family of TG2 inhibitors represented mainly by the peptidic inhibitors, this new series adds a new member to the modest, but continuously increasing, family of non-peptidic TG2 inhibitors. Sporadic examples have been disclosed so far (Duval et al., 2005; Klock et al., 2011; Ozaki et al., 2010, 2011; Pardin et al., 2008a, 2008b; Prime et al., 2012; Schaertl et al., 2010). Their pharmacological characterization in terms of potency, specificity, binding-site targeting, toxicity, and cellular permeability still remains to be revealed. In addition, a more recent report screening existing TG2 inhibitors based on a weak electrophilic 3-bromo-4,5-dihydroisoxazole (DHI) scaffold showed poor selectivity against TG1 (Klock et al., 2014). Constructed on a piperazine core, this new scaffold presented here has the advantage of an excellent selectivity profile at least against four other members of the TG family that were evaluated during our studies (TG1, TG3, TG6, and FXIIIa). It should be noted, however, that another two groups (Prime et al., 2012; Wityak et al., 2012) have reported piperazine-based derivatives with interesting TG2 activities; however, Prime et al. (2012) reported that their selectivity over the other TGs (especially over FXIIIa) requires further optimization. Wityak et al. (2012) reported that their lead inhibitor had an IC₅₀ for TG2 of 14 nM with selectivity over TG1, TG3, TG6, and FXIIIa but no cell or animal studies were undertaken on these compounds although in vitro DMPK studies indicated they had low toxicity; the authors indicated that improved ADME profiling was still required for in vivo applications because of their low plasma stability. Importantly, the straightforward synthetic route of the compounds presented in this report gives easy access to various modulations, allowing us to improve the toxicity profile of our inhibitors up to 100 μ M/72 hr, while controlling their cellular access. However, like the compounds reported by Wityak et al. (2012), further improvements on ADME characteristics are still necessary for some of our lead compounds, in particular improvements in microsomal stability and aqueous solubility for 3h, although solubility may not be such an issue for in vivo potency given that the solubility of 3h is >3,000 times the IC₅₀ of 3h. Moreover, the poor microsomal stability of 3h is unlikely to be due to the piperazinyl moiety as suggested by Wityak et al. (2012) given that compound 1h, which is a comparable structure apart from the warhead, is microsomal stable.

Physiologically, TG2 is an enzyme that exists both in the intra and extracellular environment. Inside the cell, its Ca²⁺-dependent crosslinking activity is thought to be tightly controlled by the binding of GTP/GDP, which holds the enzyme in a compact closed inactive conformation (Bergamini et al., 2011; Wang and Griffin, 2012). However, TG2 is reported to be involved in a number of human diseases where it acts both intracellularly (e.g. cystic fibrosis, cancer progression, epidermal growth factor receptor recycling) (Bergamini et al., 2011; Zhang et al., 2013) and/or extracellularly, including matrix deposition, tissue fibrosis, VEGF-dependent angiogenesis, and multiple sclerosis (Wang and Griffin, 2012; Wang et al., 2013). The development of a highly potent cell-permeable fluorescent inhibitor specific for TG2, allowed us to test for the first time whether TG2, when inside the cell, can indeed

exist in both its potentially active open conformation as well as its closed/compact conformation. Our data suggest that reactivity of TG2 with the fluorescent inhibitor probe can take place in the low Ca^{2+} intracellular environment of both HUVECs and NIH3T3 cells, which can be further enhanced by using the Ca^{2+} ionophore ionomycin. Given that the reported K_m app for Ca^{2+} for TG2 is around 3 μM (Hand et al., 1985), this suggests that the conformation of the enzyme may also be regulated by other binding factors in addition to Ca^{2+} , which permits flexibility between the open and compact conformation and which, when in the open conformation, allows the irreversible reaction with the fluorescent TG2 inhibitor probe. Earlier fluorescence resonance energy transfer studies with TG2 have also suggested that, in certain localities of the cell, the enzyme may exist in its open conformation (Pavlyukov et al., 2012). This may explain a number of observations where TG2 has been reported to regulate a several cellular processes either through conformational changes that regulate protein binding (Zhang et al., 2013) or via its transamidating activity (Colak et al., 2011).

As referred to earlier, TG2 can be secreted into the ECM by a non-conventional mechanism, which requires the cell surface binding of heparan sulfates, such as syndecan-4, for its translocation into the ECM. This binding of TG2 to syndecan-4 at the cell surface is favored by the enzyme being in its compact closed conformation, suggesting that the enzyme is secreted in this conformation or that this conformation is assumed once it reaches the cell surface (Wang et al., 2012). Therefore, our next question was to ask if the binding of an irreversible inhibitor inside the cell, which would hold the enzyme in its open conformation, would interfere with both its translocation to the cell surface and its deposition into the ECM.

Using NIH3T3 cells, we clearly show that treatment of these cells with the fluorescent permeable inhibitor 3h reduces the presence of TG2 at the cell surface and nearly completely blocks translocation of the enzyme into the ECM, a finding that is accompanied by the reduced deposition of FN. In HUVECs, where we know TG2 also reacts with our fluorescent probe inside the cell, we also observed a large reduction in the deposition of FN in the presence of this TG2 inhibitor. In relation to biological functions of endothelial cells, this intracellular acting probe is also a potent inhibitor of endothelial cord formation on Matrigel and a potent inhibitor of endothelial motility, which is required for endothelial tube formation (Wang et al., 2013). As a further means of demonstrating the potential application of the new peptidomimetic inhibitors in *in vivo* studies in a disease state where TG2 acts extracellularly, we next looked at the effects of inhibitor 3h on AngII-induced hypertensive nephrosclerosis in mice. Mice receiving AngII plus compound 3h showed significantly reduced (approx. 40%) collagen deposition across all regions of the kidney with around a 45% reduction in collagen deposition around the kidney arterioles when compared with mice receiving AngII and vehicle.

Hence, our findings demonstrate that our new peptidomimetic TG2 small-molecule inhibitors, which can react with TG2 inside the cell and prevent export of the enzyme as well as block its activity, provide an ideal therapeutic avenue for the treatment of human diseases involving TG2.

SIGNIFICANCE

TG2 has been shown to be essential in a number of human disease states, including fibrosis and angiogenesis. However, other transglutaminase family members sharing a similarity in their structures generate obstacles in generating TG2-specific inhibitors with high potency and low toxicity. Using molecular dynamics techniques, a series of new peptidomimetic inhibitors against TG2 were produced with excellent selectivity when tested against four other members of the transglutaminase family (TG1, TG3, TG6, and FXIIIa). A highly potent TG2 cell-permeable fluorescent probe ($\text{IC}_{50} = 6 \text{ nM}$; Kinact/K_i of $297,692 \text{ min}^{-1} \text{ M}^{-1}$) was designed and exploited in several biological studies. We demonstrate that the reactivity of the inhibitor can take place with TG2 in the low Ca^{2+} intracellular environment of HUVECs and NIH3T3 cells, which is enhanced by using the Ca^{2+} ionophore ionomycin. Importantly, reaction of TG2 with this fluorescent inhibitor led to a loss of binding of TG2 to cell surface syndecan-4 in NIH3T3 cells and inhibition of TG2 translocation into the ECM, which was paralleled by a reduction in the deposition of matrix FN. Further studies with HUVECs treated with this cell-permeable fluorescent inhibitor revealed a significant reduction in FN deposition, cord formation on Matrigel, and cell motility. As a means of demonstrating the potential application of the new peptidomimetic inhibitors *in vivo*, where TG2 acts extracellularly (Huang et al., 2009; Johnson et al., 2007), the effects of inhibitor 3h on Angiotensin II (AngII)-induced hypertensive nephrosclerosis in mice was investigated. Mice receiving AngII plus compound 3h showed significantly reduced (approx. 40%) collagen deposition across all regions of the kidney with around 45% reduction around blood vessels.

Hence, this new series of TG2-specific cell-permeable peptidomimetic inhibitors may be highly effective in targeting human diseases involving extracellular TG2 via their ability to block both protein crosslinking activity and enzyme export.

EXPERIMENTAL PROCEDURES

Synthetic and analytical methodology

The newly synthesized derivatives were characterised by infra-red spectroscopy (IR), proton and carbon-13 NMR spectroscopy (¹H- and ¹³C-NMR), melting points (Mp), high resolution mass spectrometry (HRMS), and had properties consistent with the proposed structures (see **Supplemental Experimental Procedures**).

Biological methodology

General Experimental procedures were performed as described previously (Wang et al., 2012 and 2013, Wang and Griffin, 2012) and experimental information is detailed in **Supplemental Experimental Procedures**.

Reagents and antibodies

The general reagents were purchased from Sigma-Aldrich (UK), unless stated below.

Chemical synthesis of the inhibitors

The synthesis of the inhibitors is described in **Supplemental Experimental Procedures**.

Cell culture

Human umbilical vein endothelial cells (HUVECs) (Lonza, Belgium) (Wang et al., 2013) and NIH3T3 cells (Wang et al., 2012) were cultured as described previously (Supplemental Experimental Procedures).

TG2 activity assays

For measurement of TG2 activity the incorporation of biotinylated cadaverine into immobilised N,N – dimethylcasein was used as previously described (Wang et al., 2012).

For determination of the activity of TG1, TG3, TG6 and FXIIIa, commercial microassays TG-CovTest were used (Covalab, Lyon, France) (Hitomi et al., 2009), according to the manufacturer's instructions. For comparable purposes, a number of TG2 assays were also undertaken using this assay. Briefly, TG-specific biotinylated peptides, including pepF11KA (FXIII pre-activated with thrombin), pepK5 (TG1), pepT26 (TG2), pepE51 (TG3) or pepY25 (TG6) (Hitomi et al., 2009; Fukui et al., 2013), were incubated with the suitable TG family members in the presence of polyamine substrates immobilized onto 96-well microplates. The incorporated biotinylated peptides were measured using HRP-conjugated streptavidin and then measured using OPD substrates. The absorbance was measured at 490 nm using a microplate reader.

Glutamate Dehydrogenase coupled assay used for Kinact/ki calculations

TG2 inhibitors were assayed in accordance with the method of Choi et al using the glutamate dehydrogenase coupled assay (Choi et al., K. 2005.). Briefly, a reaction mixture containing 4 mM CaCl₂, 10 mM α-ketoglutarate, 0.2 U/ml glutamate dehydrogenase, 0.12 mM NADH, 20µg TG2, and 10 mM Cbz-Gln-Gly in 200 mM MOPS, pH 7.1, was used in the assay. The enzyme reaction was initiated by the addition of TG2 and the consumption of NADH was monitored using different concentrations of inhibitor (10-500 nM) by UV spectroscopy (340 nm, ε= 6220 cm⁻¹M⁻¹). Kinetic parameters (kinact and ki) were obtained by using the software Dynafit 4.05.129 (Kuzmic, 2009 and Kuzmic, 1996).

Cell permeability assay

1. By measuring inactivation of intracellular TG2. To induce intracellular TG2 activity, HUVECs with high endogenous TG2 were incubated with fresh growth media with 0.5% FBS containing given 1 µM ionomycin and 1 mM biotin-cadaverine (Zedira, Germany) in the presence or absence of 50 µM of TG2 inhibitors **3h**, **1f**, **3f**, **3e** and **1e**. The non-cell permeable inhibitor **R281** and cell permeable inhibitor **R283** were used as the negative and positive controls, respectively. After a 3 h incubation, the cells were collected in homogenization buffer (50 mM Tris-HCl, pH 7.5, 150 mM NaCl, 1 mM EDTA) and sonicated on ice. The cell membrane was pelleted at 60,000 ×g for 60 min and the supernatant (the cytosol fraction) was used for the assay. 50 µg of total protein in 100 µl of the homogenization buffer was used in the biotin-cadaverine incorporation assay as described previously by Wang et al (2012).

2. By the *in vitro* passive cellular permeability (“MDCK assay”)

The permeability (P exact.) of **3h**, **1h**, **3e** across an MDCK-MDR1 cell monolayer was measured at a starting concentration of 3 μ M in the presence of GF120918, an efflux inhibitor. The pH of the donor and receiver compartments was 7.4 (Hank's Balanced Salt Solution).

Incubations were carried out in an atmosphere of 5% CO₂ with a relative humidity of 95% at 37°C for 60 min. Apical and basolateral samples were diluted for analysis by LC-MS/MS. The integrity of the monolayers throughout the experiment was checked by monitoring Lucifer yellow permeation using fluorimetric analysis (Tran et al., 2004).

Western blotting for the dansyl inhibitor interaction with rhTG2

1 μ g of recombinant human TG2 (rhTG2), wt or the active site C277S mutant protein, was incubated with the dansylated TG2 inhibitor **1h** at 100 μ M and 50 μ M in the presence of 10 mM Ca²⁺ and 1 mM DTT in Tris-HCl buffer, pH 7.4 for 30 min at room temperature. The primary amine substrate MDC, which will be incorporated into the available γ -glutamyl residues of TG2 by the enzyme was used as the positive signal control sample, while non-labelled rhTG2 was used as the negative control. The reaction was stopped by diluting the samples into 2 \times Laemmli buffer and boiling at 95°C for 5 min. The presence of dansyl was detected via Western blotting (Wang et al., 2012; Wang et al., 2013) by using a specific anti-dansyl antibody (Invitrogen, UK).

The targeting of in situ TG2 activity by fluorescence microscopy using the dansyl inhibitor 3h

HUVEC cells and TG2 ^{-/-} mouse endothelial cells were used in this study. HUVECs were treated with 1 μ M ionomycin in the presence or absence of 50 μ M of **3e** to pre-block the intracellular active TG2 for 3 h and the cells were further treated with 5 μ M **3h** for another 2 h. TG2 ^{-/-} endothelial cells were treated in a comparable manner but were not exposed to the inhibitor **3e**. For detection of endogenous TG2 activity, HUVECs were incubated without ionomycin. After the incubation, the cells were washed 3 times with pre-chilled methanol and fixed with methanol for 20 min at -20°C. Following blocking with 3% BSA in PBS, pH 7.4 for 30 min at 37°C, the cells were incubated with rabbit anti-dansyl antibody and revealed using a secondary TRITC-conjugated antibody for a 2 h/incubation at 37°C. The fluorescence signal was visualized using a Zeiss epifluorescent microscope using a 60 \times objective.

Detection of TG2 activity using co-IP

Immunoprecipitation (IP) of the intracellular TG2-dansyl inhibitor complex was performed following the treatment of cells with **3h** with or without pre-treatment of 50 μ M **3e** (as described above). Cytosol fractions of HUVEC or NIH3T3 cells transduced with TG2 were collected as described above. Anti-TG2 antibody was used to pull down the TG2 immuno-complex and SDS-PAGE and Western blotting was then performed to detect the presence of the dansyl group of **3h**. TG2 knockout (ko) endothelial cells or non-TG2 transduced NIH3T3 cells, as well as a mouse IgG negative control antibody, were used as the negative controls.

Animal study

Animal studies were undertaken with full ethical approval and all procedures carried out under license according to regulations laid down by Her Majesty's Government, United Kingdom (Animals Scientific Procedures Act, 1986) and undertaken in accordance with the 3Rs. Two groups of five animals were used. In the first group C57BL/6 male mice (14-weeks old) were infused with AngII 1.1mg/kg/day in 50% DMSO in PBS pH 7.4 for 2 weeks without TG2 inhibitor via a subcutaneously implanted osmotic pump (Alzet1002) as previously described (Murdoch et al., 2011). In the second group compound **3h** was infused in a similar manner at 25mg/kg/day together with AngII in 50% DMSO in PBS pH7.4 over 14 days. Following 14 days kidneys from the treated mice were frozen in O.C.T (CellPath) at an optimal temperature (-150⁰C) using isopentane subsequently 6 μ m sections were prepared. Picrosirius red staining was performed to measure collagen staining as previously reported (Murdoch et al., 2011). The collagen content was quantified as the percentage in a minimum of 10 images per mouse of area using ImageProPlus (v5.0). The concentration (270mM) of inhibitor used in the pump was approximated from computer simulations to give the steady state concentration in the mouse assuming an extensive distribution of the drug at 5 μ M with a half-life of 1hr.

Statistical analysis

Data are expressed as the mean \pm S.E. for at least three independent replicate experiments (n \geq 3). Statistical tests were undertaken using InStat (GraphPad, La Jolla, CA, USA). Statistical analysis of results was undertaken using one-way analysis of variance (ANOVA) using a post-test depending on the requirement.

FUNDING SOURCES

Eduard Badarau was supported by the Marie Curie research grant: "TRANSCOM", FP7 No: 251506. Andrea Costanzi was supported by the Marie Curie research grant "TRANSPATH" FP7 No 289964.

AUTHOR CONTRIBUTION

MG was the major grant holder that funded the work. M.G. and Z.W., D.R. designed the experiments. E.B. performed the compound synthesis and with D.R the modelling. Z.W., A.C., T.T., C.M., M.B. and S.E.L. performed the biological experiments, and all authors analyzed the data. M.G., Z.W., E.B. and D.R wrote the manuscript.

ACKNOWLEDGEMENTS

The authors acknowledge EPSRC National Mass Spectrometry Centre, Swansea (UK) for recording the HRMS spectra. To Glaxo Smith Kline, UK for undertaking the *in vitro* DMPK assays. The group of Prof Soichi Kojima (RIKEN, Japan) for kindly providing the TG2 ko endothelial cells. To Dr Raj K. Singh Badhan (Aston University) for help in calculating the inhibitor concentration used in the *in vivo* experiments following pharmacokinetic simulations. Fruitful discussions with Dr Alexandre Mongeot and Dr Russell Collighan (Aston University) are also acknowledged.

None of the authors of this manuscript have a financial interest related to this work.

REFERENCES

- Arnold, K., Bordoli, L., Kopp, J. and Schwede, T. (2006). The SWISS-MODEL workspace: a web-based environment for protein structure homology modelling, *Bioinformatics* 22, 195-201.
- Badarau, E., Collighan, R.J., and Griffin, M. (2013a). Recent advances in the development of tissue transglutaminase (TG2) inhibitors. *Amino Acids* 44, 119-127.
- Badarau, E., Mongeot, A., Collighan, R.J., Rathbone, D.L., and Griffin, M. (2013b). Imidazolium-based warheads strongly influence activity of water-soluble peptidic transglutaminase inhibitors. *Eur J Med Chem* 66, 526-530.
- Baumgartner, W., Golenhofen, N., Weth, A., Hiiragi, T., Saint, R., Griffin, M., and Drenckhahn, D. (2004). Role of transglutaminase 1 in stabilisation of intercellular junctions of the vascular endothelium. *Histochem Cell Biol* 122, 17-25.
- Duval, E., Case, A., Stein, R.L., and Cuny, G.D. (2005). Structure-activity relationship study of novel tissue transglutaminase inhibitors. *Bioorg Med Chem Lett* 15, 1885-1889.
- Freund, K.F., Doshi, K.P., Gaul, S.L., Claremon, D.A., Remy, D.C., Baldwin, J.J., Pitzenberger, S.M., and Stern, A.M. (1994). Transglutaminase inhibition by 2-[(2-oxopropyl)thio]imidazolium derivatives: mechanism of factor XIIIa inactivation. *Biochemistry* 33, 10109-10119.
- Griffin, M., Casadio, R., and Bergamini, C.M. (2002). Transglutaminases: nature's biological glues. *Biochem J* 368, 377-396.
- Griffin, M., Mongeot, A., Collighan, R., Saint, R.E., Jones, R.A., Coutts, I.G., and Rathbone, D.L. (2008). Synthesis of potent water-soluble tissue transglutaminase inhibitors. *Bioorg Med Chem Lett* 18, 5559-5562.
- Han, B.G., Cho, J.W., Cho, Y.D., Jeong, K.C., Kim, S.Y., and Lee, B.I. (2010). Crystal structure of human transglutaminase 2 in complex with adenosine triphosphate. *Int J Biol Macromol* 47, 190-195.
- Huang, L., Haylor, J.L., Hau, Z., Jones, R.A., Vickers, M.E., Wagner, B., Griffin, M., Saint, R.E., Coutts, I.G., El Nahas, A.M., *et al.* (2009). Transglutaminase inhibition ameliorates experimental diabetic nephropathy. *Kidney Int* 76, 383-394.
- Johnson, T.S., Fisher, M., Haylor, J.L., Hau, Z., Skill, N.J., Jones, R., Saint, R., Coutts, I., Vickers, M.E., El Nahas, A.M., *et al.* (2007). Transglutaminase inhibition reduces fibrosis and preserves function in experimental chronic kidney disease. *J. Am. Soc. Nephrol.* 18, 3078-3088.
- Klock, C., Jin, X., Choi, K., Khosla, C., Madrid, P.B., Spencer, A., Raimundo, B.C., Boardman, P., Lanza, G., and Griffin, J.H. (2011). Acylideneoxindoles: a new class of reversible inhibitors of human transglutaminase 2. *Bioorg Med Chem Lett* 21, 2692-2696.
- Liu, S., Cerione, R.A., and Clardy, J. (2002). Structural basis for the guanine nucleotide-binding activity of tissue transglutaminase and its regulation of transamidation activity. *Proc Natl Acad Sci U S A* 99, 2743-2747.
- Lortat-Jacob H, Burhan I, Scarpellini A, Thomas A, Imberty A, Vivès RR, Johnson T, Gutierrez A, Verderio EA. (2012) Transglutaminase-2 interaction with heparin: identification of a heparin binding site that regulates cell adhesion to fibronectin-transglutaminase-2 matrix. *J Biol Chem* 287, 18005-18017.

Ozaki, S., Ebisui, E., Hamada, K., Goto, J., Suzuki, A.Z., Terauchi, A., and Mikoshiba, K. (2010). Potent transglutaminase inhibitors, aryl beta-aminoethyl ketones. *Bioorg Med Chem Lett* 20, 1141-1144.

Ozaki, S., Ebisui, E., Hamada, K., Suzuki, A.Z., Terauchi, A., and Mikoshiba, K. (2011). Potent transglutaminase inhibitors, dithio beta-aminoethyl ketones. *Bioorg Med Chem Lett* 21, 377-379.

Pardin, C., Pelletier, J.N., Lubell, W.D., and Keillor, J.W. (2008a). Cinnamoyl inhibitors of tissue transglutaminase. *J Org Chem* 73, 5766-5775.

Pardin, C., Roy, I., Lubell, W.D., and Keillor, J.W. (2008b). Reversible and competitive cinnamoyl triazole inhibitors of tissue transglutaminase. *Chem Biol Drug Des* 72, 189-196.

Perez Alea, M., Kitamura, M., Martin, G., Thomas, V., Hitomi, K., and El Alaoui, S. (2009). Development of an isoenzyme-specific colorimetric assay for tissue transglutaminase 2 cross-linking activity. *Analytical Biochemistry* 389, 150-156.

Pinkas, D.M., Strop, P., Brunger, A.T., and Khosla, C. (2007). Transglutaminase 2 undergoes a large conformational change upon activation. *PLoS Biol* 5, 2788-2795.

Prime, M.E., Andersen, O.A., Barker, J.J., Brooks, M.A., Cheng, R.K., Toogood-Johnson, I., Courtney, S.M., Brookfield, F.A., Yarnold, C.J., Marston, R.W., *et al.* (2012). Discovery and structure-activity relationship of potent and selective covalent inhibitors of transglutaminase 2 for Huntington's disease. *J Med Chem* 55, 1021-1046.

Schaertl, S., Prime, M., Wityak, J., Dominguez, C., Munoz-Sanjuan, I., Pacifici, R.E., Courtney, S., Scheel, A., and Macdonald, D. (2010). A profiling platform for the characterization of transglutaminase 2 (TG2) inhibitors. *J Biomol Screen* 15, 478-487.

Schoellmann, G., and Shaw, E. (1963). Direct evidence for the presence of histidine in the active center of chymotrypsin. *Biochemistry* 2, 252-255.

Tran, T. T., A. Mittal, T. Gales, B. Maleeff, T. Aldinger, J. W. Polli, A. Ayrton, H. Ellens and J. Bentz (2004). "Exact kinetic analysis of passive transport across a polarized confluent MDCK cell monolayer modeled as a single barrier." *J Pharm Sci* 93, 2108-2123.

Wang, Z., Collighan, R.J., Pytel, K., Rathbone, D.L., Li, X., and Griffin, M. (2012). Characterization of heparin-binding site of tissue transglutaminase: its importance in cell surface targeting, matrix deposition, and cell signaling. *J Biol Chem* 287, 13063-13083.

Wang, Z., and Griffin, M. (2012). TG2, a novel extracellular protein with multiple functions. *Amino Acids* 42, 939-949.

Wang, Z., and Griffin, M. (2013). The role of TG2 in regulating S100A4-mediated mammary tumour cell migration. *PLoS One* 8, e57017.

Wang, Z., Perez, M., Caja, S., Melino, G., Johnson, T.S., Lindfors, K., and Griffin, M. (2013). A novel extracellular role for tissue transglutaminase in matrix-bound VEGF-mediated angiogenesis. *Cell Death Dis* 4, e808.

Wityak, J., Prime, M.E., Brookfield, F.A., Courtney, S.M., Erfan, S., Johnsen, S., Johnson, P.D., Li, M., Marston, R.W., Reed, L., Vaidya, D., Schaertl, S., Pedret-Dunn, A., Beconi, M., Macdonald, D., Muñoz-Sanjuan, I., and Dominguez, C. (2012) SAR Development of Lysine-Based Irreversible Inhibitors of Transglutaminase 2 for Huntington's Disease. *ACS Med Chem Lett* 3, 1024.

FIGURE LEGENDS

Figure 1. Design and Synthesis of Lead TG2 Inhibitor Precursor

(A) Examples of dihedral angles defined by N1-C2-C3-N4 recorded during the molecular dynamics trajectory.

(B) Design of new peptidomimetic derivatives starting from the water-soluble inhibitors, R = SMe2.

(C) Scheme 1 for the synthesis of the amine precursors. (a) p-NO₂-phenylchloroformate, N-methylmorpholine (NMM)/dichloromethane (DCM), 0°C, 2 hr; (b) piperazine, triethylamine (TEA)/dimethylformamide, 0°C to room temperature, 12 hr; (c) tert-butyloxycarbonyl (t-Boc)-Glu-OH, 1-ethyl-3-(3-dimethylaminopropyl) carbodiimide, HOBt, NMM/DCM, room temperature, 12 hr; (d) trifluoroacetic acid/DCM, room temperature, 24 hr. Commercially available alcohols were activated as p-nitrophenyl carbonates 7 and subsequently reacted with piperazine at room temperature in order to give the desired mono-carbamates 8. A peptidic coupling step with t-Boc-protected amino acids, followed by the acidic deprotection of the amines conducted to the key intermediates 5.

(D) Scheme 2 for the synthesis of the final derivatives. (a) Acryloyl chloride, TEA/acetonitrile, 0°C to room temperature, 3 hr; (b) bromoacetyl bromide or chloroacetyl chloride, TEA/DCM, -78°C to room temperature, 12 hr; (c) dimethylsulfide/MeOH, room temperature, 24 hr; (d) acetyl bromide, TEA/DCM, -78°C, 2 hr; (e) 2-chloroethylsulfonyl chloride, TEA/DCM, -60°C–0°C, 4 hr. Starting from the previously obtained amines 5, various acylation agents were used in order to obtain the final derivatives 1–4 as summarized in Scheme 2. In the case of polar dimethylsulfonium warhead, an additional nucleophilic substitution step was conducted on the halomethylamide precursor 6.

(E) Toxicity profile of the fluorescent derivative 3h on HUVEC lines, after 24 hr (white), 48 hr (grey), and 72 hr (black) as described in the Experimental Procedures. CNTL, control.

Figure 2. Characterization of the Lead Compounds for their Specificity and Cell Permeability

(A) Columns 2–5 show Ca²⁺-dependent binding of 3h with rhTG2. rhTG2 pre-treated with Ca²⁺ or GTP was incubated with 3h (10 nM) or 1h (1 mM) for 30 min at 4°C. Following removal of excessive inhibitors using 30-kDa cut off spin columns, bars 6 and 7 show the efficiency of the spin columns, where reaction mixes with inhibitor alone (either 3h or 1h) were prepared and filtered through the spin columns prior to assay. Bars 8–10 show the efficacy of GTP binding, where enzyme was incubated with 250 μM Ca²⁺ to show activation of rhTG2 (bar 8) in the absence of GTP and showing that 1mM Ca²⁺ activates TG2 with 250 mM GTP present (bar 10). Samples with 1 mM GTP and 250 μM calcium were prepared in duplicate and one sample was processed through the spin column (bar 10) and the other sample was not (bar 9) to evaluate whether the spin column affects GTP binding. A positive control incubated without inhibitor was used as 100% reference (bar 1).

(B) Effect of TG2 inhibitors 3h, 1h, 3e, and 1e on Caspase 3/7 activity. Following induction of apoptosis in HUVECs by staurosporine, caspase activity was measured as described in the Experimental Procedures. Ctrl represents the negative control without any inhibitor; addition of the caspase inhibitor Z-VAD-FMK to the assay represents the positive control.

(C) Western blotting showing covalent interaction of compound 1h with TG2 and demonstrating targeting of the active site Cys277 by 1h as described in the Experimental Procedures.

(D) Cell permeability of TG2 inhibitors 3h, 1f, 3f, 3e, 1e in primary HUVECs. The assay measures the inhibition of the TG2-mediated incorporation of N-(5-aminopentyl)biotinamide into intracellular proteins. R281, which is not cell permeable, was used as the 100% control. Experiments were undertaken as described in the Experimental Procedures. *p < 0.05.

(E) Detection of dansyl inhibitor 3h in NIH3T3 cells. NIH3T3 cells transduced with TG2 containing Lentivirus were treated with 3h in the presence or absence of ionomycin and 1e. Co-IP using the cell cytosol fractions was performed to detect the interaction between TG2 and 3h as described in the Experimental Procedures.

(F) Non-denaturing gel electrophoresis. rhTG2 pre-treated with Ca²⁺ or GTP (concentrations as indicated in the figure), followed by incubation with 3h or 1h as described in the Experimental Procedures. The samples were separated by non-denaturing PAGE and visualized using gel imaging.

Figure 3. Intracellular Reactivity of Fluorescent Compound 3h with TG2 and its Effect on Enzyme Externalization

(A) Detection of in situ TG2 activity using the dansyl derivative 3h, HUVECs and TG2^{-/-} mouse endothelial cells (top panel) were treated as described in the Experimental Procedures. The cells were pre-treated with (a–i) or without ionomycin (j–l), in the presence (g, h) or absence (a–f and j–l) of non-dansylated cellpermeable inhibitor 3e, while TG2 antigen was visualized using anti-TG2 antibody Cub7402 (d–l). DAPI is shown in the top right hand corner of each image.

(B) Detection of TG2-dansyl derivative 3h complex in HUVECs and mouse TG2^{-/-} endothelial cells after co-IP and western blotting. HUVECs were treated as described in (A). Cytosol fractions were collected and co-IP was undertaken using an anti-dansyl antibody as described in the Experimental Procedures. The presence of TG2 was detected via western blotting. Rabbit IgG and TG2 knockout endothelial cells were used as the negative controls.

(C) Effect of inhibitor 3h on the interaction between TG2 and syndecan-4. Swiss3T3 cells transduced with wt TG2 were pre-treated with inhibitor 3h. Co-IP was performed using anti-syndecan-4 antibody to pull down the immune complex and the presence of TG2 was detected via western blotting. The empty vector transduced cells (vector) or the heparan sulfate binding mutant (HS2) TG2-transduced cells were used as the controls.

(D) Effect of 3h on TG2 externalization and deposition. The presence of TG2 in Swiss3T3 cells from (C) was detected via biotinylation of cell surface (CS) proteins followed by western blotting. The matrix proteins were collected as described in the Experimental Procedures and the presence of TG2 was measured using anti-TG2 antibody Cub7402 via western blotting. WCL, whole-cell lysate.

Figure 4. Effect of Compound 3h on Endothelial Cell Migration and Tubule Formation.

(A) Representative images showing the effect of 3h on FN deposition by HUVECs. 7.3 × 10⁴ HUVECs were seeded into chamber slides in the presence or absence of 3h treatment for 72 hr. Immunofluorescence staining was performed to detect the extracellular FN as described in the Experimental Procedures. Fluorescence images were captured using an epifluorescence microscope from three separate experiments.

(B) Representative images showing the effect of 3h on HUVEC migration in the wound-healing assay. HUVECs were seeded into 12-well plates

until confluency. Wounds were introduced into the monolayer using 200- μ l tips. The cells were allowed to migrate for 6 hr and the closure of

the wounds was analyzed using ImageJ software (n = 3). *p < 0.05.

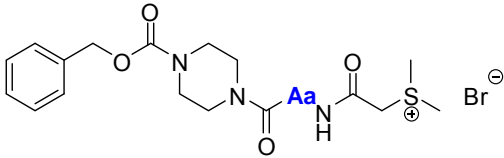
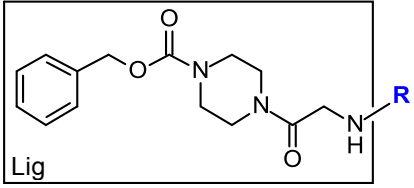
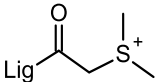
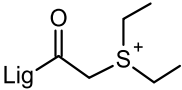
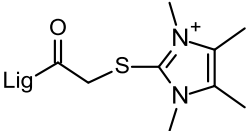
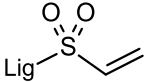
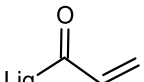
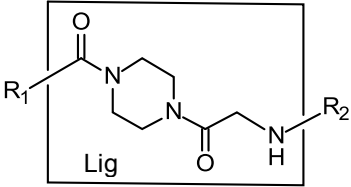
(C) Representative images demonstrating the inhibition of HUVEC cord formation on Matrigel by 3h. 96-well plates were pre-coated with Matrigel and HUVECs were allowed to form cord structures for 6 hr. The images from three separate experiments were taken using a Nikon digital camera.

Figure 5. TG2 Inhibition Attenuates Angiotensin II-Induced Renal Fibrosis Two groups of animals were used. In the first group, five C57BL/6 male mice (14 weeks old) were infused with AngII 1.1 mg/kg/day in 50% DMSO in PBS (pH 7.4) for 2 weeks without TG2 inhibitor via a subcutaneously implanted osmotic pump (Alzet 1002) as previously described (Murdoch et al., 2014). In the second group, compound 3h was infused in a similar manner at 25 mg/kg/day in 50% DMSO in PBS (pH 7.4) together with AngII over 14 days.

(A) Representative images of kidneys from the inhibitor- (lower panel) and non-inhibitor-(upper panel) treated animals.

(B and C) Averaged data of Sirius red/collagen staining in kidney sections showing staining (B) around arterioles (n = 4) and (C) total collagen staining (n = 5). *p < 0.05.

Table 1. TG2 inhibition data upon varying: **(A)** the central amino acid, **(B)** the warhead on the initial hit and **(C)** varying the substituents in the carbamate region.

(A)			(B)		
					
Cpd	Aa	IC ₅₀ ± SD [μM]	Cpd	R	IC ₅₀ ± SD [μM]
1a	Gly	1.4 ± 0.5	1a		1.4 ± 0.5
1j	D-Ala	6.8 ± 2.0	1q		1.85 ± 0
1i	L-Ala	0.7 ± 0.3	1s		100
1l	D-Phe	> 100	2a		1.725 ± 0.11
1k	L-Phe	> 100	3a		5.925 ± 0.11
(C)					
					
Cpd	R ₁		R ₂		IC ₅₀ ± SD [μM]

6c			0.029 ± 0.019	
1c			1.07 ± 0.1	
3c			0.44 ± 0.057	
6d			0.015 ± 0.007	
1d			1.5 ± 0.4	
3d			2.1 ± 0	
6n			0.00665 ± 0.00021	
6b			0.0021 ± 0.0004	
1b			3.3 ± 0.3	
3b			6.3 ± 2.9	
6e			0.0039 ± 0.0004	
6o			0.00875 ± 0.00035	
1e			0.889 ± 0.2	
3e			0.125 ± 0.066	

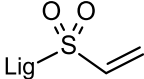
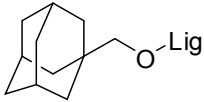
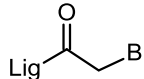
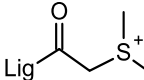
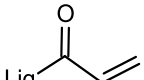
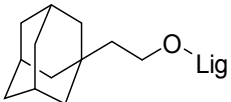
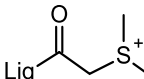
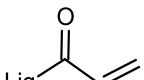
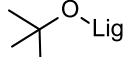
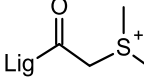
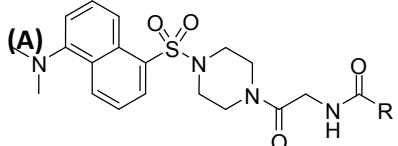
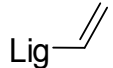
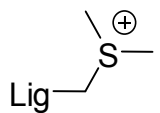
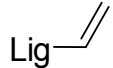
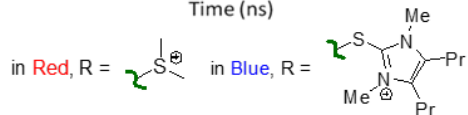
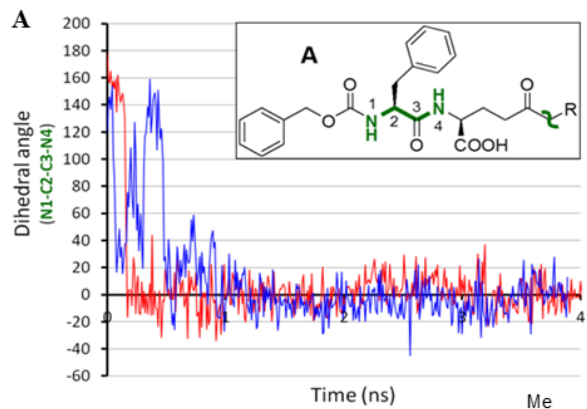
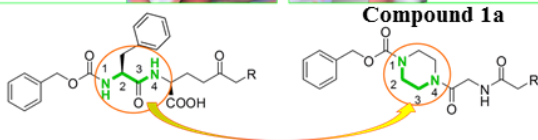
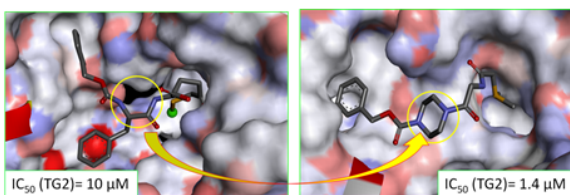
2e			0.875 ± 0.035	
6f			0.00629 ± 0.0005	
1f			0.775 ± 0.035	
3f			1.625 ± 0.035	
1g			3.15 ± 0.92	
3g			0.9 ± 0.14	
1m			0.273 ± 0.11	

Table 2. Characterisation of compounds 3h, 1h and 3e for inhibition of different TGs and PSA values (A) and inhibition profiles for other selected potent TG2 inhibitors (B).

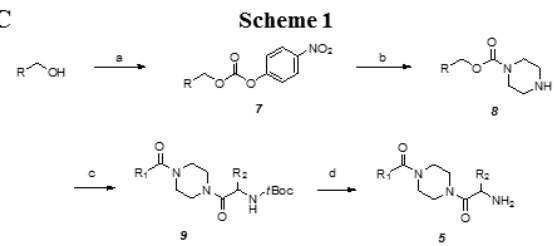
							
Cpd	FXIIIa (μM)	TG1 (μM)	TG3 (μM)	TG6 (μM)	TG2* (μM)	PSA (Å ²)	R
3h	> 100	25	20	5	0.0061 ± 0.00042	90	Lig- 
1h	> 100	> 100	> 100	>10	0.38± 0.057	112	Lig- 
3e	37	2.2	11	2μM	0.125 ±0.066	70	Lig- 
(B) Cpd	IC ₅₀ (μM)						
	TG1 (μM)	TG3 (μM)	TG6 (μM)	FXIIIa (μM)			
1a	>100	>100	NT	>100			
1c	>100	>100	NT	>100			
3c	>100	>100	NT	>100			
6d	5	65	NT	>100			
1d	>100	>100	NT	>100			
3d	>100	>100	NT	>100			
1b	>100	>100	NT	>100			
6e	1	70	NT	>100			
1e	>100	>100	>10μM	>100			
6g	3	50	NT	>100			
1f	>100	>100	>10μM	>100			
3f	>100	>100	>10μM	>100			
3g	>100	>100	NT	>100			
1m	>100	>100	NT	>100			



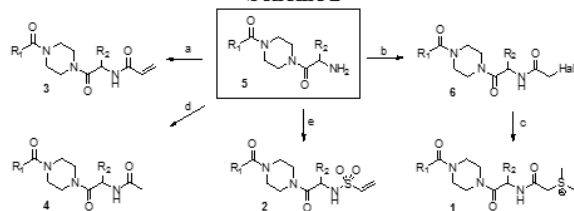
B



C



D



E

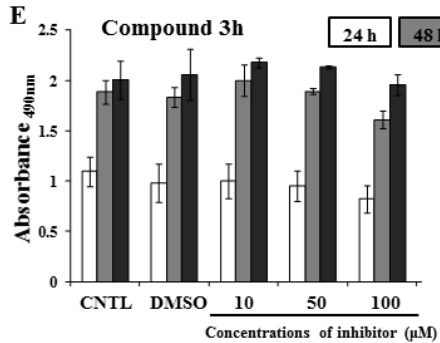


Figure 1

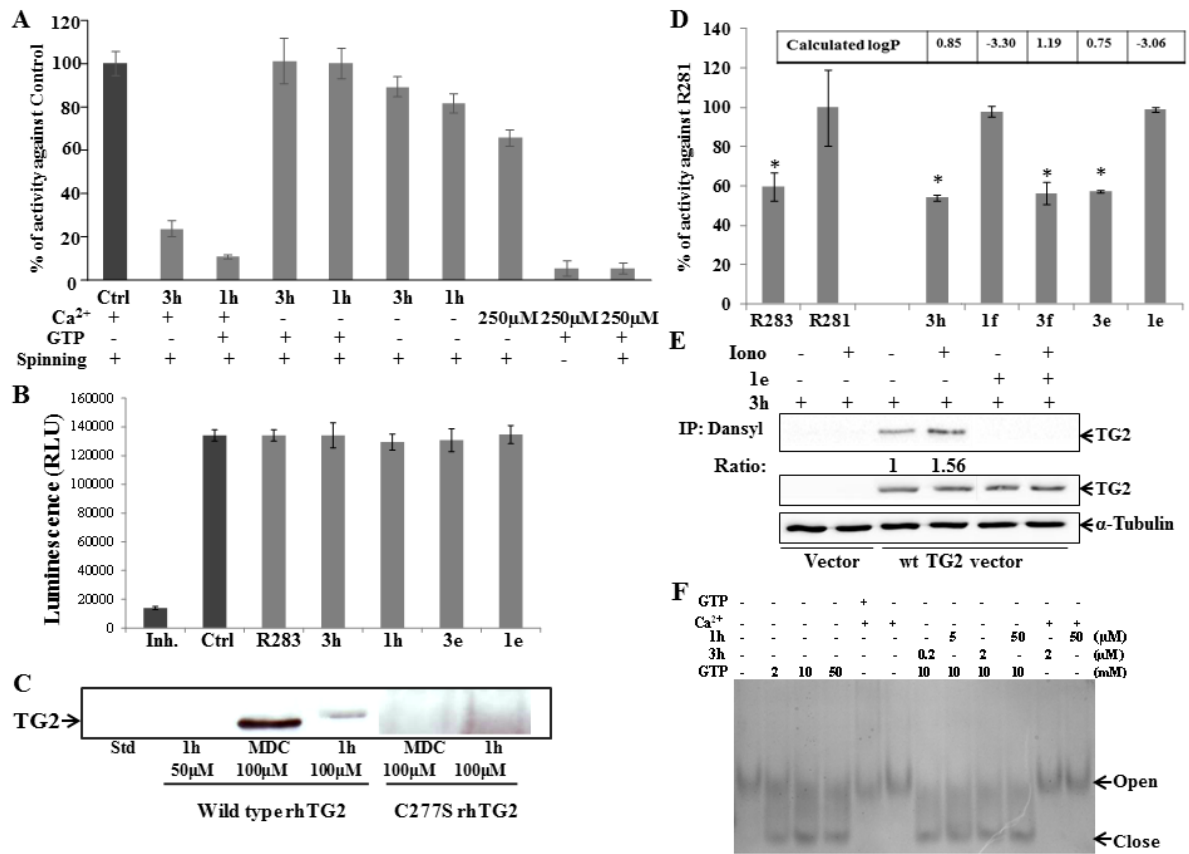


Figure 2

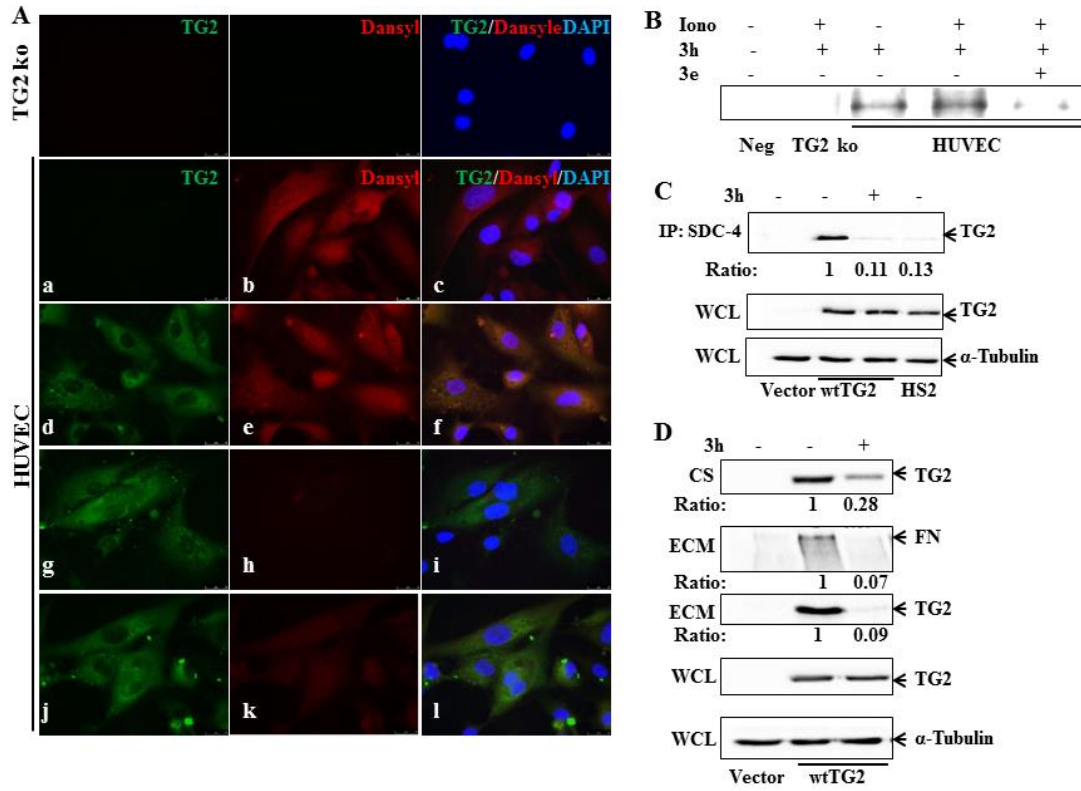


Figure 3

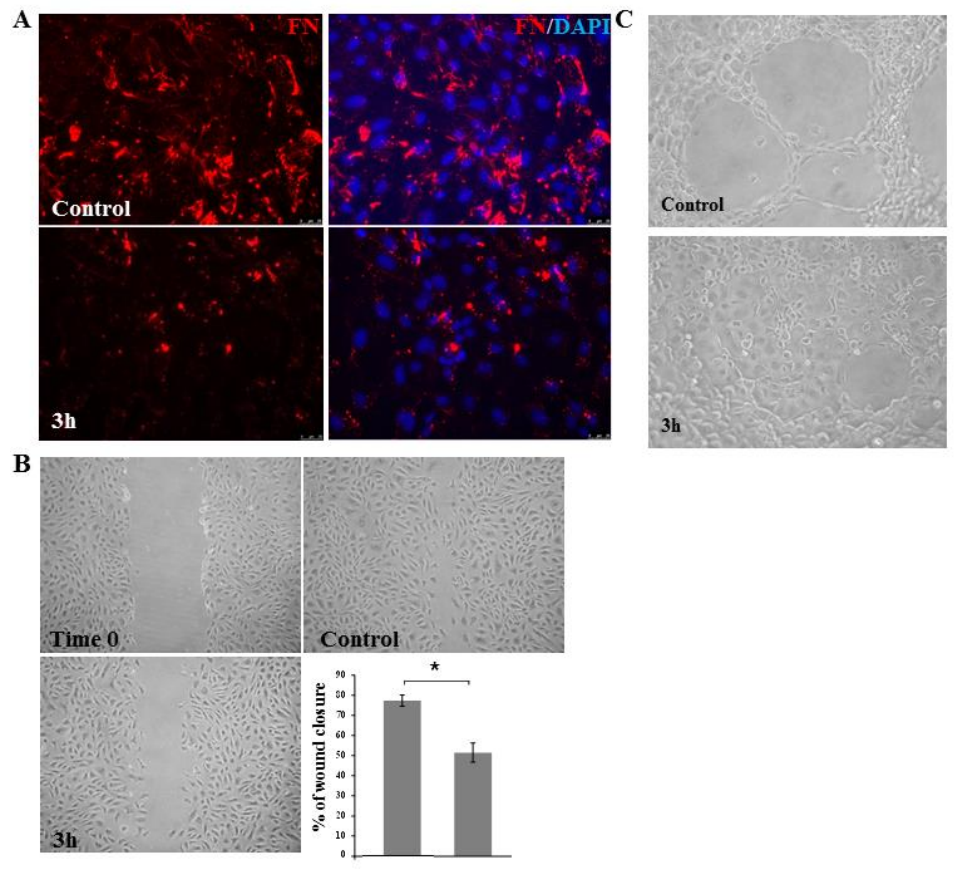


Figure 4

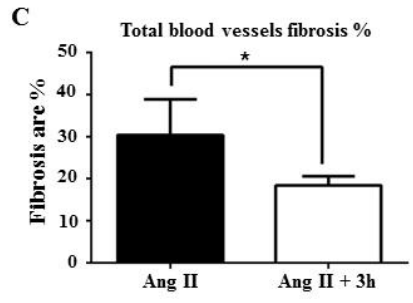
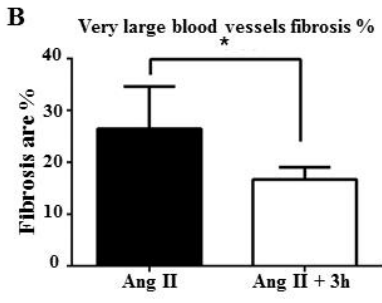
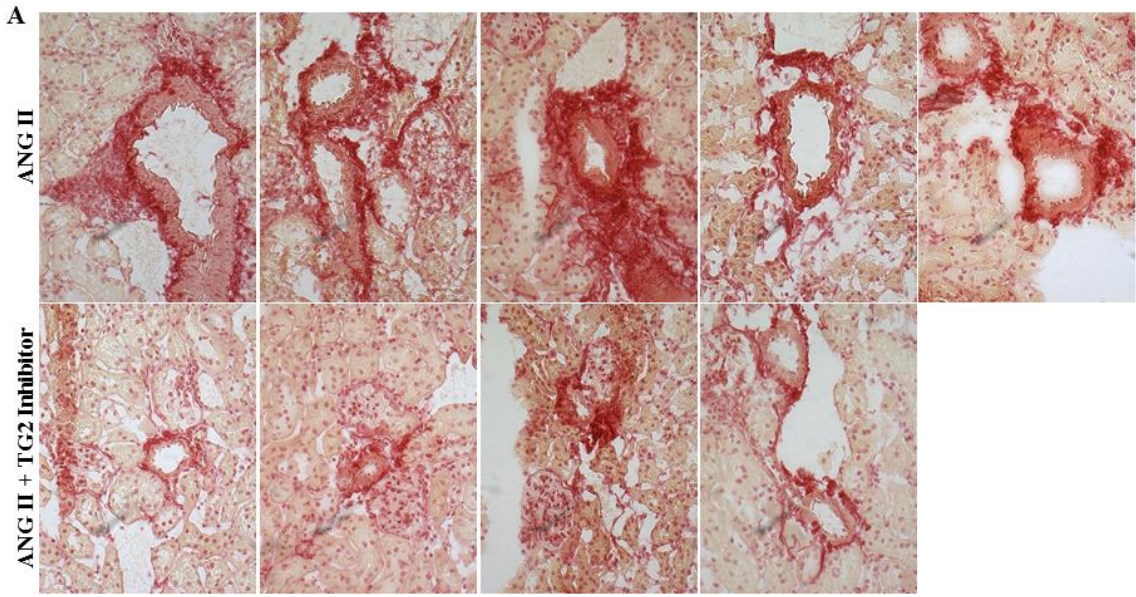
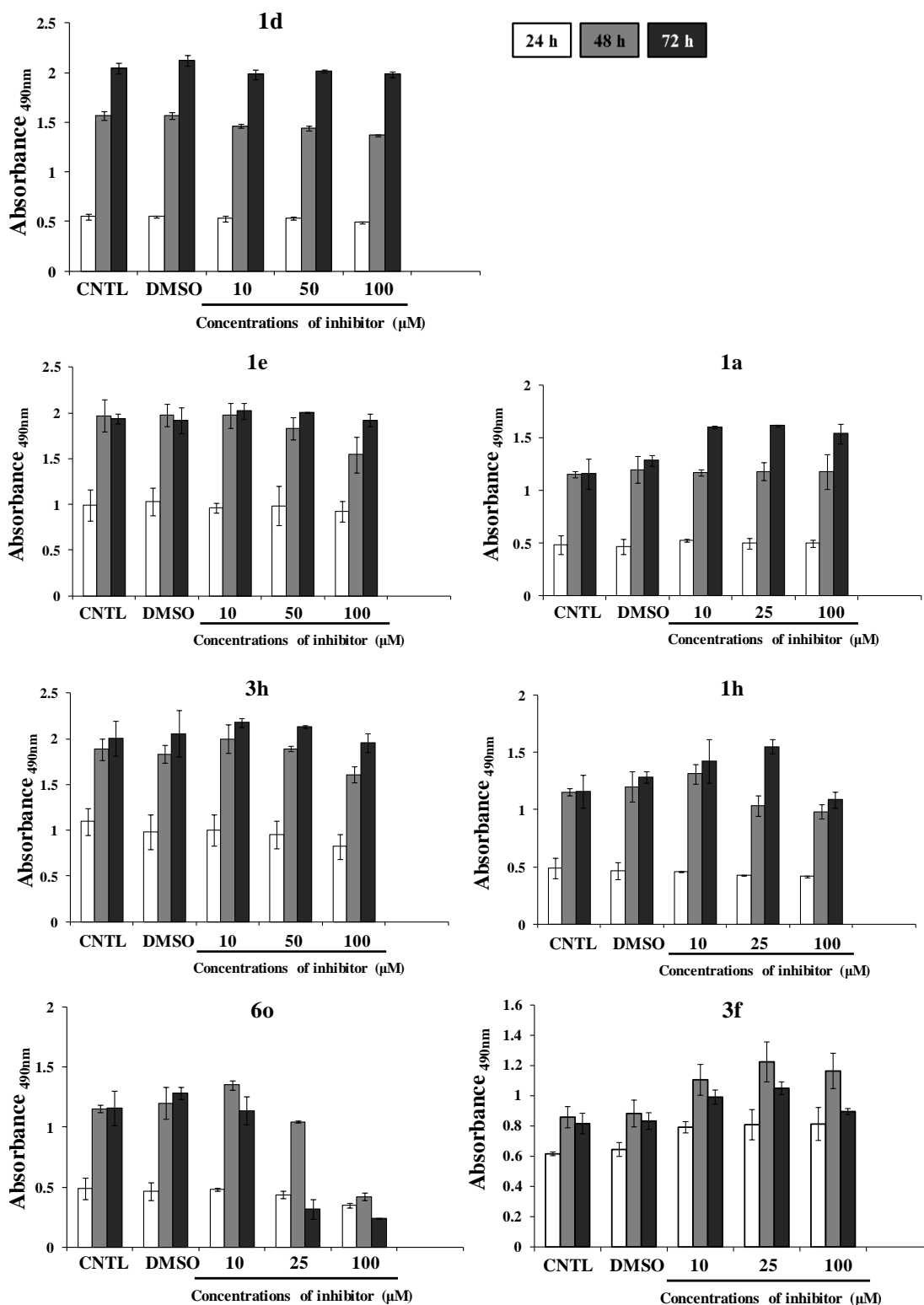
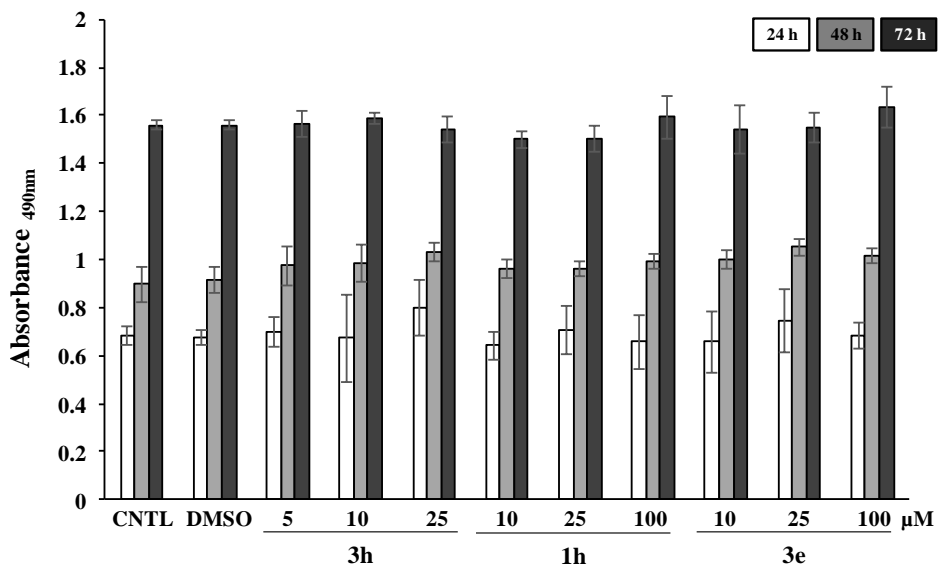


Figure 5

SUPPLEMENTAL FIGURES




Supplemental Figure 1 (related to Figure 1E). The toxicity of the inhibitors shown in following Figure was measured in HUVEC cells using the XTT assay for measuring cell viability at the time periods and inhibitor concentrations shown as described in the Supplemental Experimental procedures. The histograms show mean values \pm S.D. from 3 separate experiments at the concentration of the inhibitors shown at three time points. DMSO was used as the vehicle control treatment.




Supplemental Figure 2 (related to Figure 1E). The toxicity of the inhibitors **3h**, **1h** and **1e** was measured using the XTT assay for measurement of cell viability in HUVEC cells cultured in serum free endothelial cell culture medium as described in the Supplemental Experimental procedures. The histograms show mean values \pm S.D. from 3 separate experiments at the concentration of the inhibitors shown at three different time points. DMSO was used as the vehicle control treatment.

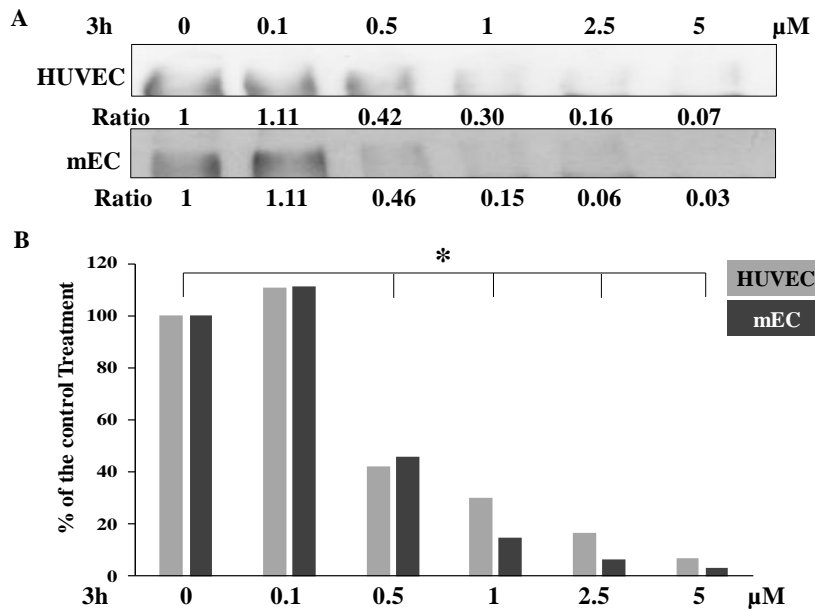
A

EDTA	-	+	-	+	-	+
Ca ²⁺	+	-	+	-	+	-
3h	100	100	1	1	100	100
						
	FXIII	FXIII	TG1	TG1	TG3	TG3

B

EDTA	-	+	-	+	-	+
Ca ²⁺	+	-	+	-	+	-
1h	100	100	100	100	100	100
						
	FXIII	FXIII	TG1	TG1	TG3	TG3

Supplemental Figure 3 (related to Table 2A). The interaction between compounds dansyl-labelled **1h** or **3h** and transglutaminase family members TG1, TG3 and FXIII (1µg of total protein/each). Recombinant human TG1, TG3 and FXIII were incubated with **1h** (A) or **3h** (B) in the presence of Ca²⁺ or EDTA for 30 min at room temperature. The detection of dansyl was performed as described in the Experimental procedures using Western blotting.



Supplemental Figure 4 (related to Figure 5). Inhibition profile for FN deposition in human HUVEC cells and mouse endothelial cells by compound 3h. (A) HUVEC cells or mouse endothelial cells were treated with compound 3h for 72 h, the extracellular matrices were collected as described in Supplemental Experimental Procedures and Western blotting was performed to detect the presence of FN which was quantified by densitometry and plotted as shown in B. (B) Percentage of the FN present in the 3h treated endothelial cells compared to the vehicle control treatment DMSO (0 μM).

SUPPLEMENTAL TABLES

Supplemental Table 1 (related to Figure 1 and Table 1). Toxicity data for the compounds listed measured over 72 h.

Cpd	R ₁	R ₂	Toxicity* / 72 h [μM]
1a			>100
6n			25
1d			>100
1f			>100
3f			100
6o			25
1e			>100
3e			>100
2e			25

* The toxicity of the inhibitors shown in the above Table and as shown in Supplemental Figure 1 was measured in HUVEC cells as described in the Experimental Procedures using the XTT assay to measure cell viability and also shown in **Supplemental Figure 1**.

Supplemental Table 2 (related to Table 2A). Characterisation of compounds 3h, 1h and 3e by *in vitro* ADME assays.

Cpd	3h	1h	3e
Cell Health (pIC ₅₀)			
Mitochondrial Potential	<3.7	<3.7	<3.7
Nuclear Morphology	<3.7	<3.7	<3.7
Microsomal Stability	3.5	0.5	1.0
3A4 (Flint Red)	4.6	4.9	<4.3
3A4 (Flint Green)	4.5	4.7	<4.3
hERG	<4.3	<4.3	<4.3
Protein Binding			
HSA (%)	89	79	61
Alpha-Glycoprotein	66	80	40

The ADME assays undertaken on compounds **3h**, **1h** and **3e**, included Cell Health (pIC₅₀), consisting of Mitochondrial Potential, Nuclear Morphology, Microsomal Stability, 3A4 (Flint Red), 3A4 (Flint Green), hERG, Protein Binding, HSA (%), Alpha-Glycoprotein, which were undertaken as described in the Supplemental Experimental Procedures. For the Cell Health Screens the values shown are the mean from 4 experiments, for microsomal stability the mean value is from two experiments and for hERG the mean is shown from 3 experiments.

SUPPLEMENTAL EXPERIMENTAL PROCEDURES

Chemistry Experimental Procedures

Analytical methodology

The newly synthesized derivatives were characterised by infra-red spectroscopy (IR), proton and carbon-13 NMR spectroscopy (^1H - and ^{13}C -NMR), melting points (m.p.), high resolution mass spectrometry (HRMS). They had properties consistent with the proposed structures and are described below.

The infrared (IR) spectra were recorded on a Thermo Scientific Nicolet iS5 FT-IR spectrometer equipped with an ID5 Diamond ATR accessory. Signal intensities were abbreviated as follows: weak (w), medium (m) and strong(s).

^1H NMR and ^{13}C NMR were recorded with Bruker Avance DPX250 (at 250.131 MHz and 62.895 MHz, respectively) in deuterated chloroform (CDCl_3) and deuterated dimethyl sulfoxide (DMSO), using tetramethylsilane (TMS) as an internal standard. Chemical shifts are reported in parts per million (ppm) and the coupling constants are reported in units of Hertz [Hz]. Multiplicities were abbreviated as follows: singlet (s), doublet (d), triplet (t), quartet (q), pentuplet (p), sextet (sx), septet (sp), apparent singlet (as), apparent doublet (ad), apparent triplet (at).

Low-resolution mass spectra (MS) were recorded with a Waters - LCT Premier. High resolution mass spectra (HRMS) were recorded with a Thermo Fischer Scientific LTQ Orbitrap XL at EPSRC National Mass Spectrometry Centre, Swansea (UK).

Melting points were recorded using a Reichert-Jung Thermo Galen - Hot Stage Microscope equipped with a Pt 100/RTD temperature sensor.

Flash chromatography was performed on Merck 40–70 μm (230–400 mesh) silica gel under nitrogen pressure. Thin-layer chromatography (TLC) was carried out on Merck silica gel 60 F254 pre-coated plates. Visualization was made with ultraviolet light ($\lambda = 254/365 \text{ nm}$) and, if necessary, using an ethanolic solution of potassium permanganate.

Synthetic methodology

General method for the synthesis of the *p*-nitrophenyl-carbonates (A)

Under nitrogen atmosphere, N-methylmorpholine (1.6 eq.) was added to a solution of the corresponding alcohols (1 eq., 3 mmol) in DCM (20 ml). The mixture was cooled to 0°C and subsequently a solution of *p*-nitrophenyl chloroformate (1.5 eq.) in DCM (5 ml) was added slowly, and the mixture was vigorously stirred at 0°C until the complete consumption of the starting material (usually 1-2 h). The reaction mixture was diluted with DCM (75 ml) and subsequently washed with sodium bicarbonate (aqueous satd. soln., 3 x 100 ml). The recovered organic layer was dried over magnesium sulfate and the solvent evaporated under vacuum.

(a) *methyl 4-[(4-nitrophenoxy)carbonyloxymethyl]benzoate (7b)*

The crude product obtained following the general protocol was washed with methanol, then with diethyl ether and further dried under reduced pressure to remove traces of solvents. $\text{C}_{16}\text{H}_{13}\text{NO}_7$; yield 88%; white solid; m.p. $95\text{--}96^\circ\text{C}$; $M = 331.28 \text{ g/mol}$; IR (ATR): $\nu = 1763 \text{ (s)}, 1706 \text{ (s)}, 1527 \text{ (s)}, 1448 \text{ (m)}, 1430 \text{ (m)}, 1281 \text{ (m)}, 1208 \text{ (m-s)}, 980 \text{ (m)}, 853 \text{ (m-s)}, 753 \text{ (s)} \text{ cm}^{-1}$; ^1H NMR (250 MHz, CDCl_3) δ 8.28 (d, $J = 9.2 \text{ Hz}$, 2H), 8.08 (d, $J = 8.3 \text{ Hz}$, 2H), 7.51 (d, $J = 8.3 \text{ Hz}$, 2H), 7.38 (d, $J = 9.2 \text{ Hz}$, 2H), 5.35 (s, 2H), 3.93 (s, 3H); ^{13}C NMR (63 MHz, CDCl_3) δ 166.7 (C_q), 155.5 (C_q), 152.5 (C_q), 145.6 (C_q), 139.2 (C_q), 130.8 (C_q), 130.2 (2CH), 128.2 (2CH), 125.5 (2CH), 121.9 (2CH), 70.2 (CH_2), 52.4 (CH_3); MS: $m/z = 354 \text{ [M + Na]}^+$;

(b) *2-naphthylmethyl (4-nitrophenyl) carbonate (7c)*

The crude product obtained following the general protocol was washed with methanol, then with diethyl ether and further dried under reduced pressure to remove traces of solvents. $\text{C}_{18}\text{H}_{13}\text{NO}_5$; yield 67%; white solid; m.p. $151\text{--}152^\circ\text{C}$; $M = 323.30 \text{ g/mol}$; IR (ATR): $\nu = 1748 \text{ (s)}, 1524 \text{ (m)}, 1351 \text{ (m)}, 1263 \text{ (s)}, 1214 \text{ (s)}, 953 \text{ (m)}, 859 \text{ (m)}, 750 \text{ (m)} \text{ cm}^{-1}$; ^1H NMR (250 MHz, CDCl_3) δ 8.31–8.24 (m, 2H), 7.92–7.84 (m, 4H), 7.56–7.50 (m, 3H), 7.42–7.36 (m, 2H), 5.47 (s, 2H); ^{13}C NMR (63 MHz, CDCl_3) δ 155.7 (C_q), 152.6 (C_q), 145.5 (C_q), 133.6 (C_q), 133.2 (C_q), 131.7 (C_q), 128.9 (CH), 128.3 (CH), 128.3 (CH), 127.9 (CH), 126.9 (CH), 126.7 (CH), 126.0 (CH), 125.4 (2CH), 121.9 (2CH), 71.3 (CH_2); MS: $m/z = 346 \text{ [M + Na]}^+$;

(c) *methyl 6-[(4-nitrophenoxy)carbonyloxymethyl]naphthalene-2-carboxylate (7d)*

The crude product obtained following the general protocol was used for the next steps without further purification. C₂₀H₁₅NO₇; white solid; yield 88%; M = 381.34 g/mol; IR (ATR): $\nu = 1754$ (s), 1715 (s), 1515 (s), 1384 (m), 1254 (m), 1208 (m-s), 853 (m-s), 750 (w) cm⁻¹; ¹H NMR (250 MHz, CDCl₃) δ 8.63 (s, 1H), 8.31-8.25 (m, 2H), 8.11 (dd, $J = 8.6$ Hz, $J = 1.6$ Hz, 1H), 8.01 (d, $J = 8.5$ Hz, 1H), 7.95 (as, 1H), 7.91 (d, $J = 8.7$ Hz, 1H), 7.60 (dd, $J = 8.4$ Hz, $J = 1.7$ Hz, 1H), 7.43-7.36 (m, 2H), 5.48 (s, 2H), 4.00 (s, 3H); ¹³C NMR (63 MHz, CDCl₃) δ 167.2 (C_q), 155.6 (C_q), 152.6 (C_q), 145.6 (C_q), 135.4 (C_q), 134.3 (C_q), 132.6 (C_q), 131.0 (CH), 130.3 (CH), 128.5 (CH), 128.4 (C_q), 127.8 (CH), 126.6 (CH), 126.1 (CH), 125.5 (2CH), 121.9 (2CH), 70.9 (CH₂), 52.5 (CH₃); MS: $m/z = 404$ [M + Na]⁺;

(d) *1-adamantylmethyl (4-nitrophenyl) carbonate (7f)*

The crude product obtained following the general protocol was washed with methanol, then with diethyl ether and further dried under reduced pressure to remove traces of solvents. C₁₈H₂₁NO₅; yield 82 %; white solid; m.p. 102-103 °C; M = 331.36 g/mol; IR (ATR): $\nu = 2913$ (m), 2847 (m), 1748 (s), 1518 (s), 1342 (m-s), 1266 (m-s), 1217 (s), 856 (m), 762 (w), 729 (w) cm⁻¹; ¹H NMR (250 MHz, CDCl₃) δ 8.31-8.25 (m, 2H), 7.42-7.36 (m, 2H), 3.89 (s, 2H), 2.03 (s, 3H), 1.79-1.70 (m, 6H), 1.61 (d, $J = 2.6$ Hz, 6H); ¹³C NMR (63 MHz, CDCl₃) δ 155.9 (C_q), 152.9 (C_q), 145.4 (C_q), 125.4 (2CH), 121.9 (2CH), 79.1 (CH₂), 39.0 (3CH₂), 36.9 (3CH₂), 33.5 (C_q), 28.0 (3CH); MS: $m/z = 354$ [M + Na]⁺;

(e) *2-(1-adamantyl)ethyl (4-nitrophenyl) carbonate (7g)*

The crude product obtained following the general protocol was washed with methanol, then with diethyl ether and further dried under reduced pressure to remove traces of solvents. C₁₉H₂₃NO₅; yield 81%; white solid; m.p. 94-95 °C; M = 345.39 g/mol; IR (ATR): $\nu = 2898$ (m), 2841 (w), 1757 (s), 1527 (s), 1342 (s), 1260 (s), 1205 (s), 950 (m), 856 (s), 668 (m) cm⁻¹; ¹H NMR (250 MHz, CDCl₃) δ 8.31-8.35 (m, 2H), 7.41-7.34 (m, 2H), 4.35 (t, $J = 7.5$ Hz, 2H), 1.98 (as, 3H), 1.75-1.62 (m, 6H), 1.59-1.53 (m, 8H); ¹³C NMR (63 MHz, CDCl₃) δ 155.7 (C_q), 152.6 (C_q), 145.4 (C_q), 125.4 (2CH), 121.9 (2CH), 66.4 (CH₂), 42.5 (3CH₂), 42.3 (CH₂), 37.0 (3CH₂), 31.8 (C_q), 28.6 (3CH); MS: $m/z = 368$ [M + Na]⁺;

General method for the piperazine alkylation step (B)

Under inert atmosphere and at 0°C, the previously obtained carbonate (1 eq., 1.5 mmol) was added to a solution of piperazine (2eq.) and TEA (5 eq.) in DMF (20 ml). The mixture was allowed to come back to room temperature and stirred vigorously overnight. After the complete consumption of the starting material, the mixture was diluted with ethyl acetate (100 ml) and washed with sodium chloride (aqueous satd. soln., 3 x 200 ml). The organic layer was dried over magnesium sulfate, filtered and the solvent evaporated under reduced pressure.

(a) *(4-methoxycarbonylphenyl)methyl piperazine-1-carboxylate (8b)*

The crude product obtained following the general protocol was further purified by flash chromatography (eluent: DCM / MeOH 9/1) to conduct to the final derivative. C₁₄H₁₈N₂O₄; yield 64%; light yellow solid; m.p. 69-70 °C; M = 278.30 g/mol; IR (ATR): $\nu = 3338$ (w), 2950 (w), 1709 (s), 1687 (s), 1433 (s), 1423 (s), 1405 (s), 1275 (s), 1226 (s), 1129 (s), 1105 (s), 798 (m), 762 (s), 750 (s) cm⁻¹; ¹H NMR (250 MHz, CDCl₃) δ 8.03 (d, $J = 8.3$ Hz, 2H), 7.41 (d, $J = 8.1$ Hz, 2H), 5.18 (s, 2H), 3.91 (s, 3H), 3.49 (t, $J = 5.1$ Hz, 4H), 2.84 (t, $J = 4.7$ Hz, 4H), 1.86 (s, 1H); ¹³C NMR (63 MHz, CDCl₃) δ 166.9 (C_q), 155.2 (C_q), 142.0 (C_q), 130.0 (2CH), 129.9 (C_q), 127.5 (2CH), 66.5 (CH₂), 52.3 (CH₃), 45.9 (2CH₂), 45.1 (2CH₂); MS: $m/z = 279$ [M + H]⁺;

(b) *2-naphthylmethyl piperazine-1-carboxylate (8c)*

The crude product obtained following the general protocol was further purified by flash chromatography (eluent: DCM / MeOH 9/1) to conduct to the final derivative. C₁₆H₁₈N₂O₂; yield 92%; white solid; m.p. 44-45°C; M = 270.33 g/mol; IR (ATR): $\nu = 3259$ (w), 2913 (w), 1681 (s), 1442 (m), 1417 (m), 1229 (s), 1129 (m), 1111 (m), 1084 (m), 744 (m) cm⁻¹; ¹H NMR (250 MHz, CDCl₃) δ 7.85-7.81 (m, 4H), 7.51-7.44 (m, 3H), 5.29 (s, 2H), 3.49 (t, $J = 5.1$ Hz, 4H), 2.82 (as, 4H), 2.25 (s, 1H); ¹³C NMR (63 MHz, CDCl₃) δ 155.4 (C_q), 134.2 (C_q), 133.3 (C_q), 133.2 (C_q), 128.4 (CH), 128.1 (CH), 127.8 (CH), 127.1 (CH), 126.3 (CH), 126.3 (CH), 125.9 (CH), 67.7 (CH₂), 45.8 (2CH₂), 44.8 (2CH₂); MS: $m/z = 271$ [M + H]⁺;

(c) *(6-methoxycarbonyl-2-naphthyl)methyl piperazine-1-carboxylate (8d)*

The crude product obtained following the general protocol was further purified by flash chromatography (eluent: DCM / MeOH 9/1) to conduct to the final derivative. C₁₈H₂₀N₂O₄; yield 85%; white solid; m.p. 94-95 °C; M = 328.36 g/mol; IR (ATR): $\nu = 3320$ (w), 2950 (w), 1712 (m), 1681 (s), 1433 (m), 1287 (m), 1226 (m), 1193 (m), 1120 (m), 1075 (m), 756 (m) cm⁻¹; ¹H NMR (250 MHz,

CDCl₃) δ 8.60 (s, 1H), 8.07 (dd, $J = 8.6$ Hz, $J = 1.7$ Hz, 1H), 7.95 (d, $J = 8.5$ Hz, 1H), 7.88 (d, $J = 8.7$ Hz, 1H), 7.84 (s, 1H), 7.53 (dd, $J = 8.5$ Hz, $J = 1.6$ Hz, 1H), 5.31 (s, 2H), 3.98 (s, 3H), 3.51 (t, $J = 5.1$ Hz, 4H), 2.85 (at, $J = 4.6$ Hz, 4H); ¹³C NMR (63 MHz, CDCl₃) δ 167.3 (C_q), 155.3 (C_q), 137.0 (C_q), 135.5 (C_q), 132.3 (C_q), 130.9 (CH), 129.9 (CH), 128.4 (CH), 127.8 (C_q), 126.6 (CH), 126.5 (CH), 125.8 (CH), 67.1 (CH₂), 52.4 (CH₃), 46.0 (2CH₂), 45.1 (2CH₂); MS: $m/z = 329$ [M + H]⁺ and 351 [M + Na]⁺;

(d) *1-adamantylmethyl piperazine-1-carboxylate* (8f)
The crude product obtained following the general protocol was subsequently used without further purification. C₁₆H₂₆N₂O₂; yield 62%; light yellow solid; M = 278.39 g/mol; IR (ATR): $\nu = 2883$ (m-s), 2841 (m), 1678 (s), 1427 (s), 1232 (s), 1120 (m), 765 (m) cm⁻¹; ¹H NMR (250 MHz, CDCl₃) δ 3.66 (s, 2H), 3.44 (t, $J = 5.1$ Hz, 4H), 2.82 (t, $J = 5.1$ Hz, 4H), 2.13 (s, 1H), 1.96 (as, 3H), 1.73-1.60 (m, 6H), 1.51 (d, $J = 2.5$ Hz, 6H); ¹³C NMR (63 MHz, CDCl₃) δ 155.9 (C_q), 75.2 (CH₂), 46.0 (2CH₂), 44.9 (2CH₂), 39.5 (3CH₂), 37.1 (3CH₂), 33.6 (C_q), 28.2 (3CH); MS: $m/z = 279$ [M + H]⁺;

(e) *2-(1-adamantyl)ethyl piperazine-1-carboxylate* (8g)
The crude product obtained following the general protocol was further purified by flash chromatography (eluent: DCM / MeOH 95/5) to conduct to the final derivative. C₁₇H₂₈N₂O₂; yield 77%; light yellow oil becoming a light yellow solid on standing; m.p. 56-57 °C; M = 292.42 g/mol; IR (ATR): $\nu = 2895$ (s), 2837 (m), 1687 (s), 1436 (s), 1232 (s), 1120 (s), 1087 (m) cm⁻¹; ¹H NMR (250 MHz, CDCl₃) δ 4.12 (t, $J = 7.3$ Hz, 2H), 3.42 (t, $J = 5.0$ Hz, 4H), 2.81 (t, $J = 5.0$ Hz, 4H), 1.93 (as, 3H), 1.71-1.58 (m, 6H), 1.52-1.51 (m, 6H), 1.41 (t, $J = 7.3$ Hz, 2H); ¹³C NMR (63 MHz, CDCl₃) δ 155.8 (C_q), 61.9 (CH₂), 46.0 (2CH₂), 44.9 (2CH₂), 43.0 (CH₂), 42.7 (3CH₂), 37.2 (3CH₂), 31.9 (C_q), 28.7 (3CH); MS: $m/z = 293$ [M + H]⁺;

(f) *tert-butyl N-[2-[4-[[5-(dimethylamino)-1-naphthyl]sulfonyl]piperazin-1-yl]-2-oxo-ethyl]-carbamate* (8h)

The coupling compound was obtained following the general protocol described before. The crude product was purified by flash-chromatography (DCM/MeOH 98/2) to give the titled derivative. C₂₃H₃₂N₄O₅S; yield 89%; light yellow solid; m.p. 176-177 °C; M = 476.59 g/mol; IR (ATR): $\nu = 3287$ (w), 2977 (w), 1703 (m), 1642 (s), 1339 (m), 1232 (m), 1160 (s), 1141 (s), 932 (m), 798 (s), 710 (m), 616 (m) cm⁻¹; ¹H NMR (250 MHz, CDCl₃) δ 8.58 (d, $J = 8.5$ Hz, 1H), 8.35 (d, $J = 8.7$ Hz, 1H), 8.19 (dd, $J = 7.4$ Hz, $J = 1.3$ Hz, 1H), 7.54 (dd, $J = 8.6$ Hz, $J = 7.5$ Hz, 2H), 7.19 (d, $J = 7.0$ Hz, 1H), 5.36 (as, 1H), 3.86 (d, $J = 4.5$ Hz, 2H), 3.67 – 3.63 (m, 2H), 3.44 – 3.40 (m, 2H), 3.19 – 3.15 (m, 4H), 2.88 (s, 6H), 1.40 (s, 9H); ¹³C NMR (63 MHz, CDCl₃) δ 167.0 (C_q), 155.8 (C_q), 152.0 (C_q), 132.2 (C_q), 131.3 (CH), 131.0 (CH), 130.4 (C_q), 130.2 (C_q), 128.5 (CH), 123.3 (CH), 119.4 (CH), 115.5 (CH), 79.9 (C_q), 45.6 (CH₂), 45.5 (2CH₃), 45.4 (CH₂), 44.2 (CH₂), 42.2 (CH₂), 41.6 (CH₂), 28.4 (3CH₃); MS: $m/z = 499$ [M + Na]⁺;

General method for the peptide coupling step (C)

Under inert atmosphere and at room temperature, to a solution of the previously obtained piperazine (1.85 mmol, 1 eq.) in dichloromethane (DCM, 15 ml) were successively added: N-(3-Dimethylaminopropyl)-N'-ethylcarbodiimide (EDC, 1.85 mmol, 1 eq.), 1-hydroxybenzotriazole (0.37 mmol, 0.2 eq.), the corresponding Boc-protected aminoacid (1.85 mmol, 1 eq.) and N-methylmorpholine (5.55 mmol, 3 eq.). After 12 hours of stirring, the reaction mixture was diluted by addition of 75 ml of DCM and washed with citric acid (aq soln. 10%, 3 x 50 ml) and then with brine. The organic phase was subsequently dried over magnesium sulfate, filtered and the solvent evaporated under vacuum. The crude product was purified by flash-chromatography to give the desired coupling product.

(a) *benzyl 4-[2-(tert-butoxycarbonylamino)acetyl]piperazine-1-carboxylate* (9a)

The crude derivative obtained following the general protocol described before was purified by flash-chromatography (eluent: EtOAc/PE 5/5). C₁₉H₂₇N₃O₅; yield 95%; white solid; m.p. 66-67 °C; M = 377.43 g/mol; IR (ATR): $\nu = 3329$ (w), 2971 (w), 1691 (s), 1627 (m), 1527 (m), 1420 (m), 1223 (s), 1153 (m), 756 (m), 695 (m) cm⁻¹; ¹H NMR (250 MHz, CDCl₃) δ 7.40-7.32 (m, 5H), 5.48 (as, 1H), 5.14 (s, 2H), 3.96 (d, $J = 4.4$ Hz, 2H), 3.69-3.60 (m, 2H), 3.53-3.49 (m, 4H), 3.45-3.47 (m, 2H), 1.44 (s, 9H); ¹³C NMR (63 MHz, CDCl₃) δ 167.2 (C_q), 155.9 (C_q), 155.2 (C_q), 136.4 (C_q), 128.7 (2CH), 128.4 (CH), 128.2 (2CH), 79.9 (C_q), 67.7 (CH₂), 44.3 (CH₂), 43.7 (CH₂), 43.6 (CH₂), 42.4 (CH₂), 41.8 (CH₂), 28.5 (3CH₃); MS: $m/z = 400$ [M + Na]⁺;

(b) *(4-methoxycarbonylphenyl)methyl 4-[2-(tert-butoxycarbonylamino)acetyl]piperazine-1-carboxylate* (9b)

The crude derivative obtained following the general protocol described before was purified by flash-chromatography (eluent: EtOAc/PE 5/5) C₂₁H₂₉N₃O₇; yield 80%; white solid; m.p. 90-91 °C; M = 435.47 g/mol; IR (ATR): $\nu = 2977$ (w), 1703 (s), 1651 (s), 1430 (m), 1278 (m), 1223 (m), 1160 (m), 1105 (m), 1017 (m), 756 (m) cm⁻¹; ¹H NMR (250 MHz, CDCl₃) δ 8.04 (d, $J = 8.4$ Hz, 2H), 7.41 (d, $J = 8.4$ Hz, 2H), 5.47 (as, 1H), 5.20 (s, 2H), 3.97 (d, $J = 4.5$ Hz, 2H), 3.92 (s, 3H), 3.70-3.62 (m, 2H), 3.56-3.50 (m, 4H), 3.41-3.37 (m, 2H), 1.44 (s, 9H); ¹³C NMR (63 MHz, CDCl₃) δ 167.3 (C_q), 166.8 (C_q), 154.9 (C_q), 141.4 (2C_q), 130.1 (C_q), 130.0 (2CH), 127.7 (2CH), 80.0 (C_q), 67.0 (CH₂), 52.3 (CH₃), 44.3 (CH₂), 43.7 (2CH₂), 42.4 (CH₂), 41.8 (CH₂), 28.5 (3CH₃); MS: $m/z = 458$ [M + Na]⁺;

(c) *2-naphthylmethyl 4-[2-(tert-butoxycarbonylamino)acetyl]piperazine-1-carboxylate (9c)*

The crude derivative obtained following the general protocol described before was purified by flash-chromatography (eluent: EtOAc/PE 5/5). C₂₃H₂₉N₃O₅; yield 91%; white solid; m.p. 41-42 °C; M = 427.49 g/mol; IR (ATR): $\nu = 3332$ (w), 2971 (w), 1697 (s), 1645 (s), 1460 (m), 1427 (s), 1214 (s), 1160 (m), 1117 (w), 1017 (w), 747 (w) cm⁻¹; ¹H NMR (250 MHz, CDCl₃) δ 7.87-7.82 (m, 4H), 7.53-7.45 (m, 3H), 5.48 (as, 1H), 5.31 (s, 2H), 3.96 (d, $J = 4.4$ Hz, 2H), 3.69-3.61 (m, 2H), 3.56-3.50 (4H), 3.42-3.33 (m, 2H), 1.44 (s, 9H); ¹³C NMR (63 MHz, CDCl₃) δ 167.3 (C_q), 155.9 (C_q), 155.2 (C_q), 133.8 (C_q), 133.3 (C_q), 133.3 (C_q), 128.6 (CH), 128.1 (CH), 127.9 (CH), 127.5 (CH), 126.5 (CH), 126.5 (CH), 126.0 (CH), 79.9 (C_q), 67.9 (CH₂), 44.3 (CH₂), 43.7 (2CH₂), 42.4 (CH₂), 41.8 (CH₂), 28.5 (3CH₃); MS: $m/z = 450$ [M + Na]⁺;

(d) *(6-methoxycarbonyl-2-naphthyl)methyl 4-[2-(tert-butoxycarbonylamino)acetyl]-piperazine-1-carboxylate (9d)*

The crude derivative obtained following the general protocol described before was purified by flash-chromatography (eluent: DCM/MeOH 95/5). C₂₅H₃₁N₃O₇; yield 97%; white solid; m.p. 43-44 °C; M = 485.53 g/mol; IR (ATR): $\nu = 3350$ (w), 2974 (w), 1697 (s), 1651 (s), 1460 (m), 1423 (s), 1366 (m), 1284 (m), 1220 (m-s), 1163 (m), 762 (w) cm⁻¹; ¹H NMR (250 MHz, CDCl₃) δ 8.60 (s, 1H), 8.08 (dd, $J = 8.6$ Hz, $J = 1.6$ Hz, 1H), 7.96 (d, $J = 8.5$ Hz, 1H), 7.88 (d, $J = 1$ Hz, 1H), 7.84 (s, 1H), 7.52 (dd, $J = 8.4$ Hz, $J = 1.6$ Hz, 1H), 5.47 (s, 1H), 5.33 (s, CH₂), 3.99-3.98 (m, 5H), 3.70-3.62 (m, 2H), 3.58-3.52 (m, 4H), 3.41-3.36 (m, 2H), 1.44 (s, 9H); ¹³C NMR (63 MHz, CDCl₃) δ 167.3 (C_q), 155.1 (C_q), 136.4 (C_q), 135. (C_q), 132.3 (C_q), 130.9 (CH), 130.0 (CH), 128.4 (CH), 128.0 (C_q), 127.0 (CH), 126.6 (CH), 125.9 (CH), 80.0 (C_q), 67.6 (CH₂), 52.4 (CH₃), 44.3 (CH₂), 43.8 (CH₂), 43.7 (CH₂), 42.4 (CH₂), 41.8 (CH₂), 28.5 (3CH₃); MS: $m/z = 508$ [M + Na]⁺;

(e) *tert-butyl N-[2-[4-(adamantane-1-carbonyl)piperazin-1-yl]-2-oxo-ethyl]carbamate (9e)*

The crude derivative obtained following the general protocol described before was subsequently purified by flash chromatography (eluent: PE/EtOAc 5/5) to conduct to the desired derivative. C₂₂H₃₅N₃O₄; yield 78 %; white solid; m.p. 187-188 °C; M = 405.53 g/mol; IR (ATR): $\nu = 3423$ (w), 2904 (m), 1712 (s), 1642 (s), 1615 (s), 1442 (m-s), 1399 (m), 1153 (m), 1008 (m) cm⁻¹; ¹H NMR (250 MHz, DMSO) δ 6.75 (t, $J = 5.7$ Hz, 1H), 3.78 (d, $J = 5.8$ Hz, 2H), 3.65-3.49 (m, 4H), 3.47-3.36 (m, 4H), 1.97 (as, 3H), 1.90 (as, 6H), 1.73-1.63 (m, 6H), 1.38 (s, 9H); ¹³C NMR (63 MHz, DMSO) δ 174.6 (C_q), 167.6 (C_q), 155.8 (C_q), 77.9 (C_q), 44.6 (2CH₂), 44.1 (CH₂), 41.7 (2CH₂), 40.9 (C_q), 28.4 (3CH₂), 36.0 (3CH₂), 28.2 (3CH), 27.9 (3CH₃); MS: $m/z = 428$ [M + Na]⁺;

(f) *1-adamantylmethyl 4-[2-(tert-butoxycarbonylamino)acetyl]piperazine-1-carboxylate (9f)*

The crude derivative obtained following the general protocol described before was subsequently purified by flash chromatography (eluent: PE/EtOAc 5/5). C₂₃H₃₇N₃O₅; yield 78%; white solid; m.p. 156-157 °C; M = 435.56 g/mol; IR (ATR): $\nu = 3405$ (w), 2907 (m), 1712 (s), 1678 (s), 1639 (s), 1475 (m-s), 1430 (s), 1229 (m-s), 1163 (m-s) cm⁻¹; ¹H NMR (250 MHz, CDCl₃) δ 5.48 (as, 1H), 3.97 (d, $J = 4.4$ Hz, 2H), 3.71 (s, 2H), 3.65-3.59 (m, 2H), 3.53-3.47 (m, 4H), 3.40-3.37 (m, 2H), 1.99 (as, 3H), 1.76-1.62 (m, 6H), 1.53 (d, $J = 2.5$ Hz, 6H), 1.45 (s, 9H); ¹³C NMR (63 MHz, CDCl₃) δ 167.3 (C_q), 155.9 (C_q), 155.7 (C_q), 79.9 (C_q), 75.6 (CH₂), 44.3 (CH₂), 43.7 (CH₂), 43.6 (CH₂), 42.4 (CH₂), 41.9 (CH₂), 39.5 (3CH₂), 37.1 (3CH₂), 33.6 (C_q), 28.5 (3CH₃), 28.1 (3CH); MS: $m/z = 458$ [M + Na]⁺;

(g) *2-(1-adamantyl)ethyl 4-[2-(tert-butoxycarbonylamino)acetyl]piperazine-1-carboxylate (9g)*

The crude derivative obtained following the general protocol described before was subsequently purified by flash chromatography (eluent: PE/EtOAc 5/5). C₂₄H₃₉N₃O₅; yield 78%; white solid; m.p. 167-168 °C; M = 449.58 g/mol; IR (ATR): $\nu = 3362$ (w), 2898 (m), 2844 (w), 1706 (m-s), 1687 (m-s), 1645 (s), 1463 (m), 1427 (m-s), 1217 (s), 1156 (m), 1123 (m) cm⁻¹; ¹H NMR (250 MHz, CDCl₃) δ 5.48 (as, 1H), 4.14 (t, $J = 7.3$ Hz, 2H), 3.95 (d, $J = 4.4$ Hz, 2H), 3.62-3.58 (m, 2H), 3.47-3.41 (m, 4H), 3.37-3.34 (m, 2H), 1.93 (as, 3H), 1.72-1.58 (m, 6H), 1.51 (d, $J = 2.5$ Hz, 6H), 1.43-1.39 (m, 11H); ¹³C NMR

(63 MHz, CDCl₃) δ 167.2 (C_q), 155.9 (C_q), 155.5 (C_q), 79.9 (C_q), 62.5 (CH₂), 44.3 (CH₂), 43.6 (CH₂), 43.5 (CH₂), 42.9 (CH₂), 42.7 (3CH₂), 42.4 (CH₂), 41.9 (CH₂), 37.1 (3CH₂), 31.9 (C_q), 28.7 (3CH), 28.5 (3CH₃); MS: $m/z = 472$ [M + Na]⁺;

(h) *benzyl 4-[(2R)-2-(tert-butoxycarbonylamino)propanoyl]piperazine-1-carboxylate (9i)*

The crude derivative obtained following the general protocol described before was subsequently used without any further purification. C₂₀H₂₉N₃O₅; colorless viscous oil; yield 90%; M = 391.46 g/mol; IR (ATR): $\nu = 2980$ (w), 1700 (s), 1645 (s), 1423 (m), 1217 (m), 1160 (m), 1014 (m), 765 (w), 695 (w) cm⁻¹; ¹H NMR (250 MHz, CDCl₃) δ 7.39-7.32 (m, 5H), 5.49 (d, $J = 8.1$ Hz, 1H), 5.15 (s, 2H), 4.60 (p, $J = 7.1$ Hz, 1H), 3.74-3.39 (m, 8H), 1.43 (s, 9H), 1.29 (d, $J = 6.9$ Hz, 3H); ¹³C NMR (63 MHz, CDCl₃) δ 171.6 (C_q), 155.2 (2C_q), 136.4 (C_q), 128.7 (2CH), 128.4 (CH), 128.2 (2CH), 79.9 (C_q), 67.7 (CH₂), 46.2 (CH), 45.3 (CH₂), 44.0 (CH₂), 43.7 (CH₂), 42.0 (CH₂), 28.5 (3CH₃), 19.3 (CH₃); MS: $m/z = 414$ [M + Na]⁺;

(i) *benzyl 4-[(2S)-2-(tert-butoxycarbonylamino)propanoyl]piperazine-1-carboxylate (9j)*

The crude derivative obtained following the general protocol described before was subsequently used without any further purification. C₂₀H₂₉N₃O₅; colorless viscous oil; yield 90%; M = 391.46 g/mol; IR (ATR): $\nu = 2974$ (w), 1694 (s), 1639 (s), 1433 (m), 1220 (m), 1163 (m), 1014 (m), 762 (w), 698 (w) cm⁻¹; ¹H NMR (250 MHz, CDCl₃) δ 7.40-7.30 (m, 5H), 5.47 (d, $J = 7.9$ Hz, 1H), 5.15 (s, 2H), 4.60 (p, $J = 7.1$ Hz, 1H), 3.76-3.39 (m, 8H), 1.43 (s, 9H), 1.29 (d, $J = 6.9$ Hz, 3H); ¹³C NMR (63 MHz, CDCl₃) δ 184.8 (C_q), 171.6 (C_q), 155.2 (2C_q), 136.4 (C_q), 128.7 (2CH), 128.4 (CH), 128.2 (2CH), 79.9 (C_q), 67.7 (CH₂), 46.2 (CH), 45.3 (CH₂), 44.0 (CH₂), 43.7 (CH₂), 42.0 (CH₂), 28.5 (3CH₃), 19.5 (CH₃); MS: $m/z = 414$ [M + Na]⁺;

(j) *benzyl 4-[(2R)-2-(tert-butoxycarbonylamino)-3-phenyl-propanoyl]piperazine-1-carboxylate (9k)*

The crude derivative obtained following the general protocol described before was subsequently used without any further purification. C₂₆H₃₃N₃O₅; colorless viscous oil; yield 97%; M = 467.56 g/mol; IR (ATR): $\nu = 3314$ (w), 2968 (w), 1700 (s), 1636 (s), 1423 (m), 1220 (m-s), 1163 (m-s), 1011 (w-m), 750 (w), 698 (m) cm⁻¹; ¹H NMR (250 MHz, CDCl₃) δ 7.41-7.17 (m, 10H), 5.41 (d, $J = 8.6$ Hz, 1H), 5.10 (s, 2H), 4.85-4.75 (m, 1H), 3.60-3.14 (m, 6H), 3.06-2.87 (m, 3H), 2.66-2.57 (m, 1H), 1.42 (s, 9H); ¹³C NMR (63 MHz, CDCl₃) δ 170.6 (C_q), 155.2 (C_q), 155.1 (C_q), 136.5 (C_q), 136.4 (C_q), 129.7 (2CH), 128.8 (2CH), 128.7 (2CH), 128.4 (CH), 128.2 (2CH), 127.3 (CH), 80.1 (C_q), 67.6 (CH₂), 51.1 (CH), 45.4 (CH₂), 43.4 (CH₂), 43.4 (CH₂), 41.8 (CH₂), 40.6 (CH₂), 28.5 (3CH₃); MS: $m/z = 490$ [M + Na]⁺;

(k) *benzyl 4-[(2S)-2-(tert-butoxycarbonylamino)-3-phenyl-propanoyl]piperazine-1-carboxylate (9l)*

The crude derivative obtained following the general protocol described before was subsequently used without any further purification. C₂₆H₃₃N₃O₅; colorless viscous oil; yield 97%; M = 467.56 g/mol; IR (ATR): $\nu = 2971$ (w), 1700 (s), 1633 (s), 1420 (m), 1220 (s), 1163 (s), 1011 (m), 695 (s) cm⁻¹; ¹H NMR (250 MHz, CDCl₃) δ 7.41-7.17 (m, 10H), 5.41 (d, $J = 8.5$ Hz, 1H), 5.10 (s, 2H), 4.85-4.75 (m, 1H), 3.60-3.38 (m, 3H), 3.33-3.14 (m, 3H), 3.06-2.87 (m, 3H), 2.67-2.57 (m, 1H), 1.42 (s, 9H); ¹³C NMR (63 MHz, CDCl₃) δ 170.6 (C_q), 155.2 (C_q), 155.1 (C_q), 136.5 (C_q), 136.4 (C_q), 129.7 (2CH), 128.8 (2CH), 128.7 (2CH), 128.4 (CH), 128.2 (2CH), 127.3 (CH), 80.1 (C_q), 67.6 (CH₂), 51.1 (CH), 45.4 (CH₂), 43.4 (2CH₂), 41.8 (CH₂), 40.6 (CH₂), 28.5 (3CH₃); MS: $m/z = 490$ [M + Na]⁺;

General protocol for the carbamate deprotection step (D)

The previously obtained carbamate (1.2 mmol) was dissolved in DCM (15 ml) and reacted with an excess of trifluoroacetic acid (9.6 mmol, 8 eq.) at room temperature, until the complete consumption of the starting material (generally 3h). At the end of the reaction, the mixture was diluted with DCM (35 ml) and washed with hydrogen chloride (aq. soln. 0.5 M, 3 x 50 ml). The pH of the combined aqueous layers was adjusted to 9-10 by addition of potassium carbonate (satd. soln.), then extracted with DCM (3 x 75 ml). The combined organic layers were dried over magnesium sulfate and the solvent evaporated under reduced pressure. The obtained amine was used further without any other purification.

(a) *benzyl 4-(2-aminoacetyl)piperazine-1-carboxylate (5a)*

C₁₄H₁₉N₃O₃; yield 82%; white solid; m.p. 52-53 °C; M = 277.32 g/mol; IR (ATR): $\nu = 3526$ (w), 2901 (w), 1678 (s), 1642 (s), 1420 (m-s), 1363 (w), 1281 (w), 1229 (s), 1123 (m-s) cm⁻¹; ¹H NMR (250 MHz, CDCl₃) δ 7.38-7.32 (m, 5H), 5.14 (s, 2H), 3.70-3.58 (m, 2H), 3.52-3.50 (m, 4H), 3.47 (s, 2H), 3.43-3.30 (m, 2H), 1.80 (s, 2H); ¹³C NMR (63 MHz, CDCl₃) δ 171.5 (C_q), 155.2 (C_q), 136.4 (C_q), 128.6 (2CH), 128.3 (CH), 128.1 (2CH), 67.6 (CH₂), 44.1 (CH₂), 43.7 (2CH₂), 43.4 (CH₂), 41.8 (CH₂); MS: $m/z = 278$ [M + H]⁺;

(b) *(4-methoxycarbonylphenyl)methyl 4-(2-aminoacetyl)piperazine-1-carboxylate (5b)*

C₁₆H₂₁N₃O₅; yield 88%; light-yellow solid; m.p. 94-95 °C; M = 335.36 g/mol; IR (ATR): $\nu = 3520$ (w), 3350 (w), 2904 (w), 1715 (s), 1691 (s), 1624 (m-s), 1448 (m-s), 1430 (s), 1275 (s), 1226 (s), 1111 (s), 1065 (m), 759 (s) cm⁻¹; ¹H NMR (250 MHz, CDCl₃) δ 8.03 (d, $J = 8.3$ Hz, 2H), 7.41 (d, $J = 8.3$ Hz, 2H), 5.20 (s, 2H), 3.92 (s, 3H), 3.69-3.59 (m, 2H), 3.54-3.52 (m, 4H), 3.47 (s, 2H), 3.40-3.33 (m, 2H), 1.62 (s, 2H); ¹³C NMR (63 MHz, CDCl₃) δ 171.6 (C_q), 166.8 (C_q), 155.0 (C_q), 141.5 (C_q), 130.1 (C_q), 130.0 (2CH), 127.7 (2CH), 66.9 (CH₂), 52.3 (CH₃), 44.1 (CH₂), 43.8 (2CH₂), 43.5 (CH₂), 41.8 (CH₂); MS: $m/z = 336$ [M + H]⁺;

(c) *2-naphthylmethyl 4-(2-aminoacetyl)piperazine-1-carboxylate (5c)*

C₁₈H₂₁N₃O₃; yield 61%; white solid; m.p. 109-110 °C; M = 327.38 g/mol; IR (ATR): $\nu = 3526$ (w), 3350 (w), 2907 (w), 1691 (s), 1618 (s), 1445 (m), 1433 (s), 1281 (m-s), 1220 (s), 804 (s), 735 (m) cm⁻¹; ¹H NMR (250 MHz, CDCl₃) δ 7.86-7.82 (m, 4H), 7.53-7.45 (m, 3H), 5.31 (s, 2H), 3.70-3.58 (m, 2H), 3.57-3.50 (m, 4H), 3.46 (s, 2H), 3.43-3.30 (m, 2H), 1.64 (s, 2H); ¹³C NMR (63 MHz, CDCl₃) δ 171.6 (C_q), 133.8 (C_q), 133.3 (C_q), 128.6 (CH), 128.1 (CH), 127.9 (CH), 127.4 (CH), 126.5 (CH), 126.5 (CH), 126.0 (CH), 67.9 (CH₂), 44.1 (CH₂), 43.8 (2CH₂), 43.5 (CH₂), 41.9 (CH₂); MS: $m/z = 328$ [M + H]⁺;

(d) *(6-methoxycarbonyl-2-naphthyl)methyl 4-(2-aminoacetyl)piperazine-1-carboxylate (5d)*

C₂₀H₂₃N₃O₅; yield 79%; light yellow solid; m.p. 91-92 °C; M = 385.41 g/mol; IR (ATR): $\nu = 2953$ (w), 1718 (m), 1687 (s), 1639 (m), 1423 (m), 1281 (m), 1226 (m), 1196 (m), 1126 (m), 1075 (w), 759 (w-m) cm⁻¹; ¹H NMR (250 MHz, CDCl₃) δ 8.60 (s, 1H), 8.08 (dd, $J = 8.6$ Hz, $J = 1.7$ Hz, 1H), 7.96 (d, $J = 8.5$ Hz, 1H), 7.88 (d, $J = 8.7$ Hz, 1H), 7.84 (s, 1H), 7.53 (dd, $J = 8.5$ Hz, $J = 1.6$ Hz, 1H), 5.33 (s, 2H), 3.99 (s, 3H), 3.69-3.63 (m, 2H), 3.57-3.54 (m, 4H), 3.47 (s, 2H), 3.40-3.34 (m, 2H), 1.60 (s, 2H); ¹³C NMR (63 MHz, CDCl₃) δ 171.7 (C_q), 167.3 (C_q), 155.1 (C_q), 136.5 (C_q), 135.5 (C_q), 132.3 (C_q), 130.9 (CH), 130.0 (CH), 128.4 (CH), 128.0 (C_q), 126.9 (CH), 126.6 (CH), 125.9 (CH), 67.5 (CH₂), 52.4 (CH₃), 44.1 (CH₂), 43.8 (2CH₂), 43.5 (CH₂), 41.9 (CH₂); MS: $m/z = 386$ [M + H]⁺;

(e) *1-[4-(adamantane-1-carbonyl)piperazin-1-yl]-2-amino-ethanone (5e)*

C₁₇H₂₇N₃O₂; yield 47 %; white solid; m.p. 231-132 °C; M = 305.42 g/mol; IR (ATR): $\nu = 2904$ (m), 2844 (w), 1697 (w), 1606 (s), 1414 (m), 1226 (m), 1005 (m-s) cm⁻¹; ¹H NMR (250 MHz, CDCl₃) δ 3.70-3.62 (m, 6H), 3.47 (s, 2H), 3.38-3.34 (m, 2H), 2.04 (as, 3H), 1.98-1.97 (m, 6H), 1.77-1.66 (m, 6H), 1.60 (s, 2H); ¹³C NMR (63 MHz, CDCl₃) δ 176.2 (C_q), 171.7 (C_q), 45.6 (CH₂), 44.8 (CH₂), 44.4 (CH₂), 43.5 (CH₂), 42.3 (CH₂), 41.9 (C_q), 39.2 (3CH₂), 36.7 (3CH₂), 28.5 (3CH); MS: $m/z = 306$ [M + H]⁺;

(f) *1-adamantylmethyl 4-(2-aminoacetyl)piperazine-1-carboxylate (5f)*

C₁₈H₂₉N₃O₃; yield 60%; colorless viscous oil; M = 335.44 g/mol; IR (ATR): $\nu = 3384$ (w), 2901 (m-s), 2847 (m), 1694 (s), 1627 (s), 1457 (m), 1423 (s), 1223 (s) cm⁻¹; ¹H NMR (250 MHz, CDCl₃) δ 3.70 (s, 2H), 3.66-3.59 (m, 2H), 3.53-3.48 (m, 6H), 3.41-3.35 (m, 2H), 2.04 (as, 3H), 1.76-1.61 (m, 8H), 1.53 (d, $J = 2.5$ Hz, 6H); ¹³C NMR (63 MHz, CDCl₃) δ 171.5 (C_q), 155.7 (C_q), 75.6 (CH₂), 44.1 (CH₂), 43.6 (2CH₂), 43.4 (CH₂), 41.9 (CH₂), 39.5 (3CH₂), 37.1 (3CH₂), 33.6 (C_q), 28.1 (3CH); MS: $m/z = 336$ [M + H]⁺;

(g) *2-(1-adamantyl)ethyl 4-(2-aminoacetyl)piperazine-1-carboxylate (5g)*

C₁₉H₃₁N₃O₃; yield 72%; light yellow viscous oil becoming light yellow solid on standing; m.p. 58-59 °C; M = 349.47 g/mol; IR (ATR): $\nu = 3375$ (m), 2892 (s), 2844 (m), 1697 (s), 1639 (s), 1448 (m), 1417 (s), 1375 (m), 1220 (s), 1123 (m) cm⁻¹; ¹H NMR (250 MHz, CDCl₃) δ 4.15 (t, $J = 7.2$ Hz, 2H), 3.67-3.59 (m, 2H), 3.54-3.48 (m, 6H), 3.37-3.33 (m, 2H), 1.93 (as, 3H), 1.72-1.58 (m, 6H), 1.51 (d, $J = 2.5$ Hz, 6H), 1.42 (t, $J = 7.3$ Hz, 2H); ¹³C NMR (63 MHz, CDCl₃) δ 171.1 (C_q), 155.5 (C_q), 62.4 (CH₂), 44.2 (CH₂), 43.6 (2CH₂), 43.2 (CH₂), 42.9 (CH₂), 42.7 (3CH₂), 41.9 (CH₂), 37.1 (3CH₂), 31.9 (C_q), 28.7 (3CH); MS: $m/z = 350$ [M + H]⁺;

(h) *2-amino-1-[4-[[5-(dimethylamino)-1-naphthyl]sulfonyl]piperazin-1-yl]ethanone (5h)*

C₁₈H₂₄N₄O₃S; yield 95%; yellow solid; m.p. 82-83 °C; M = 376.47 g/mol; IR (ATR): $\nu = 3441$ (w), 2932 (w), 1654 (m-s), 1636 (m-s), 1451 (m), 1342 (m), 1323 (m), 1156 (s), 1144 (s), 941 (m-s), 896 (m), 789 (s), 707 (s), 619 (m) cm⁻¹; ¹H NMR (250 MHz, CDCl₃) δ 8.58 (d, $J = 8.5$ Hz, 1H), 8.36 (d, $J = 8.7$ Hz, 1H), 8.19 (dd, $J = 7.4$ Hz, $J = 1.2$ Hz, 1H), 7.53 (dd, $J = 8.5$ Hz, $J = 7.6$ Hz, 2H), 7.18 (d, $J = 7.5$ Hz, 1H), 3.72-3.57 (m, 2H), 3.50-3.31 (m, 4H), 3.23-3.10 (m, 4H), 2.88 (s, 6H); ¹³C NMR (63 MHz, CDCl₃) δ 171.2 (C_q), 152.0 (C_q), 132.2 (C_q), 131.2 (CH), 130.9 (CH), 130.4 (C_q), 130.2 (C_q), 128.4 (CH), 123.3 (CH), 119.4 (CH), 115.5 (CH), 45.6 (CH₂), 45.5 (2CH₃), 45.5 (CH₂), 44.0 (CH₂), 43.2 (CH₂), 41.6 (CH₂); MS: $m/z = 377$ [M + H]⁺;

(i) *benzyl 4-[(2R)-2-aminopropanoyl]piperazine-1-carboxylate (5i)*

C₁₅H₂₁N₃O₃; colorless viscous oil; yield 41%; M = 291.35 g/mol; IR (ATR): ν = 3372 (w), 2922 (w), 1694 (s), 1639 (s), 1466 (w), 1417 (m-s), 1223 (s), 1117 (m), 1072 (m), 1020 (m), 729 (m), 698 (m) cm⁻¹; ¹H NMR (250 MHz, CDCl₃) δ 7.38-7.31 (m, 5H), 5.15 (s, 2H), 3.90-3.36 (m, 9H), 1.83 (s, 2H), 1.25 (d, J = 6.7 Hz, 3H); ¹³C NMR (63 MHz, CDCl₃) δ 174.9 (C_q), 155.2 (C_q), 136.4 (C_q), 128.7 (2CH), 128.4 (CH), 128.2 (2CH), 67.7 (CH₂), 47.1 (CH), 45.0 (CH₂), 44.0 (CH₂), 43.8 (CH₂), 42.0 (CH₂), 21.7 (CH₃); MS: m/z = 292 [M + H]⁺;

(j) *benzyl 4-[(2S)-2-aminopropanoyl]piperazine-1-carboxylate (5j)*

C₁₅H₂₁N₃O₃; colorless viscous oil becoming white solid on standing; m.p.: 53-54 °C; yield 35%; M = 291.35 g/mol; IR (ATR): ν = 2965 (w), 1697 (s), 1633 (s), 1420 (s), 1366 (m), 1223 (s), 1129 (m-s), 984 (m), 886 (m), 732 (m) cm⁻¹; ¹H NMR (250 MHz, CDCl₃) δ 7.40-7.31 (m, 5H), 5.14 (s, 2H), 3.85-3.36 (m, 9H), 1.81 (s, 2H), 1.25 (d, J = 6.8 Hz, 3H); ¹³C NMR (63 MHz, CDCl₃) δ 174.9 (C_q), 155.2 (C_q), 136.4 (C_q), 128.7 (2CH), 128.4 (CH), 128.2 (2CH), 67.7 (CH₂), 47.1 (CH), 45.0 (CH₂), 44.0 (CH₂), 43.8 (CH₂), 41.9 (CH₂), 21.8 (CH₃); MS: m/z = 292 [M + H]⁺;

(k) *benzyl 4-[(2R)-2-amino-3-phenyl-propanoyl]piperazine-1-carboxylate (5k)*

C₂₁H₂₅N₃O₃; light yellow viscous oil; yield 64%; M = 367.44 g/mol; IR (ATR): ν = 3365 (w), 2913 (w), 1697 (s), 1633 (s), 1427 (m), 1223 (s), 1117 (w), 747 (m), 695 (m-s); ¹H NMR (250 MHz, CDCl₃) δ 7.41-7.16 (m, 10H), 5.10 (s, 2H), 3.94 (as, 1H), 3.66-3.19 (m, 6H), 3.05-2.97 (m, 1H), 2.94-2.81 (m, 2H), 2.76-2.68 (m, 1H), 1.89 (broad s, 2H); MS: m/z = 368 [M + H]⁺;

(l) *benzyl 4-[(2S)-2-amino-3-phenyl-propanoyl]piperazine-1-carboxylate (5l)*

C₂₁H₂₅N₃O₃; light yellow viscous oil; yield 46%; M = 367.44 g/mol; IR (ATR): ν = 3372 (w), 2919 (w), 1694 (s), 1636 (s), 1423 (s), 1226 (s), 1114 (m), 741 (m), 692 (s) cm⁻¹; ¹H NMR (250 MHz, CDCl₃) δ 7.41-7.16 (m, 10H), 5.11 (CH₂), 3.69-2.83 (m, 10H), 2.74-2.67 (m, 1H), 1.76 (broad s, 2H); MS: m/z = 368 [M + H]⁺;

(m) *Synthesis of tert-butyl 4-(2-aminoacetyl)piperazine-1-carboxylate (5m)*

4-(2-bromoacetyl)piperazine-1-carboxylate (9.77 mmol, 1 eq.) in methanol (26 ml) at 0°C. The reaction vial was sealed and the mixture stirred vigorously overnight at room temperature. The solvent was subsequently evaporated, the residue dissolved in hydrogen chloride (aqueous soln., 0.1 N, 100 ml) and extracted with ethyl acetate (3 x 100 ml). The pH of the recovered aqueous layer was adjusted to 10 by addition of sodium hydroxide (aqueous soln., 1N), then the organics extracted with ethyl acetate (3 x 100 ml). The combined organic layers were dried over magnesium sulfate, filtered and the solvent evaporated under vacuum to give a light yellow crude product. Further trituration in diethyl ether conducted to the desired amine as a white solid used for the next step without additional purification. C₁₁H₂₁N₃O₃; yield 58%; white solid; m.p. 159-160 °C; M = 243.30 g/mol; IR (ATR): ν = 2974 (w), 1675 (s), 1627 (s), 1417 (m), 1360 (m), 1235 (m), 1172 (m), 1123 (m), 990 (m), 759 (m) cm⁻¹; ¹H NMR (250 MHz, CDCl₃) δ 3.71-3.41 (m, 10H), 1.46 (s, 9H); ¹³C NMR (63 MHz, CDCl₃) δ 169.5 (C_q), 154.6 (C_q), 80.5 (C_q), 50.4 (CH₂), 44.6 (2CH₂), 41.7 (2CH₂); HRMS: calcd. for C₁₁H₂₁N₃O₃ 244.1661, found. 244.1657;

Synthesis of the acrylamide derivatives (E)

Triethylamine (1.25 mmol, 5 eq.) was added to a solution of the previously obtained amine (0.25 mmol, 1 eq.) in acetonitrile (5 ml). The mixture was cooled to 0°C and acryloyl chloride (0.63 mmol, 2.5 eq.) was subsequently added under nitrogen. After 3h of stirring at 0°C, the reaction mixture was diluted with ethyl acetate (100 ml) and washed with sodium bicarbonate (satd. aq. soln., 3 x 50 ml). The recovered organic phase was dried over magnesium sulfate and then the solvent evaporated under reduced pressure to give the crude product.

(a) *benzyl 4-[2-(prop-2-enoylamino)acetyl]piperazine-1-carboxylate (3a)*

The crude derivative obtained following the general protocol described before was subsequently purified by flash chromatography (eluent: DCM/MeOH 96/4). C₁₇H₂₁N₃O₄; yield 56%; colorless viscous oil; M = 331.37 g/mol; IR (ATR): ν = 3004 (w), 1691 (s), 1636 (s), 1420 (s), 1223 (s), 744 (s) cm⁻¹; ¹H NMR (250 MHz, CDCl₃) δ 7.42-7.32 (m, 5H), 6.73 (as, 1H), 6.32 (dd, J = 17.0 Hz, J = 1.9 Hz, 1H), 6.18 (dd, J = 17.0 Hz, J = 9.8 Hz, 1H), 5.68 (dd, J = 9.8 Hz, J = 1.9 Hz, 1H), 5.15 (s, 2H), 4.15 (d, J = 4.0 Hz, 2H), 3.70-3.62 (m, 2H), 3.57-3.50 (m, 4H), 3.43-3.36 (m, 2H); ¹³C NMR (63 MHz, CDCl₃) δ 166.8 (C_q), 165.5 (C_q), 155.2 (C_q), 136.3 (C_q), 130.4 (CH), 128.7 (2CH), 128.4 (CH), 128.2 (2CH), 127.1 (CH₂), 67.8 (CH₂), 44.4 (CH₂), 43.7 (CH₂), 43.6 (CH₂), 41.9 (CH₂), 41.4 (CH₂); MS: m/z = 354 [M + Na]⁺; HRMS: calcd. for C₁₇H₂₂O₄N₃ 332.1605, found 332.1610 (1.6 ppm).

(b) *(4-methoxycarbonylphenyl)methyl 4-[2-(prop-2-enoylamino)acetyl]piperazine-1-carboxylate (3b)*

The crude derivative obtained following the general protocol described before was subsequently purified by flash chromatography (eluent: DCM/MeOH 97/3). C₁₉H₂₃N₃O₆; yield 60%; white solid; m.p. 159-160 °C; M = 389.40 g/mol; IR (ATR): $\nu = 3284$ (w), 2898 (w), 1703 (s), 1648 (s), 1427 (s), 1278 (m), 1214 (m), 1105 (m), 759 (m) cm⁻¹; ¹H NMR (250 MHz, CDCl₃) δ 8.04 (d, $J = 8.4$ Hz, 2H), 7.42 (d, $J = 8.4$ Hz, 2H), 6.68 (as, 1H), 6.33 (dd, $J = 17.0$ Hz, $J = 1.9$ Hz, 1H), 6.18 (dd, $J = 17.0$ Hz, 9.9 Hz, 1H), 5.69 (dd, $J = 9.8$ Hz, $J = 1.9$ Hz, 1H), 5.21 (s, 2H), 4.15 (d, $J = 4.1$ Hz, 2H), 3.92 (s, 3H), 3.68-3.63 (m, 2H), 3.59-3.52 (m, 4H), 3.49-3.39 (m, 2H); ¹³C NMR (63 MHz, CDCl₃) δ 166.8 (C_q), 165.5 (C_q), 154.9 (C_q), 141.4 (C_q), 130.4 (CH), 130.2 (C_q), 130.0 (2CH), 127.7 (2CH), 127.0 (CH₂), 67.0 (CH₂), 52.3 (CH₃), 44.3 (CH₂), 43.8 (CH₂), 43.7 (CH₂), 41.9 (CH₂), 41.4 (CH₂); MS: $m/z = 412$ [M + Na]⁺; HRMS: calcd. for C₁₉H₂₄O₆N₃ 390.1660, found 390.1663 (0.9 ppm).

(c) *2-naphthylmethyl 4-[2-(prop-2-enoylamino)acetyl]piperazine-1-carboxylate (3c)*

The crude derivative obtained following the general protocol described before was subsequently purified by flash chromatography (eluent: EtOAc). C₂₁H₂₃N₃O₄; yield 59%; white solid; m.p. 125-126 °C; M = 381.43 g/mol; IR (ATR): $\nu = 3332$ (w), 2925 (w), 1703 (s), 1663 (m), 1642 (s), 1621 (s), 1460 (m), 1436 (m), 1417 (m), 1220 (s), 817 (w), 750 (w) cm⁻¹; ¹H NMR (250 MHz, CDCl₃) δ 7.86-7.82 (m, 4H), 7.53-7.54 (m, 3H), 6.71 (as, 1H), 6.31 (dd, $J = 17.0$ Hz, $J = 2.0$ Hz, 1H), 6.18 (dd, $J = 17.0$ Hz, $J = 9.7$ Hz, 1H), 5.67 (dd, $J = 9.7$ Hz, $J = 2.0$ Hz, 1H), 5.32 (s, 2H), 4.14 (d, $J = 4.0$ Hz, 2H), 3.65-3.42 (m, 8H); ¹³C NMR (63 MHz, CDCl₃) δ 166.7 (C_q), 165.5 (C_q), 155.2 (C_q), 133.7 (C_q), 133.3 (C_q), 133.3 (C_q), 130.4 (CH), 128.6 (CH), 128.1 (CH), 127.9 (CH), 127.5 (CH), 127.1 (CH₂), 126.5 (CH), 126.5 (CH), 126.0 (CH), 68.0 (CH₂), 44.4 (CH₂), 43.8 (CH₂), 43.6 (CH₂), 41.9 (CH₂), 41.4 (CH₂); MS: $m/z = 404$ [M + Na]⁺; HRMS: calcd. for C₂₁H₂₄O₄N₃ 382.1761, found 382.1765 (1.0 ppm).

(d) *(6-methoxycarbonyl-2-naphthyl)methyl 4-[2-(prop-2-enoylamino)acetyl]piperazine-1-carboxylate (3d)*

The crude derivative obtained following the general protocol described before was subsequently purified by flash chromatography (eluent: EtOAc). C₂₃H₂₅N₃O₆; yield 71%; white solid; m.p. 159-160 °C; M = 439.46 g/mol; IR (ATR): $\nu = 3338$ (w), 2938 (w), 1697 (s), 1666 (s), 1648 (s), 1618 (s), 1430 (s), 1290 (s), 1217 (m), 1123 (m), 804 (s) cm⁻¹; ¹H NMR (250 MHz, CDCl₃) δ 8.60 (s, 1H), 8.08 (dd, $J = 8.6$ Hz, $J = 1.7$ Hz, 1H), 7.96 (d, $J = 8.5$ Hz, 1H), 7.88 (d, $J = 8.7$ Hz, 1H), 7.85 (s, 1H), 7.53 (dd, $J = 8.5$ Hz, $J = 1.6$ Hz, 1H), 6.70 (as, 1H), 6.32 (dd, $J = 17.0$ Hz, $J = 1.9$ Hz, 1H), 6.18 (dd, $J = 17.0$ Hz, $J = 9.8$ Hz, 1H), 5.68 (dd, $J = 9.8$ Hz, $J = 1.9$ Hz, 1H), 5.33 (s, 2H), 4.15 (d, $J = 4.1$ Hz, 2H), 3.98 (s, 3H), 3.68-3.64 (m, 2H), 3.60-3.53 (m, 4H), 3.50-3.38 (m, 2H); ¹³C NMR (63 MHz, CDCl₃) δ 167.2 (C_q), 166.8 (C_q), 165.5 (C_q), 155.1 (C_q), 136.4 (C_q), 135.5 (C_q), 132.2 (C_q), 130.9 (CH), 130.4 (CH), 130.0 (CH), 128.4 (CH), 128.0 (C_q), 127.1 (CH₂), 127.0 (CH), 126.6 (CH), 125.9 (CH), 67.6 (CH₂), 52.4 (CH₃), 44.3 (CH₂), 43.8 (CH₂), 43.7 (CH₂), 41.9 (CH₂), 41.4 (CH₂); MS: $m/z = 462$ [M + Na]⁺; HRMS: calcd. for C₂₃H₂₆O₆N₃ 440.1816, found 440.1814 (0.5 ppm).

(e) *N-[2-[4-(adamantane-1-carbonyl)piperazin-1-yl]-2-oxo-ethyl]prop-2-enamide (3e)*

The crude derivative obtained following the general protocol described before was subsequently purified by flash chromatography (eluent: EtOAc). C₂₀H₂₉N₃O₃; yield 41%; white solid; m.p. 195-196 °C; M = 359.46 g/mol; IR (ATR): $\nu = 3311$ (w), 2910 (m), 1675 (m-s), 1642 (m), 1599 (s), 1557 (m), 1417 (m), 1223 (s), 1008 (m-s), 947 (m) cm⁻¹; ¹H NMR (250 MHz, CDCl₃) δ 6.68 (as, 1H), 6.32 (dd, $J = 17.0$ Hz, $J = 1.9$ Hz, 1H), 6.18 (dd, $J = 17.0$ Hz, $J = 9.9$ Hz, 1H), 5.69 (dd, $J = 9.8$ Hz, $J = 1.9$ Hz, 1H), 4.15 (d, $J = 4.1$ Hz, 2H), 3.75-3.71 (m, 4H), 3.66-3.63 (m, 2H), 3.45-3.41 (m, 2H), 2.06 (as, 3H), 1.99-1.98 (m, 6H), 1.79-1.68 (m, 6H); ¹³C NMR (63 MHz, CDCl₃) δ 176.3 (C_q), 166.8 (C_q), 165.5 (C_q), 130.5 (CH), 127.1 (CH₂), 45.3 (CH₂), 44.9 (CH₂), 44.7 (CH₂), 42.4 (CH₂), 42.0 (C_q), 41.4 (CH₂), 39.2 (3CH₂), 36.7 (3CH₂), 28.5 (3CH); MS: $m/z = 382$ [M + Na]⁺; HRMS: calcd. for C₂₀H₃₀O₃N₃ 360.2282, found 360.2287 (1.5 ppm).

(f) *1-adamantylmethyl 4-[2-(prop-2-enoylamino)acetyl]piperazine-1-carboxylate (3f)*

The crude derivative obtained following the general protocol described before was subsequently purified by flash chromatography (eluent: EtOAc). C₂₁H₃₁N₃O₄; yield 48%; white solid; m.p. 176-177 °C; M = 389.49 g/mol; IR (ATR): $\nu = 3335$ (w), 2892 (m), 2844 (w), 1687 (s), 1672 (m), 1621 (s), 1469 (m), 1420 (s), 1251 (m), 1223 (s) cm⁻¹; ¹H NMR (250 MHz, CDCl₃) δ 6.70 (as, 1H), 6.32 (dd, $J = 17.0$ Hz, $J = 1.9$ Hz, 1H), 6.18 (dd, $J = 17.0$ Hz, $J = 9.8$ Hz, 1H), 5.68 (dd, $J = 9.8$ Hz, $J = 1.9$ Hz, 1H), 4.16 (d, $J = 4.1$ Hz, 2H), 3.71 (s, 2H), 3.68-3.62 (m, 2H), 3.56-3.49 (m, 4H), 3.46-3.42 (m, 2H), 1.99 (as, 3H), 1.77-1.62 (m, 6H), 1.53 (d, $J = 2.5$ Hz, 6H); ¹³C NMR (63 MHz, CDCl₃) δ 166.8 (C_q), 165.5 (C_q),

155.7 (C_q), 130.5 (CH), 127.1 (CH₂), 75.7 (CH₂), 44.4 (CH₂), 43.7 (CH₂), 43.5 (CH₂), 42.0 (CH₂), 41.5 (CH₂), 39.5 (3CH₂), 37.1 (3CH₂), 33.6 (C_q), 28.1 (3CH); MS: *m/z* = 412 [M + Na]⁺; HRMS: calcd. for C₂₁H₃₂O₄N₃ 390.2387, found 390.2391 (0.9 ppm).

(g) *2-(1-adamantyl)ethyl 4-[2-(prop-2-enoylamino)acetyl]piperazine-1-carboxylate (3g)*

The crude derivative obtained following the general protocol described before was subsequently purified by flash chromatography (eluent: EtOAc). C₂₂H₃₃N₃O₄; yield 54 %; white solid; m.p. 155-156 °C; M = 403.52 g/mol; IR (ATR): ν = 3317 (w), 2901 (m-s), 2847 (w), 1684 (s), 1624 (s), 1469 (m), 1427 (s), 1223 (s) cm⁻¹; ¹H NMR (250 MHz, CDCl₃) δ 6.73 (as, 1H), 6.32 (dd, *J* = 17.0 Hz, *J* = 1.9 Hz, 1H), 6.18 (dd, *J* = 17.0 Hz, *J* = 9.8 Hz, 1H), 5.68 (dd, *J* = 9.8 Hz, *J* = 1.9 Hz, 1H), 4.19-4.13 (m, 4H), 3.65-3.61 (m, 2H), 3.50-3.46 (m, 4H), 3.43-3.39 (m, 2H), 1.94 (as, 3H), 1.73-1.59 (m, 6H), 1.52 (d, *J* = 2.4 Hz, 6H), 1.43 (t, *J* = 7.3 Hz, 2H); ¹³C NMR (63 MHz, CDCl₃) δ 166.7 (C_q), 165.5 (C_q), 155.5 (C_q), 130.5 (CH), 127.0 (CH₂), 62.5 (CH₂), 44.4 (CH₂), 43.6 (CH₂), 43.5 (CH₂), 42.9 (CH₂), 42.7 (3CH₂), 42.0 (CH₂), 41.4 (CH₂), 37.1 (3CH₂), 31.9 (C_q), 28.7 (3CH); MS: *m/z* = 426 [M + Na]⁺; HRMS: calcd. for C₂₂H₃₄O₄N₃ 404.2544, found 404.2547 (0.8 ppm).

(h) *N-[2-[4-[[5-(dimethylamino)-1-naphthyl]sulfonyl]piperazin-1-yl]-2-oxo-ethyl]prop-2-enamide (3h)*

The crude derivative obtained following the general protocol described before was subsequently purified by flash chromatography (eluent: EtOAc). C₁₈H₂₄N₄O₃S; yield 39%; light yellow solid; m.p. 185-186 °C; M = 430.52 g/mol; IR (ATR): ν = 2935 (w), 1651 (s), 1454 (m), 1436 (m), 1311 (m), 1141 (s), 941 (s), 789 (s), 704 (m) cm⁻¹; ¹H NMR (250 MHz, CDCl₃) δ 8.59 (d, *J* = 8.5 Hz, 1H), 8.35 (d, *J* = 8.7 Hz, 1H), 8.21 (dd, *J* = 7.4 Hz, *J* = 1.2 Hz, 1H), 7.55 (dd, *J* = 8.5 Hz, *J* = 7.5 Hz, 2H), 7.19 (d, *J* = 7.5 Hz, 1H), 6.58 (as, 1H), 6.28 (dd, *J* = 17.0 Hz, *J* = 1.8 Hz, 1H), 6.13 (dd, *J* = 17.0 Hz, *J* = 9.9 Hz, 1H), 5.65 (dd, *J* = 9.9 Hz, *J* = 1.8 Hz, 1H), 4.05 (d, *J* = 4.1 Hz, 2H), 3.68 (t, *J* = 5.1 Hz, 2H), 3.47 (t, *J* = 5.0 Hz, 2H), 3.21 (dt, *J* = 9.8 Hz, *J* = 4.7 Hz, 4H), 2.89 (s, 6H); ¹³C NMR (63 MHz, CDCl₃) δ 166.5 (C_q), 165.4 (C_q), 152.1 (C_q), 132.2 (C_q), 131.4 (CH), 131.0 (CH), 130.4 (C_q), 130.3 (CH), 130.3 (C_q), 128.5 (CH), 127.1 (CH₂), 123.3 (CH), 119.3 (CH), 115.6 (CH), 45.6 (CH₂), 45.6 (2CH₃), 45.4 (CH₂), 44.3 (CH₂), 41.8 (CH₂), 41.3 (CH₂); MS: *m/z* = 453 [M + Na]⁺; HRMS: calcd. for C₂₁H₂₇O₄N₄S 431.1748, found 431.1751 (0.8 ppm).

(i) *benzyl 4-[(2R)-2-(prop-2-enoylamino)propanoyl]piperazine-1-carboxylate (3i)*

The crude derivative obtained following the general protocol described before was subsequently purified by flash chromatography (eluent: EtOAc). C₁₈H₂₃N₃O₄; colorless viscous oil; yield 73%; M = 345.39 g/mol; IR (ATR): ν = 3290 (w), 2929 (w), 1697 (s), 1621 (s), 1423 (s), 1220 (s), 1020 (m), 759 (m), 695 (m) cm⁻¹; ¹H NMR (250 MHz, CDCl₃) δ 7.41-7.32 (m, 5H), 6.71 (d, *J* = 7.1 Hz, 1H), 6.30 (dd, *J* = 17.0 Hz, *J* = 1.7 Hz, 1H), 6.12 (dd, *J* = 17.0 Hz, *J* = 10.0 Hz, 1H), 5.66 (dd, *J* = 10.0 Hz, *J* = 1.7 Hz, 1H), 5.15 (s, 2H), 4.96 (p, *J* = 6.9 Hz, 1H), 3.79-3.40 (m, 8H), 1.36 (d, *J* = 6.8 Hz, 3H); ¹³C NMR (63 MHz, CDCl₃) δ 171.2 (C_q), 164.7 (C_q), 155.2 (C_q), 136.4 (C_q), 130.7 (CH), 128.7 (2CH), 128.4 (CH), 128.2 (2CH), 127.0 (CH₂), 67.7 (CH₂), 45.4 (CH₂), 45.3 (CH), 44.0 (CH₂), 43.7 (CH₂), 42.1 (CH₂), 19.2 (CH₃); MS: *m/z* = 368 [M + Na]⁺; HRMS: calcd. for C₁₈H₂₄O₄N₃ 346.1761, found 346.1767 (1.6 ppm).

(j) *benzyl 4-[(2S)-2-(prop-2-enoylamino)propanoyl]piperazine-1-carboxylate (3j)*

The crude derivative obtained following the general protocol described before was subsequently purified by flash chromatography (eluent: EtOAc). C₁₈H₂₃N₃O₄; white solid; m.p. 121-122 °C; yield 72 %; M = 345.39 g/mol; IR (ATR): ν = 3271 (w), 2929 (w), 1697 (s), 1624 (s), 1423 (s), 1223 (s), 1117 (w-m), 1011 (m), 759 (m), 695 (m) cm⁻¹; ¹H NMR (250 MHz, CDCl₃) δ 7.40-7.35 (m, 5H), 6.71 (d, *J* = 7.1 Hz, 1H), 6.29 (dd, *J* = 17.0 Hz, *J* = 1.6 Hz, 1H), 6.12 (dd, *J* = 17.0 Hz, *J* = 10.0 Hz, 1H), 5.66 (dd, *J* = 10.0 Hz, *J* = 1.6 Hz, 1H), 5.15 (d, 2H), 4.96 (p, *J* = 7.0 Hz, 1H), 3.81-3.40 (m, 8H), 1.35 (d, *J* = 6.8 Hz, 3H); ¹³C NMR (63 MHz, CDCl₃) δ 171.1 (C_q), 164.6 (C_q), 155.1 (C_q), 136.3 (C_q), 130.7 (CH), 128.7 (2CH), 128.4 (CH), 128.2 (2CH), 127.0 (CH₂), 67.7 (CH₂), 45.3 (CH₂), 45.2 (CH), 43.9 (CH₂), 43.6 (CH₂), 42.0 (CH₂), 19.2 (CH₃); MS: *m/z* = 368 [M + Na]⁺; HRMS: calcd. for C₁₈H₂₄O₄N₃ 346.1761, found 346.1767 (1.6 ppm).

(k) *benzyl 4-[(2R)-3-phenyl-2-(prop-2-enoylamino)propanoyl]piperazine-1-carboxylate (3k)*

The crude derivative obtained following the general protocol described before was subsequently purified by flash chromatography (eluent: EtOAc). C₂₄H₂₇N₃O₄; colorless viscous oil; yield 79 %; M = 421.49 g/mol; IR (ATR): ν = 3284 (w), 2929 (w), 1700 (s), 1621 (s), 1423 (s), 1220 (s), 729 (m), 692 (m) cm⁻¹; ¹H NMR (250 MHz, CDCl₃) δ 7.41-7.18 (m, 10H), 6.77 (d, *J* = 8.0 Hz, 1H), 6.31 (dd, *J* =

17.0 Hz, $J = 1.6$ Hz, 1H), 6.12 (dd, $J = 17.0$ Hz, $J = 10.1$ Hz, 1H), 5.67 (dd, $J = 10.1$ Hz, $J = 1.6$ Hz, 1H), 5.20 (td, $J = 9.0$ Hz, $J = 5.3$ Hz, 1H), 5.10 (s, 2H), 3.59-2.92 (m, 9H), 2.68-2.58 (m, 1H); ^{13}C NMR (63 MHz, CDCl_3) δ 170.2 (C_q), 164.9 (C_q), 155.0 (C_q), 136.4 (C_q), 136.0 (C_q), 130.5 (CH), 129.6 (2CH), 128.8 (2CH), 128.7 (2CH), 128.3 (CH), 128.1 (2CH), 127.5 (CH), 127.3 (CH_2), 67.6 (CH_2), 49.9 (CH), 45.4 (CH_2), 43.3 (2 CH_2), 41.8 (CH_2), 40.1 (CH_2); MS: $m/z = 444$ [$\text{M} + \text{Na}$] $^+$; HRMS: calcd. for $\text{C}_{24}\text{H}_{28}\text{O}_4\text{N}_3$ 422.2074, found 422.2077 (0.6 ppm).

(l) *benzyl 4-[(2S)-3-phenyl-2-(prop-2-enoylamino)propanoyl]piperazine-1-carboxylate (3l)*

The crude derivative obtained following the general protocol described before was subsequently purified by flash chromatography (eluent: EtOAc). $\text{C}_{24}\text{H}_{27}\text{N}_3\text{O}_4$; colorless viscous oil; yield 65 %; $M = 421.49$ g/mol; IR (ATR): $\nu = 3287$ (w), 2925 (w), 1697 (s), 1621 (s), 1423 (s), 1220 (s), 1123 (w), 729 (m), 695 (m) cm^{-1} ; ^1H NMR (250 MHz, CDCl_3) δ 7.41-7.18 (m, 10H), 6.77 (d, $J = 8.0$ Hz, 1H), 6.31 (dd, $J = 17.0$ Hz, $J = 1.6$ Hz, 1H), 6.12 (dd, $J = 17.0$ Hz, $J = 10.1$ Hz, 1H), 5.67 (dd, $J = 10.1$ Hz, $J = 1.6$ Hz, 1H), 5.23 (td, $J = 9.0$ Hz, $J = 5.3$ Hz, 1H), 5.10 (s, 2H), 3.64-2.92 (m, 9H), 2.68-2.58 (m, 1H); ^{13}C NMR (63 MHz, CDCl_3) δ 170.2 (C_q), 164.9 (C_q), 155.0 (C_q), 136.4 (C_q), 136.0 (C_q), 130.5 (CH), 129.6 (2CH), 128.8 (2CH), 128.7 (2CH), 128.3 (CH), 128.1 (2CH), 127.5 (CH), 127.3 (CH_2), 67.6 (CH_2), 49.9 (CH), 45.4 (CH_2), 43.3 (2 CH_2), 41.8 (CH_2), 40.1 (CH_2); MS: $m/z = 444$ [$\text{M} + \text{Na}$] $^+$; HRMS: calcd. for $\text{C}_{24}\text{H}_{28}\text{O}_4\text{N}_3$ 422.2074, found 422.2077 (0.6 ppm).

General method for the acetylation step (F)

Under inert atmosphere and at -78°C , the corresponding acetylation reagent, bromoacetyl bromide or chloroacetyl chloride, (1.65 mmol, 1.1 eq.) was slowly added to a solution of the corresponding amine (1.5 mmol, 1 eq.) and TEA (7.5 mmol, 5 eq.) in DCM (15 ml). The reaction mixture was stirred at -78°C for 3h, diluted with DCM (75 ml) and washed with hydrogen chloride (aqueous soln. 0.2 M, 3 x 50 ml). The recovered organic layer was dried over magnesium sulfate and the solvent was evaporated under vacuum to give the crude product.

(a) *benzyl 4-[2-[(2-bromoacetyl)amino]acetyl]piperazine-1-carboxylate (6a)*

The crude derivative obtained using the general protocol described previously was further triturated in diethyl ether to give the desired acetylated compound as a solid. $\text{C}_{16}\text{H}_{20}\text{BrN}_3\text{O}_4$; yield 84%; white solid; m.p. 132-133 $^\circ\text{C}$; $M = 398.25$ g/mol; IR (ATR): $\nu = 3344$ (w), 2904 (w), 1681 (s), 1621 (s), 1478 (m), 1423 (s), 1263 (m-s), 1223 (s), 750 (m) cm^{-1} ; ^1H NMR (250 MHz, CDCl_3) δ 7.51 (as, 1H), 7.38-7.32 (m, 5H), 5.15 (s, 2H), 4.08 (d, $J = 4.1$ Hz, 2H), 3.89 (s, 2H), 3.70-3.62 (m, 2H), 3.57-3.48 (m, 4H), 3.46-3.32 (m, 2H); ^{13}C NMR (63 MHz, CDCl_3) δ 166.1 (C_q), 165.8 (C_q), 155.1 (C_q), 136.3 (C_q), 128.7 (2CH), 128.4 (CH), 128.2 (2CH), 67.8 (CH_2), 44.3 (CH_2), 43.7 (CH_2), 43.6 (CH_2), 42.0 (CH_2), 41.9 (CH_2), 28.6 (CH_2); MS: $m/z = 420$ [$\text{M} + \text{Na}$] $^+$ for ^{79}Br and 422 [$\text{M} + \text{Na}$] for ^{81}Br ; HRMS: calcd. for $\text{C}_{16}\text{H}_{21}\text{O}_4\text{N}_3\text{Br}$ 398.0710, found 398.0713 (0.8 ppm).

(b) *(4-methoxycarbonylphenyl)methyl 4-[2-[(2-bromoacetyl)amino]acetyl]piperazine-1-carboxylate (6b)*

The crude derivative obtained using the general protocol described previously was further triturated in diethyl ether to give the desired acetylated compound as a solid. $\text{C}_{18}\text{H}_{22}\text{BrN}_3\text{O}_6$; yield 95%; light beige solid, m.p. 134-135 $^\circ\text{C}$; $M = 456.29$ g/mol; IR (ATR): $\nu = 3284$ (m), 2898 (w), 1715 (m), 1697 (s), 1675 (m), 1642 (s), 1433 (m), 1278 (m), 1223 (s), 1102 (m), 1026 (m), 759 (s) cm^{-1} ; ^1H NMR (250 MHz, CDCl_3) δ 8.04 (d, $J = 8.4$ Hz, 2H), 7.51 (as, 1H), 7.41 (d, $J = 8.4$ Hz, 2H), 5.20 (s, 2H), 4.09 (d, $J = 4.1$ Hz, 2H), 3.92 (s, 3H), 3.90 (s, 2H), 3.68-3.62 (m, 2H), 3.59-3.52 (m, 4H), 3.46-3.36 (m, 2H); ^{13}C NMR (63 MHz, CDCl_3) δ 166.2 (C_q), 165.9 (C_q), 154.9 (C_q), 141.3 (C_q), 130.2 (C_q), 130.1 (2CH), 127.8 (2CH), 67.0 (CH_2), 52.3 (CH_3), 44.3 (CH_2), 43.8 (CH_2), 43.7 (CH_2), 41.9 (2 CH_2), 28.6 (CH_2); MS: $m/z = 480$ [$\text{M} + \text{Na}$] $^+$; HRMS: calcd. for $\text{C}_{18}\text{H}_{23}\text{O}_6\text{N}_3\text{Br}$ 456.0765, found 456.0768 (0.7 ppm).

(c) *2-naphthylmethyl 4-[2-[(2-bromoacetyl)amino]acetyl]piperazine-1-carboxylate (6c)*

The crude derivative obtained using the general protocol described previously was further triturated in diethyl ether to give the desired acetylated compound as a solid. $\text{C}_{20}\text{H}_{22}\text{BrN}_3\text{O}_4$; yield 77%; light beige solid; m.p. 133-134 $^\circ\text{C}$; $M = 448.31$ g/mol; IR (ATR): $\nu = 3338$ (w), 2922 (w), 1687 (s), 1621 (s), 1478 (w), 1423 (s), 1217 (s), 826 (w), 765 (m) cm^{-1} ; ^1H NMR (250 MHz, CDCl_3) δ 7.87-7.83 (m, 4H), 7.52-7.45 (m, 4H), 5.31 (s, 2H), 4.08 (d, $J = 4.0$ Hz, 2H), 3.90 (s, 2H), 3.66-3.40 (m, 8H); ^{13}C NMR (63 MHz, CDCl_3) δ 166.1 (C_q), 165.8 (C_q), 155.2 (C_q), 133.7 (C_q), 133.3 (2 C_q), 128.6 (CH), 128.1 (CH), 127.9 (CH), 127.5 (CH), 126.5 (CH), 126.5 (CH), 126.0 (CH), 68.0 (CH_2), 44.3 (CH_2), 43.7 (CH_2), 43.6 (CH_2), 42.0 (CH_2), 41.9 (CH_2), 28.6 (CH_2); MS: $m/z = 472$ [$\text{M} + \text{Na}$] $^+$; HRMS: calcd. for $\text{C}_{20}\text{H}_{23}\text{O}_4\text{N}_3\text{Br}$ 448.0866, found 448.0867 (0.1 ppm).

(d) (6-methoxycarbonyl-2-naphthyl)methyl 4-[2-[(2-bromoacetyl)amino]acetyl]piperazine-1-carboxylate (6d)

The crude derivative obtained using the general protocol described previously was further triturated in diethyl ether to give the desired acetylated compound as a solid. C₂₂H₂₄BrN₃O₆; yield 80%; white solid; m.p. 136-137 °C; M = 506.35 g/mol; IR (ATR): ν = 3326 (w), 2916 (w), 1706 (s), 1621 (s), 1423 (s), 1214 (m), 1202 (m), 814 (m) cm⁻¹; ¹H NMR (250 MHz, CDCl₃) δ 8.61 (s, 1H), 8.08 (dd, *J* = 8.6 Hz, *J* = 1.6 Hz, 1H), 7.96 (d, *J* = 8.5 Hz, 1H), 7.88 (d, *J* = 8.7 Hz, 1H), 7.85 (s, 1H), 7.53 (dd, *J* = 8.5 Hz, 1H), 7.53-7.47 (m, 1H), 5.33 (s, 2H), 4.09 (d, *J* = 4.1 Hz, 2H), 3.98 (s, 3H), 3.90 (s, 2H), 3.69-3.65 (m, 2H), 3.60-3.54 (m, 4H), 3.43-3.36 (m, 2H); ¹³C NMR (63 MHz, CDCl₃) δ 167.2 (C_q), 166.1 (C_q), 165.9 (C_q), 155.1 (C_q), 136.4 (C_q), 135.5 (C_q), 132.3 (C_q), 130.9 (CH), 130.0 (CH), 128.4 (CH), 128.0 (C_q), 127.0 (CH), 126.6 (CH), 125.9 (CH), 67.6 (CH₂), 52.4 (CH₃), 44.3 (CH₂), 43.7 (CH₂), 43.7 (CH₂), 42.0 (CH₂), 41.9 (CH₂), 28.6 (CH₂); MS: *m/z* = 528 [M + Na]⁺ for ⁷⁹Br and 530 [M + Na]⁺ for ⁸¹Br; HRMS: calcd. for C₂₂H₂₅O₆N₃Br 506.0921, found 506.0918 (0.6 ppm).

(e) 2-N-[2-[4-(adamantane-1-carbonyl)piperazin-1-yl]-2-oxo-ethyl]-2-bromo-acetamide (6e)

The crude derivative obtained using the general protocol described previously was further triturated in diethyl ether to give the desired acetylated compound as a solid. C₁₉H₂₈BrN₃O₃; yield 86%; white solid; m.p. 203-204 °C; M = 426.35 g/mol; IR (ATR): ν = 3305 (m-s), 2932 (m-s), 1681 (s), 1645 (s), 1590 (s), 1563 (m), 1420 (s), 1223 (s), 1205 (m-s), 1014 (s) cm⁻¹; ¹H NMR (250 MHz, CDCl₃) δ 7.50 (as, 1H), 4.09 (d, *J* = 4.1 Hz, 2H), 3.90 (s, 2H), 3.74-3.70 (m, 4H), 3.66-3.63 (m, 2H), 3.43-3.39 (m, 2H), 2.06 (as, 3H), 1.99-1.97 (m, 6H), 1.79-1.67 (m, 6H); ¹³C NMR (63 MHz, CDCl₃) δ 176.3 (C_q), 166.2 (C_q), 165.8 (C_q), 45.4 (CH₂), 44.8 (CH₂), 44.7 (CH₂), 42.4 (CH₂), 41.9 (CH₂), 41.9 (C_q), 39.2 (3CH₂), 36.7 (3CH₂), 28.6 (CH₂), 28.5 (3CH); MS: *m/z* = 448 [M + Na]⁺ for ⁷⁹Br and 450 [M + Na] for ⁸¹Br; HRMS: calcd. for C₁₉H₂₉O₃N₃Br 426.1387, found 426.1389 (0.5 ppm).

(f) 1-adamantylmethyl 4-[2-[(2-bromoacetyl)amino]acetyl]piperazine-1-carboxylate (6f)

The crude derivative obtained using the general protocol described previously was further triturated in diethyl ether to give the desired acetylated compound as a solid. C₂₀H₃₀BrN₃O₄; yield 76%; light beige solid; m.p. 210-211 °C; M = 456.37 g/mol; IR (ATR): ν = 3335 (w), 2898 (m-s), 2847 (w), 1678 (s), 1621 (s), 1466 (m), 1430 (m), 1247 (m), 1220 (s), 1205 (m) cm⁻¹; ¹H NMR (250 MHz, CDCl₃) δ 7.52 (s, 1H), 4.09 (d, *J* = 4.0 Hz, 2H), 3.90 (s, 2H), 3.71 (s, 2H), 3.68-3.64 (m, 2H), 3.56-3.50 (m, 4H), 3.45-3.41 (m, 2H), 1.99 (as, 3H), 1.76-1.61 (m, 6H), 1.53 (d, *J* = 2.9 Hz, 6H); ¹³C NMR (63 MHz, CDCl₃) δ 166.2 (C_q), 165.8 (C_q), 155.6 (C_q), 75.7 (CH₂), 44.4 (CH₂), 43.7 (CH₂), 43.5 (CH₂), 42.0 (CH₂), 42.0 (CH₂), 39.5 (3CH₂), 37.1 (3CH₂), 33.6 (C_q), 28.6 (CH₂), 28.1 (3CH); MS: *m/z* = 480 [M + Na]⁺; HRMS: calcd. for C₂₀H₃₁O₄N₃Br 456.1492, found 456.1491 (0.3 ppm).

(g) 2-(1-adamantyl)ethyl 4-[2-[(2-bromoacetyl)amino]acetyl]piperazine-1-carboxylate (6g)

The crude derivative obtained using the general protocol described previously was further triturated in diethyl ether to give the desired acetylated compound as a solid. C₂₁H₃₂BrN₃O₄; yield 39 %; light beige solid; m.p. 111-112 °C; M = 470.40 g/mol; IR (ATR): ν = 3335 (w), 2895 (m-s), 2844 (m), 1700 (s), 1612 (s), 1427 (s), 1284 (w), 1226 (s) cm⁻¹; ¹H NMR (250 MHz, CDCl₃) δ 7.51 (as, 1H), 4.16 (t, *J* = 7.3 Hz, 2H), 4.09 (d, *J* = 4.0 Hz, 2H), 3.90 (s, 2H), 3.66-3.59 (m, 2H), 3.57-3.45 (m, 4H), 3.41-3.34 (m, 2H), 1.95 (as, 3H), 1.73-1.59 (m, 6H), 1.52 (as, 6H), 1.43 (t, *J* = 7.3 Hz, 2H); ¹³C NMR (63 MHz, CDCl₃) δ 166.1 (C_q), 165.8 (C_q), 155.5 (C_q), 62.6 (CH₂), 44.4 (CH₂), 43.6 (CH₂), 43.5 (CH₂), 42.9 (CH₂), 42.7 (3CH₂), 42.1 (CH₂), 42.0 (CH₂), 37.1 (3CH₂), 31.9 (C_q), 28.7 (3CH), 28.6 (CH₂); MS: *m/z* = 494 [M + Na]⁺; HRMS: calcd. for C₂₁H₃₃O₄N₃Br 470.1649, found 470.1646 (0.6 ppm).

(h) 22-bromo-N-[2-[4-[[5-(dimethylamino)-1-naphthyl]sulfonyl]piperazin-1-yl]-2-oxo-ethyl]-acetamide (6h)

The crude compound obtained after the aqueous work-up (sodium bicarbonate satd. soln. / DCM extraction) was triturated in diethyl ether to conduct to the desired derivative. C₂₀H₂₅BrN₄O₄S; yield 79 %; yellow solid; m.p. 173-174 °C; M = 497.41 g/mol; IR (ATR): ν = 3381 (w), 2925 (w), 1651 (s), 1451 (m), 1339 (m), 1144 (s), 941 (s), 792 (s), 707 (s) cm⁻¹; ¹H NMR (250 MHz, CDCl₃) δ 8.64 (d, *J* = 8.1 Hz, 1H), 8.38 (d, *J* = 8.6 Hz, 1H), 8.21 (dd, *J* = 7.4 Hz, *J* = 1.2 Hz, 1H), 7.60-7.53 (m, 2H), 7.39 (as, 1H), 7.22 (d, *J* = 7.4 Hz, 1H), 3.99 (d, *J* = 4.1 Hz, 2H), 3.85 (s, 2H), 3.70-3.66 (m, 2H), 3.47-3.43 (m, 2H), 3.21 (dd, *J* = 10.1 Hz, *J* = 5.2 Hz, 4H), 2.92 (s, 6H); ¹³C NMR (63 MHz, CDCl₃) δ 165.9 (C_q), 165.9 (C_q), 132.1 (C_q), 131.2 (CH), 131.0 (CH), 130.3 (C_q), 129.9 (C_q), 128.4 (CH), 123.5 (CH), 119.7 (CH), 115.7 (CH), 45.6 (2CH₃), 45.5 (CH₂), 45.3 (CH₂), 44.2 (CH₂), 41.7 (2CH₂), 28.5 (CH₂);

(i) benzyl 4-[(2R)-2-[(2-bromoacetyl)amino]propanoyl]piperazine-1-carboxylate (6i)

The crude derivative obtained using the general protocol described previously was further triturated in diethyl ether to give the desired acetylated compound as a solid. C₁₇H₂₂BrN₃O₄; light beige solid; m.p. 104-105 °C; yield 78 %; M = 412.28 g/mol; IR (ATR): $\nu = 3302$ (m), 2929 (w), 1700 (s), 1678 (s), 1615 (s), 1475 (m), 1427 (s), 1257 (m), 1226 (s), 1120 (m), 741 (m) cm⁻¹; ¹H NMR (250 MHz, CDCl₃) δ 7.53 (d, $J = 6.9$ Hz, 1H), 7.40-7.30 (m, 5H), 5.15 (s, 2H), 4.83 (p, $J = 6.9$ Hz, 1H), 3.85 (ad, $J = 1.3$ Hz, 2H), 3.70-3.35 (m, 8H), 1.35 (d, $J = 6.8$ Hz, 3H); ¹³C NMR (63 MHz, CDCl₃) δ 170.5 (C_q), 165.0 (C_q), 155.1 (C_q), 136.3 (C_q), 128.7 (2CH), 128.4 (CH), 128.2 (2CH), 67.7 (CH₂), 46.1 (CH), 45.3 (CH₂), 43.9 (CH₂), 43.6 (CH₂), 42.1 (CH₂), 28.8 (CH₂), 18.9 (CH₃); MS: $m/z = 434$ [M + Na]⁺ for ⁷⁹Br and 436 [M + Na]⁺ for ⁸¹Br; HRMS: calcd. for C₁₇H₂₃O₄N₃Br 412.0866, found 412.0870 (0.9 ppm).

(j) *benzyl 4-[(2S)-2-[(2-bromoacetyl)amino]propanoyl]piperazine-1-carboxylate (6j)*

The crude derivative obtained using the general protocol described previously was further triturated in diethyl ether to give the desired acetylated compound as a solid. C₁₇H₂₂BrN₃O₄; light beige solid; m.p. 104-105 °C; yield 83 %; M = 412.28 g/mol; IR (ATR): $\nu = 3305$ (m), 2929 (w), 1697 (s), 1675 (s), 1612 (s), 1484 (m), 1427 (s), 1254 (m), 1226 (s), 1120 (m), 741 (m) cm⁻¹; ¹H NMR (250 MHz, CDCl₃) δ 7.55 (d, $J = 4.7$ Hz, 1H), 7.47-7.28 (m, 5H), 5.14 (s, 2H), 4.92-4.74 (m, 1H), 3.85 (s, 2H), 3.79-3.33 (m, 8H), 1.34 (m, $J = 6.1$ Hz, 3H); ¹³C NMR (63 MHz, CDCl₃) δ 170.5 (C_q), 165.0 (C_q), 155.1 (C_q), 136.3 (C_q), 128.7 (2CH), 128.4 (CH), 128.2 (2CH), 67.7 (CH₂), 46.0 (CH), 45.3 (CH₂), 43.9 (CH₂), 43.6 (CH₂), 42.1 (CH₂), 28.8 (CH₂), 18.9 (CH₃); MS: $m/z = 434$ [M + Na]⁺ for ⁷⁹Br and 436 [M + Na]⁺ for ⁸¹Br; HRMS: calcd. for C₁₇H₂₃O₄N₃Br 412.0866, found 412.0871 (1.1 ppm).

(k) *benzyl 4-[(2R)-2-[(2-bromoacetyl)amino]-3-phenyl-propanoyl]piperazine-1-carboxylate (6k)*

The crude derivative obtained using the protocol described previously was subsequently used without any further purification. C₂₃H₂₆BrN₃O₄; colorless viscous oil; yield 85%; M = 488.37 g/mol; IR (ATR): $\nu = 3293$ (w), 3026 (w), 1694 (s), 1621 (s), 1420 (s), 1226 (s), 1120 (w), 750 (w), 732 (w), 695 (m-s) cm⁻¹; ¹H NMR (250 MHz, CDCl₃) δ 7.46 (d, $J = 8.0$ Hz, 1H), 7.41-7.17 (m, 10H), 5.14-5.05 (m, 3H), 3.85 (s, 2H), 3.66-3.39 (m, 3H), 3.34-3.15 (m, 3H), 3.11-2.88 (m, 3H), 2.70-2.60 (m, 1H); ¹³C NMR (63 MHz, CDCl₃) δ 169.8 (C_q), 165.5 (C_q), 155.0 (C_q), 136.3 (C_q), 135.6 (C_q), 129.7 (2CH), 128.9 (2CH), 128.7 (2CH), 128.4 (CH), 128.2 (2CH), 127.7 (CH), 67.7 (CH₂), 50.6 (CH), 45.5 (CH₂), 43.3 (2CH₂), 42.0 (CH₂), 39.9 (CH₂), 28.7 (CH₂); MS: $m/z = 510$ [M + Na]⁺ for ⁷⁹Br and 512 [M + Na]⁺ for ⁸¹Br; HRMS: calcd. for C₂₃H₂₇O₄N₃Br 488.1179, found 488.1178 (0.3 ppm).

(l) *benzyl 4-[(2S)-2-[(2-bromoacetyl)amino]-3-phenyl-propanoyl]piperazine-1-carboxylate (6l)*

The crude derivative obtained using the general protocol described previously was subsequently used without any further purification. C₂₃H₂₆BrN₃O₄; colorless viscous oil; yield 98 %; M = 488.37 g/mol; IR (ATR): $\nu = 3274$ (w), 3032 (w), 1697 (s), 1624 (s), 1427 (s), 1223 (s), 1117 (m), 750 (m), 695 (s) cm⁻¹; ¹H NMR (250 MHz, CDCl₃) δ 7.41-7.17 (m, 11H), 5.14-5.05 (m, 3H), 3.85 (s, 2H), 3.62-3.40 (m, 3H), 3.34-3.18 (m, 3H), 3.11-2.88 (m, 3H), 2.72-2.62 (m, 1H); ¹³C NMR (63 MHz, CDCl₃) δ 169.6 (C_q), 165.3 (C_q), 155.0 (C_q), 136.3 (C_q), 135.6 (C_q), 129.7 (2CH), 128.9 (2CH), 128.7 (2CH), 128.4 (CH), 128.2 (2CH), 127.6 (CH), 67.6 (CH₂), 50.6 (CH), 45.5 (CH₂), 43.3 (2CH₂), 42.0 (CH₂), 39.9 (CH₂), 28.7 (CH₂); MS: $m/z = 510$ [M + Na]⁺ for ⁷⁹Br and 512 [M + Na]⁺ for ⁸¹Br; HRMS: calcd. for C₂₃H₂₇O₄N₃Br 488.1179, found 488.1178 (0.3 ppm).

(m) *tert-butyl 4-[2-[(2-bromoacetyl)amino]acetyl]piperazine-1-carboxylate (6m)*

The crude derivative obtained using the general protocol described previously was further triturated in diethyl ether to give the desired acetylated compound as a solid. C₁₃H₂₂BrN₃O₄; yield 42%; white solid; m.p. 148-149 °C; M = 364.24 g/mol; IR (ATR): $\nu = 3323$ (w), 2968 (w), 1687 (m), 1615 (s), 1405 (m), 1247 (m), 1223 (m), 1156 (s), 1123 (m), 1023 (m), 859 (w) cm⁻¹; ¹H NMR (250 MHz, CDCl₃) δ 7.52 (as, 1H), 4.09 (d, $J = 4.0$ Hz, 2H), 3.90 (s, 2H), 3.65-3.61 (m, 2H), 3.49-3.42 (m, 4H), 3.40-3.36 (m, 2H), 1.47 (s, 9H); ¹³C NMR (63 MHz, CDCl₃) δ 166.1 (C_q), 165.8 (C_q), 154.5 (C_q), 80.7 (C_q), 44.4 (2CH₂), 42.1 (2CH₂), 41.9 (CH₂), 28.6 (CH₂), 28.5 (3CH₃); MS: $m/z = 386$ [M + Na]⁺ for ⁷⁹Br and MS: $m/z = 388$ [M + Na]⁺ for ⁸¹Br; HRMS: calcd. for C₁₃H₂₃O₄N₃Br 364.0866, found 364.0872 (1.5 ppm).

(n) *(6-methoxycarbonyl-2-naphthyl)methyl 4-[2-[(2-chloroacetyl)amino]acetyl]piperazine-1-carboxylate (6n)*

The crude derivative obtained using the general protocol described previously was further purified by flash chromatography (eluent: EtOAc). C₂₂H₂₄ClN₃O₆; yield 96 %; white solid; m.p. 56-57 °C; M = 461.90 g/mol; IR (ATR): $\nu = 2950$ (w), 1697 (s), 1642 (s), 1430 (m-s), 1284 (m), 1223 (m-s), 753 (w) cm⁻¹; ¹H NMR (250 MHz, CDCl₃) δ 8.61 (s, 1H), 8.09 (dd, $J = 8.6$ Hz, $J = 1.7$ Hz, 1H), 7.96 (d, $J = 8.5$ Hz, 1H), 7.88 (d, $J = 8.7$ Hz, 1H), 7.85 (s, 1H), 7.60 (as, 1H), 7.53 (dd, $J = 8.5$ Hz, $J = 1.6$ Hz, 1H),

5.33 (s, 2H), 4.10 (d, $J = 4.2$ Hz, 2H), 4.08 (s, 2H), 3.99 (s, 3H), 3.69-3.65 (m, 2H), 3.60-3.54 (m, 4H), 3.44-3.41 (m, 2H); ^{13}C NMR (63 MHz, CDCl_3) δ 167.2 (C_q), 166.3 (C_q), 166.1 (C_q), 155.1 (C_q), 136.4 (C_q), 135.4 (C_q), 132.3 (C_q), 130.9 (CH), 130.0 (CH), 128.4 (CH), 128.0 (C_q), 127.0 (CH), 126.6 (CH), 125.9 (CH), 67.6 (CH_2), 52.4 (CH_3), 44.3 (CH_2), 43.7 (CH_2), 43.6 (CH_2), 42.5 (CH_2), 42.0 (CH_2), 41.6 (CH_2); MS: $m/z = 484$ [$\text{M} + \text{Na}$] $^+$; HRMS: calcd. for $\text{C}_{22}\text{H}_{24}\text{O}_6\text{N}_3\text{ClNa}$ 484.1246, found 484.1246 (0.0 ppm).

(o) *N*-[2-[4-(adamantane-1-carbonyl)piperazin-1-yl]-2-oxo-ethyl]-2-chloro-acetamide (6o)

The crude material obtained following the general procedure was purified by flash chromatography using ethyl acetate as eluent. $\text{C}_{19}\text{H}_{28}\text{ClN}_3\text{O}_3$; yield 36 %; white solid; m.p. 201-202 °C; $M = 381.90$ g/mol; IR (ATR): $\nu = 3305$ (m), 2904 (m), 1687 (s), 1648 (s), 1599 (s), 1560 (m), 1451 (m), 1414 (m-s), 1223 (s), 1011 (s) cm^{-1} ; ^1H NMR (250 MHz, CDCl_3) δ 7.60 (as, 1H), 4.11 (d, $J = 4.2$ Hz, 2H), 4.08 (s, 2H), 3.74-3.70 (m, 4H), 3.67-3.63 (m, 2H), 3.43-3.39 (m, 2H), 2.06 (as, 3H), 1.99 (d, $J = 2.6$ Hz, 6H), 1.79-1.68 (m, 6H); ^{13}C NMR (63 MHz, CDCl_3) δ 176.3 (C_q), 166.3 (C_q), 166.2 (C_q), 45.4 (CH_2), 44.8 (CH_2), 44.7 (CH_2), 42.5 (CH_2), 42.4 (CH_2), 41.9 (C_q), 41.6 (CH_2), 39.2 (3 CH_2), 36.7 (3 CH_2), 28.5 (3CH); MS: $m/z = 404$ [$\text{M} + \text{Na}$] $^+$; HRMS: calcd. for $\text{C}_{19}\text{H}_{29}\text{O}_3\text{N}_3\text{Cl}$ 382.1892, found 382.1896 (1.1 ppm).

(p) 2-chloro-*N*-[2-[4-[[5-(dimethylamino)-1-naphthyl]sulfonyl]piperazin-1-yl]-2-oxo-ethyl]-acetamide (6p)

The crude material obtained following the general protocol mentioned above was further purified by flash-chromatography (eluent: AcOEt) to conduct to the titled compound. $\text{C}_{20}\text{H}_{25}\text{ClN}_4\text{O}_4\text{S}$; yield 80 %; yellow-green solid; m.p. 68-69 °C; $M = 452.95$ g/mol; IR (ATR): $\nu = 3314$ (w), 2938 (w), 1648 (s), 1454 (m), 1436 (m), 1141 (s), 938 (m-s), 786 (s) cm^{-1} ; ^1H NMR (250 MHz, CDCl_3) δ 8.59 (d, $J = 8.5$ Hz, 1H), 8.35 (d, $J = 8.7$ Hz, $J = 1$ Hz), 8.20 (dd, $J = 7.4$ Hz, $J = 1.3$ Hz, 1H), 7.56 (d, $J = 7.4$ Hz, 1H), 7.53 (d, $J = 7.5$ Hz, 1H), 7.49 (as, 1H), 7.19 (d, $J = 7.5$ Hz, 1H), 4.02 (s, 2H), 4.00 (d, $J = 4.2$ Hz, 2H), 3.70-3.66 (m, 2H), 3.47-3.43 (m, 2H), 3.24-3.18 (m, 4H), 2.89 (s, 6H); ^{13}C NMR (63 MHz, CDCl_3) δ 166.2 (C_q), 165.9 (C_q), 152.1 (C_q), 132.1 (C_q), 131.4 (CH), 131.0 (CH), 130.4 (C_q), 130.2 (C_q), 128.5 (CH), 123.3 (CH), 119.3 (CH), 115.6 (CH), 45.5 (2 CH_3), 45.5 (CH_2), 45.4 (CH_2), 44.3 (CH_2), 42.4 (CH_2), 41.8 (CH_2), 41.4 (CH_2); MS: $m/z = 475$ [$\text{M} + \text{Na}$] $^+$; HRMS: calcd. for $\text{C}_{20}\text{H}_{26}\text{O}_4\text{N}_4\text{SCl}$ 453.1358, found 453.1358 (0.0 ppm).

(q) *tert*-butyl 4-(2-bromoacetyl)piperazine-1-carboxylate (6q)

Under inert atmosphere and at -78°C, bromoacetyl bromide (53.7 mmol, 1 eq.) was slowly added to a solution of Boc-piperazine (53.7 mmol, 1 eq.) and TEA (59.1 mmol, 1.1 eq.) in DCM (150 ml). The reaction mixture was stirred at -78°C for 3h, diluted with DCM (75 ml) and washed with water. The recovered organic layer was dried over magnesium sulfate and the solvent was evaporated under vacuum. The obtained crude product was further triturated with diethyl ether, filtered and dried under vacuum to conduct to the desired acetylated compound. $\text{C}_{11}\text{H}_{19}\text{BrN}_2\text{O}_3$; yield 78%; white solid; m.p. 243-244 °C; $M = 307.18$ g/mol; IR (KBr): $\nu = 2965$ (m), 1689 (s), 1632 (s), 1417 (s), 1246 (s), 1167 (s), 1023 (m); cm^{-1} ; ^1H NMR (250 MHz, CDCl_3) δ 3.87 (s, 2H), 3.61-3.57 (m, 2H), 3.55-3.47 (m, 4H), 3.46-3.41 (m, 2H), 1.46 (s, 9H); ^{13}C NMR (63 MHz, CDCl_3) δ 165.5 (C_q), 154.5 (C_q), 80.5 (C_q), 46.6 (2 CH_2), 40.9 (2 CH_2), 28.4 (3 CH_3), 25.7 (CH_2);

(r) *benzyl* 4-(2-acetamidoacetyl)piperazine-1-carboxylate (4)

Under inert atmosphere and at -78°C, acetyl bromide (1.1 eq.) was slowly added to a solution of the corresponding amine (0.36 mmol, 1 eq.) and TEA (1.5 eq.) in DCM (5 ml). The reaction mixture was stirred at -78°C for 2h, diluted with DCM (50 ml) and subsequently washed with hydrogen chloride (aq. soln. 0.1 M, 3 x 50 ml). The recovered organic layer was dried over magnesium sulfate and the solvent was evaporated under vacuum to give the crude product further triturated in diethyl ether to conduct to the desired acetylated derivative. $\text{C}_{16}\text{H}_{21}\text{N}_3\text{O}_4$; yield 90%; white solid; m.p. 134-135 °C; $M = 319.36$ g/mol; IR (ATR): $\nu = 3356$ (m), 2919 (s), 1681 (m), 1657 (s), 1636 (s), 1563 (m), 1420 (m), 1229 (s), 1120 (m), 1068 (m), 1023 (m) cm^{-1} ; ^1H NMR (250 MHz, CDCl_3) δ 7.39-7.33 (m, 5H), 6.56 (as, 1H), 5.15 (s, 2H), 4.06 (d, $J = 3.8$ Hz, 2H), 3.64-3.59 (m, 2H), 3.56-3.50 (m, 4H), 3.45-3.40 (m, 2H), 2.05 (s, 3H); ^{13}C NMR (63 MHz, CDCl_3) δ 170.3 (C_q), 166.9 (C_q), 155.2 (C_q), 136.4 (C_q), 128.8 (2CH), 128.5 (CH), 128.3 (2CH), 67.8 (CH_2), 44.3 (CH_2), 43.7 (CH_2), 43.6 (CH_2), 41.9 (CH_2), 41.5 (CH_2), 23.2 (CH_3); MS: $m/z = 342$ [$\text{M} + \text{Na}$] $^+$; HRMS: calcd. for $\text{C}_{16}\text{H}_{22}\text{O}_4\text{N}_3$ 320.1605, found 320.1608 (1.0 ppm).

Preparation of the dimethylsulfonium salts (G)

Dimethyl sulfide (2.5 mmol, 10 eq.) was added to a solution of the previously obtained bromoacetylated compounds (0.25 mmol, 1 eq.) in methanol (5 ml). The reaction vessel was sealed and the mixture vigorously stirred for 48 h at room temperature. The solvent was evaporated, the residue was dissolved in water (15 ml) and washed with ethyl acetate (3 x 20 ml). The recovered aqueous layer was freeze-dried to give the final dimethylsulfonium bromide salts as solids.

(a) [2-[[2-(4-benzyloxycarbonylpiperazin-1-yl)-2-oxo-ethyl]amino]-2-oxo-ethyl]-dimethyl-sulfonium bromide (1a)

C₁₈H₂₆BrN₃O₄S; yield 83%; white solid / hygroscopic; M = 460.39 g/mol; IR (ATR): $\nu = 2919$ (w), 1681 (s), 1642 (s), 1427 (m), 1223 (s), 1123 (w), 1020 (w), 762 (w), 695 (w) cm⁻¹; ¹H NMR (250 MHz, DMSO₃) δ 7.38-7.32 (m, 5H), 5.10 (s, 2H), 4.47 (s, 2H), 4.08 (d, $J = 5.4$ Hz, 2H), 3.53-3.40 (m, 8H), 2.94 (s, 6H); ¹³C NMR (63 MHz, DMSO₃) δ 166.2 (C_q), 163.2 (C_q), 154.4 (C_q), 136.7 (C_q), 128.4 (2CH), 127.9 (CH), 127.6 (2CH), 66.4 (CH₂), 46.4 (CH₂), 43.7 (CH₂), 43.4 (CH₂), 43.1 (CH₂), 41.1 (CH₂), 41.0 (CH₂), 24.5 (2CH₃); MS: $m/z = 380$ [M-Br]⁺; HRMS: calcd. for C₁₈H₂₆O₄N₃S 380.1639, found 380.1638 (0.1 ppm).

(b) [2-[[2-[4-[(4-methoxycarbonylphenyl)methoxycarbonyl]piperazin-1-yl]-2-oxo-ethyl]-amino]-2-oxo-ethyl]-dimethyl-sulfonium bromide (1b)

C₂₀H₂₈BrN₃O₆S; yield 94%; light beige solid / hygroscopic; M = 518.42 g/mol; IR (ATR): $\nu = 3211$ (w), 2913 (w), 1694 (s), 1645 (s), 1423 (m-s), 1407 (m), 1278 (m-s), 1220 (m-s), 1102 (m), 1017 (m), 753 (m) cm⁻¹; ¹H NMR (250 MHz, DMSO) δ 8.90 (t, $J = 5.4$ Hz, 1H), 7.96 (d, $J = 8.4$ Hz, 2H), 7.51 (d, $J = 8.4$ Hz, 2H), 5.19 (s, 2H), 4.48 (s, 2H), 4.09 (d, $J = 5.4$ Hz, 2H), 3.85 (s, 3H), 3.86-3.38 (m, 8H), 2.94 (s, 6H); ¹³C NMR (63 MHz, DMSO) δ 166.3 (C_q), 166.0 (C_q), 163.2 (C_q), 154.2 (C_q), 142.3 (C_q), 129.3 (2CH), 129.0 (C_q), 127.4 (2CH), 65.7 (CH₂), 52.2 (CH₃), 46.4 (CH₂), 43.7 (CH₂), 43.4 (CH₂), 43.2 (CH₂), 41.1 (CH₂), 41.0 (CH₂), 24.5 (2CH₃); MS: $m/z = 438$ [M]⁺; HRMS: calcd. for C₂₀H₂₈O₆N₃S 438.1693, found 438.1693 (0.1 ppm).

(c) dimethyl-[2-[[2-[4-(2-naphthylmethoxycarbonyl)piperazin-1-yl]-2-oxo-ethyl]amino]-2-oxo-ethyl]sulfonium bromide (1c)

C₂₂H₂₈BrN₃O₄S; yield 47%; light beige solid / hygroscopic; M = 510.44 g/mol; IR (ATR): $\nu = 2910$ (w), 1678 (s), 1639 (s), 1463 (m), 1427 (s), 1223 (s), 817 (w), 747 (m) cm⁻¹; ¹H NMR (250 MHz, CDCl₃) δ 8.88 (t, $J = 4.9$ Hz, 1H), 7.86-7.80 (m, 4H), 7.51-7.43 (m, 3H), 5.29 (s, 2H), 5.05 (s, 2H), 4.12 (d, $J = 5.3$ Hz, 2H), 3.61-3.41 (m, 8H), 3.32 (s, 6H); ¹³C NMR (63 MHz, CDCl₃) δ 166.3 (C_q), 163.3 (C_q), 154.5 (C_q), 134.3 (C_q), 132.7 (C_q), 132.6 (C_q), 128.1 (CH), 127.8 (CH), 127.6 (CH), 126.5 (CH), 126.4 (CH), 126.3 (CH), 125.8 (CH), 66.6 (CH₂), 46.5 (CH₂), 43.8 (CH₂), 43.4 (CH₂), 43.2 (CH₂), 41.2 (CH₂), 41.1 (CH₂), 24.6 (2CH₃); MS: $m/z = 430$ [M-Br]⁺; HRMS: calcd. for C₂₂H₂₈O₄N₃S 430.1795, found 430.1793 (0.5 ppm).

(d) [2-[[2-[4-[(6-methoxycarbonyl-2-naphthyl)methoxycarbonyl]piperazin-1-yl]-2-oxo-ethyl]amino]-2-oxo-ethyl]-dimethyl-sulfonium bromide (1d)

C₂₄H₃₀BrN₃O₆S; yield 81%; white solid; m.p. 125-126 °C; M = 568.48 g/mol; IR (ATR): $\nu = 3320$ (w), 2980 (w), 1712 (m), 1675 (m), 1639 (s), 1433 (m), 1287 (m), 1232 (s), 1199 (m), 1126 (m), 759 (w) cm⁻¹; ¹H NMR (250 MHz, DMSO) δ 8.88 (t, $J = 5.4$ Hz, 1H), 8.65 (s, 1H), 8.16 (d, $J = 8.6$ Hz, 1H), 8.08-7.99 (m, 3H), 7.62 (dd, $J = 8.5$ Hz, $J = 1.6$ Hz, 1H), 5.30 (s, 2H), 4.43 (s, 2H), 4.10 (d, $J = 5.4$ Hz, 2H), 3.92 (s, 3H), 3.56-3.40 (m, 8H), 2.91 (s, 6H); ¹³C NMR (63 MHz, DMSO) δ 166.3 (C_q), 166.3 (C_q), 163.2 (C_q), 154.3 (C_q), 137.3 (C_q), 134.9 (C_q), 131.6 (C_q), 130.4 (CH), 129.7 (CH), 128.5 (CH), 127.1 (C_q), 126.5 (CH), 125.9 (CH), 125.2 (CH), 66.3 (CH₂), 52.3 (CH₃), 46.5 (CH₂), 43.7 (CH₂), 43.4 (CH₂), 43.3 (CH₂), 41.1 (CH₂), 41.1 (CH₂), 24.6 (2CH₃). MS: $m/z = 488$ [M]⁺; HRMS: calcd. for C₂₄H₃₀O₆N₃S 488.1850, found 488.1841 (1.8 ppm).

(e) [2-[[2-[4-(adamantane-1-carbonyl)piperazin-1-yl]-2-oxo-ethyl]amino]-2-oxo-ethyl]-dimethyl-sulfonium bromide (1e)

C₂₁H₃₄BrN₃O₃S; yield 98%; white solid; m.p. 157-158 °C; M = 488.48 g/mol; IR (ATR): $\nu = 3417$ (w), 2901 (m-s), 2844 (w), 1645 (s), 1612 (s), 1445 (w), 1408 (m), 1241 (m), 1214 (m), 1008 (s) cm⁻¹; ¹H NMR (250 MHz, DMSO) δ 8.87 (t, $J = 5.3$ Hz, 1H), 4.42 (s, 2H), 4.08 (d, $J = 5.3$ Hz, 2H), 3.65-3.54 (m, 4H), 3.48-3.38 (m, 4H), 2.90 (s, 6H), 1.98 (as, 3H), 1.92-1.86 (m, 6H), 1.74-1.62 (m, 6H); ¹³C NMR (63 MHz, DMSO) δ 174.6 (C_q), 166.2 (C_q), 163.2 (C_q), 46.5 (CH₂), 44.5 (2CH₂), 44.2 (CH₂), 41.7 (CH₂), 41.0 (CH₂), 40.9 (C_q), 38.4 (3CH₂), 36.0 (3CH₂), 27.9 (3CH), 24.6 (2CH₃); MS: $m/z = 408$ [M-Br]⁺; HRMS: calcd. for C₂₁H₃₄O₃N₃S 408.2315, found 408.2317 (0.4 ppm).

(f) [2-[[2-[4-(1-adamantylmethoxycarbonyl)piperazin-1-yl]-2-oxo-ethyl]amino]-2-oxo-ethyl]-dimethyl-sulfonium bromide (1f)

C₂₂H₃₆BrN₃O₄S; yield 67%; light beige solid / hygroscopic; M = 518.51 g/mol; IR (ATR): $\nu = 3414$ (w), 2895 (s), 2844 (m), 1669 (s), 1642 (s), 1466 (m), 1423 (m-s), 1220 (s) cm⁻¹; ¹H NMR (250 MHz, DMSO) δ 8.89 (t, $J = 5.3$ Hz, 1H), 4.46 (s, 2H), 4.08 (d, $J = 5.4$ Hz, 2H), 3.62 (s, 2H), 3.54-3.40 (m, 8H), 2.93 (s, 6H), 1.94 (as, 3H), 1.71-1.58 (m, 6H), 1.50 (as, 6H); ¹³C NMR (63 MHz, DMSO) δ 166.3 (C_q), 163.2 (C_q), 154.8 (C_q), 74.3 (CH₂), 46.4 (CH₂), 43.7 (CH₂), 43.3 (CH₂), 43.0 (CH₂), 41.1 (CH₂), 41.0 (CH₂), 38.7 (3CH₂), 36.4 (3CH₂), 33.1 (C_q), 27.4 (3CH), 24.6 (2CH₃); MS: $m/z = 438$ [M-Br]⁺; HRMS: calcd. for C₂₂H₃₆O₄N₃S 438.2421, found 438.2419 (0.5 ppm).

(g) [2-[[2-[4-[2-(1-adamantyl)ethoxycarbonyl]piperazin-1-yl]-2-oxo-ethyl]amino]-2-oxo-ethyl]-dimethyl-sulfonium bromide (1g)

C₂₃H₃₈BrN₃O₄S; yield 75 %; light beige solid / hygroscopic; M = 532.53 g/mol; IR (ATR): $\nu = 2895$ (m-s), 2847 (w), 1684 (s), 1423 (s), 1226 (s), 1020 (w) cm⁻¹; ¹H NMR (250 MHz, DMSO) δ 8.89 (t, $J = 5.3$ Hz, 1H), 4.47 (s, 2H), 4.09-4.03 (m, 4H), 3.50-3.38 (m, 8H), 2.93 (s, 6H), 1.91 (as, 3H), 1.69-1.57 (m, 6H), 1.49 (as, 6H), 1.37 (t, $J = 7.3$, 2H); ¹³C NMR (63 MHz, DMSO) δ 166.2 (C_q), 163.2 (C_q), 154.6 (C_q), 61.2 (CH₂), 46.4 (CH₂), 43.7 (CH₂), 43.3 (CH₂), 43.0 (CH₂), 42.4 (CH₂), 41.9 (3CH₂), 41.1 (CH₂), 41.0 (CH₂), 36.5 (3CH₂), 31.3 (C_q), 27.9 (3CH), 24.6 (2CH₃); MS: $m/z = 452$ [M-Br]⁺; HRMS: calcd. for C₂₃H₃₈O₄N₃S 452.2578, found 452.2575 (0.6 ppm).

(h) [2-[[2-[4-[[5-(dimethylamino)-1-naphthyl]sulfonyl]piperazin-1-yl]-2-oxo-ethyl]amino]-2-oxo-ethyl]-dimethyl-sulfonium bromide (1h)

C₂₂H₃₁BrN₄O₄S₂; yield 76%; light yellow solid; m.p. 98-99 °C; M = 559.54 g/mol; IR (ATR): $\nu = 3475$ (m), 2992 (w), 1672 (s), 1648 (s), 1345 (s), 1153 (s), 1144 (s), 935 (s), 795 (s), 713 (s) cm⁻¹; ¹H NMR (250 MHz, DMSO) δ 8.79 (t, $J = 5.4$ Hz, 1H), 8.54 (d, $J = 8.5$ Hz, 1H), 8.30 (d, $J = 8.7$ Hz, 1H), 8.14 (dd, $J = 7.4$ Hz, $J = 1.1$ Hz, 1H), 7.68 (dd, $J = 8.5$ Hz, $J = 7.4$ Hz, 1H), 7.63 (dd, $J = 8.5$ Hz, $J = 7.7$ Hz, 1H), 7.28 (d, $J = 7.3$ Hz, 1H), 4.38 (s, 2H), 4.01 (d, $J = 5.3$ Hz, 2H), 3.55-3.43 (m, 4H), 3.18-3.05 (m, 4H), 2.87 (s, 6H), 2.83 (s, 6H); ¹³C NMR (63 MHz, DMSO) δ 166.2 (C_q), 163.2 (C_q), 151.5 (C_q), 132.4 (C_q), 130.5 (CH), 130.2 (CH), 129.6 (C_q), 129.2 (C_q), 128.3 (CH), 123.8 (CH), 118.9 (CH), 115.4 (CH), 46.5 (CH₂), 45.3 (CH₂), 45.2 (CH₂), 45.1 (2CH₃), 43.7 (CH₂), 41.0 (CH₂), 40.9 (CH₂), 24.5 (2CH₃); MS: $m/z = 479$ [M]⁺; HRMS: calcd. for C₂₂H₃₁O₄N₄S₂ 479.1781, found 479.1779 (0.5 ppm).

(i) [2-[[[1S]-2-(4-benzyloxycarbonylpiperazin-1-yl)-1-methyl-2-oxo-ethyl]amino]-2-oxo-ethyl]-dimethyl-sulfonium bromide (1j)

C₁₉H₂₈BrN₃O₄S; light beige solid / hygroscopic; yield 78%; M = 474.41 g/mol; IR (ATR): $\nu = 2986$ (w), 1694 (s), 1636 (s), 1420 (s), 1220 (s), 1020 (m), 759 (m), 698 (m) cm⁻¹; ¹H NMR (250 MHz, DMSO) δ 9.07 (d, $J = 7.3$ Hz, 1H), 7.39-7.32 (m, 5H), 5.10 (s, 2H), 4.78 (p, $J = 6.6$ Hz, 1H), 4.40 (s, 2H), 3.51-3.46 (m, 8H), 2.90 (s, 3H), 2.89 (s, 3H), 1.21 (d, $J = 6.9$ Hz, 3H); ¹³C NMR (63 MHz, DMSO) δ 169.8 (C_q), 162.4 (C_q), 154.4 (C_q), 136.7 (C_q), 128.4 (2CH), 127.9 (CH), 127.7 (2CH), 66.4 (CH₂), 46.6 (CH₂), 45.3 (CH), 44.5 (CH₂), 43.6 (CH₂), 43.2 (CH₂), 41.3 (CH₂), 24.7 (CH₃), 24.6 (CH₃), 17.6 (CH₃); MS: $m/z = 394$ [M-Br]⁺; HRMS: calcd. for C₁₉H₂₈O₄N₃S 394.1795, found 394.1800 (1.3 ppm).

(j) [2-[[2-(4-tert-butoxycarbonylpiperazin-1-yl)-2-oxo-ethyl]amino]-2-oxo-ethyl]-dimethyl-sulfonium bromide (1m)

C₁₅H₂₈BrN₃O₄S; light yellow solid / hygroscopic; yield 48%; M = 426.37 g/mol; IR (ATR): $\nu = 3429$ (w), 2974 (w), 1672 (s), 1645 (s), 1408 (s), 1460 (w), 1363 (m), 1232 (m), 1163 (m-s), 1107 (w) cm⁻¹; ¹H NMR (250 MHz, DMSO) δ 8.87 (t, $J = 5.4$ Hz, 1H), 4.43 (s, 2H), 4.08 (d, $J = 5.4$ Hz, 2H), 3.45-3.32 (m, 8H), 2.91 (s, 6H), 1.41 (s, 9H); ¹³C NMR (63 MHz, DMSO) δ 166.2 (C_q), 163.2 (C_q), 153.8 (C_q), 79.2 (C_q), 46.5 (2CH₂), 43.8 (CH₂), 41.2 (CH₂), 41.0 (2CH₂), 28.0 (3CH₃), 24.6 (2CH₃); MS: $m/z = 346$ [M]⁺; HRMS: calcd. for C₁₅H₂₈O₄N₃S 346.1795, found 346.1797 (0.6 ppm).

(k) benzyl 4-[2-[[2-(1,3,4,5-tetramethylimidazol-1-ium-2-yl)sulfanylacetyl]amino]-acetyl]-piperazine-1-carboxylate bromide (1s)

C₂₃H₃₂BrN₅O₄S; light beige solid / hygroscopic; yield 79%; M = 554.50 g/mol; IR (ATR): $\nu = 3402$ (w), 3192 (w), 2922 (w), 1696 (s), 1645 (s), 1423 (s), 1226 (s), 1026 (w) cm⁻¹; ¹H NMR (250 MHz, DMSO) δ 8.35 (t, $J = 5.3$ Hz, 1H), 7.38-7.32 (m, 5H), 5.10 (s, 2H), 3.96 (d, $J = 5.4$ Hz, 2H), 3.77 (s, 6H), 3.68 (s, 2H), 3.50-3.39 (m, 8H), 2.29 (s, 6H); ¹³C NMR (63 MHz, DMSO) δ 167.0 (C_q), 166.6 (C_q), 154.4 (C_q), 136.7 (C_q), 135.9 (C_q), 129.2 (C_q), 128.4 (2CH), 127.9 (CH), 127.6 (2CH), 66.4 (CH₂), 43.7 (CH₂), 43.3 (CH₂), 43.1 (CH₂), 41.0 (CH₂), 40.7 (CH₂), 36.8 (CH₂), 33.5 (2CH₃), 8.8 (2CH₃); MS: $m/z = 474$ [M]⁺; HRMS: calcd. for C₂₃H₃₂O₄N₅S 474.2170, found 474.2161 (1.8 ppm).

General method for the preparation of vinyl sulfonamides (H)

Under inert atmosphere, triethylamine (1.1 eq.) was added at -60 °C to a solution of 2-chloroethylsulfonfyl chloride (0.3 mmol, 1 eq.) in DCM (6 mL). The mixture was stirred at -60 °C for 2h before adding the corresponding amine (1.1 eq.) and triethylamine (1.1 eq.), then the reaction was stirred for two additional hours at 0 °C. The reaction was quenched by addition of HCl (aq. soln., 0.1 N, 20 mL) and extracted with DCM (3 x 20 mL). The recovered organic layers were dried over magnesium sulfate and the solvent evaporated under reduced pressure. The crude material was further purified by flash-chromatography (eluent: ethyle acetate) to conduct to the desired vinyl sulfonamide.

(a) *benzyl 4-[2-(vinylsulfonylamino)acetyl]piperazine-1-carboxylate (2a)*

C₁₆H₂₁N₃O₅S; yield 53%; colorless viscous oil becoming whitish solid on standing; m.p. 66-67 °C; M = 367.42 g/mol; IR (ATR): $\nu = 3220$ (w), 2865 (w), 1694 (s), 1648 (s), 1423 (m), 1326 (w), 1223 (s), 1141 (m), 1123 (m), 762 (m), 729 (m), 695 (m) cm⁻¹; ¹H NMR (250 MHz, CDCl₃) δ 7.41-7.30 (m, 5H), 6.51 (dd, $J = 16.5$ Hz, $J = 9.8$ Hz, 1H), 6.25 (d, $J = 16.5$ Hz, 1H), 5.95 (d, $J = 9.8$ Hz, 1H), 5.44 (t, $J = 4.2$ Hz, 1H), 5.15 (s, 2H), 3.84 (d, $J = 4.4$ Hz, 2H), 3.68-3.62 (m, 2H), 3.57-3.50 (m, 4H), 3.41-3.28 (m, 2H); ¹³C NMR (63 MHz, CDCl₃) δ 165.9 (C_q), 155.1 (C_q), 136.3 (C_q), 135.5 (CH), 128.8 (2CH), 128.5 (CH), 128.3 (2CH), 127.2 (CH₂), 67.8 (CH₂), 44.3 (CH₂), 43.9 (CH₂), 43.7 (CH₂), 43.6 (CH₂), 42.2 (CH₂); MS: $m/z = 390$ [M + Na]⁺; HRMS: calcd. for C₁₆H₂₂O₅N₃S 368.1275, found 368.1280 (1.4 ppm).

(b) *N-[2-[4-(adamantane-1-carbonyl)piperazin-1-yl]-2-oxo-ethyl]ethenesulfonamide (2e)*

C₁₉H₂₉N₃O₄S; yield 49%; white solid; m.p. 159-160 °C; M = 395.52 g/mol; IR (ATR): $\nu = 3232$ (w), 2895 (m), 2850 (w), 1645 (m-s), 1612 (m-s), 1402 (m-s), 1320 (m), 1232 (m-s), 1153 (s), 1011 (m-s), 984 (m), 738 (m) cm⁻¹; ¹H NMR (250 MHz, DMSO) δ 7.35 (t, $J = 5.5$ Hz, 1H), 6.71 (dd, $J = 16.6$ Hz, $J = 10.0$ Hz, 1H), 6.03 (d, $J = 16.6$ Hz, 1H), 5.94 (d, $J = 10.0$ Hz, 1H), 3.82 (d, $J = 5.6$ Hz, 2H), 3.57-3.46 (m, 4H), 3.42-3.38 (m, 4H), 1.97 (as, 3H), 1.89 (s, 6H), 1.73-1.62 (m, 6H); ¹³C NMR (63 MHz, DMSO) δ 174.6 (C_q), 166.4 (C_q), 137.0 (CH), 125.1 (CH₂), 44.5 (2CH₂), 44.3 (CH₂), 43.7 (CH₂), 41.7 (CH₂), 40.9 (C_q), 38.4 (3CH₂), 36.0 (3CH₂), 27.9 (3CH); HRMS: calcd. for C₁₉H₃₀O₄N₃S 396.1952, found 396.1954 (0.6 ppm).

Measurement of Thermodynamic Solubility

Inhibitor (1-1.5mg) in a suitable 2ml vial was shaken with 1.0ml of Phosphate Buffered Saline (PBS), pH 7.4. After 2hours, the vial and contents were centrifuged at 4,000 xg for 10 min. Approximately 150-200 μ l of supernatant was then filtered through a 0.22 μ m PTFE into a microvial for DAD-LCMS analysis. The original 2 ml vial and contents are then shaken again for another 22 h. After a total of 24 h, the vial and contents were centrifuged again for 10min. Approximately 150-200 μ l of supernatant was then filtered through a 0.22 μ m PTFE into a microvial for DAD-LCMS analysis. A 1,000 μ g/ml standard solution of the inhibitor was prepared in 100% DMSO. A further dilution was prepared to provide an additional standard of 100 μ g/ml in DMSO. The concentration of compound in the PBS filtrate was determined by comparing the UV DAD (210-400 nm) absorbance peak area with that of the two DMSO calibration standards. A range of injection volumes (typically 1-40 μ l) was performed to ensure an appropriate match between the analyte and standard peak areas. Mass spectrometry was used to confirm the presence of the expected molecular ion in the UV DAD (210-400 nm) peak measured. The effective range of the assay is typically 1- 2,000 μ M dependent upon the chromophore present.

Molecular Modelling Methodology

The core region (GLU155 - GLU585) of the open-conformation of tissue transglutaminase (PDB code: 2Q3Z, Pinkas et al., 2009) was used in our studies. The crystal structure was prepared by removing the covalently-bound irreversible inhibitor and other co-crystallisation factors. The catalytic cysteine residue (CYS 277) was modelled in its deprotonated state and the HIS335 in its protonated state, respectively. Docking was conducted with the Gold software (GOLD, version 5.1; CCDC, <http://www.ccdc.cam.ac.uk>), using a distance constraint between the sulphur atom (CYS277) and the electrophilic carbon (inhibitor). The default settings as implemented in Gold were used (ChemPLP scoring function), except for the GA runs (20) and search efficiency (200%). The highly ranked poses were subsequently validated by molecular dynamics. The missing loops of the enzyme were constructed by homology with a TG2 closed-conformation (PDB code: 1KV3, Liu et al., 2002) using SwissPDB server (Arnold et al., 2006), and then minimized using MM3FF in Cache (CACHe, version 7.5; Fujitsu Ltd). The ligand-enzyme complex was subjected to unrestrained molecular dynamics in explicit water using Sander module of Amber package (Amber, version 11, <http://ambermd.org/>), as follows: input

files were prepared with the Antechamber module using ff99SB force field; the systems were neutralized by addition of 10 Na⁺ counter ions then solvated using a TIP3P water model. The complexes were subsequently minimized for 2,000 steps using a nonbonding cut-off of 12 Å, then gradually heated from 0 to 300 K over 20 ps (constant volume, time step = 1 fs). Molecular dynamics trajectories were carried out for 4 ns (constant pressure, SHAKE on, time step = 2 fs) using the Particle– Mesh–Ewald (PME) method to treat the long range electrostatic interactions with a 12 Å non-bonded cut-off. The MD simulation was analyzed with VMD (Humphrey et al., 1996) and the same distance described before was monitored.

In vitro microsomal stability

The metabolic stability of **3h**, **1h**, **3e** was tested in male Wistar Han rat and mixed gender pooled human liver microsomes. Microsomes (final protein concentration 0.5 mg/mL), 0.1 M phosphate buffer pH 7.4 and test compound (final substrate concentration = 0.5 μM) were pre-incubated at 37°C prior to the addition of NADPH (final concentration = 1 mM) to initiate the reaction. The test compound was incubated for 0, 5, 15, 30 and 45 min. The control (minus NADPH) was incubated for 45 min only. The reactions were stopped by the addition of 50 μl methanol containing internal standard at the appropriate time points. Following protein precipitation, the compound remaining in the supernatants was measured using specific LC-MS/MS methods as a ratio to the internal standard in the absence of a calibration curve. Peak area ratios (Compound to IS) were fitted to an unweighted logarithmic decline in substrate. Using the first order rate constant, clearance was calculated by adjustment for protein concentration, volume of the incubation and hepatic scaling factor (52.5 mg microsomal protein/g liver for all species).

Protein binding assay

Chemically bonded Human Serum Albumin (HSA) and Alpha-1-acidglycoprotein HPLC stationary phases (Chiral Technologies, France) were used for measuring compounds' binding to plasma proteins, applying linear gradient elution up to 30% iso-propanol. The run time was 6 minutes including the re-equilibration of the stationary phases with the 50 mM pH7.4 ammonium acetate buffer. The obtained gradient retention times were standardised using a calibration set of mixtures as described in the references [4]. The average standard error of the assay depends on the bindings strength and kinetic of the compounds. It ranges from ±5% in the medium binding range which reduces to 0.1% at binding above 99% with fast kinetic.

hERG Electrophysiological Methods

Compounds **3h**, **1h** and **3e** were assessed for potential hERG liabilities in a high-throughput electrophysiological assay, using the Molecular Devices (Sunnyvale, CA) Barracuda™ platform, as fully described in Gillies et al (2013). The concentration – response relationship was determined for each compound on 3 separate occasions, and in each instance the test compounds were completely inactive in this assay.

Cell Health Profiling

HepG2 cells were seeded at 5,000 cells/well/50 μl in 384-well black, clear bottomed plates in growth media (EMEM + 10 % FBS + 1 % NEAA) and incubated at 37 °C, 5 % CO₂ for 24 h. Compounds stamped at 10 mM, 0.5 μl in V bottomed PP plates were intermediately diluted with 100 μl assay media (EMEM + 1 % NEAA, +1 % Pen/Strep). 80 μl of this compound solution was transferred to the cell plates yielding a final assay concentration of 200 μM. Cells were incubated for 72 h at 37 °C, 5 % CO₂. On the day of acquisition, a cocktail of dyes was made in PBS – 0.22 % pluronic acid, 16.5 μM Hoechst 33342, 880 nM TMRM, 6.25 μM TOTO-3. 5 μl of this solution was added to all wells and left for 45 min at 37 °C, 5 % CO₂.

Images were acquired using the INCell Analyzer 2000 system with the following filter settings Hoechst: DAPI, TMRM: Cy3, TOTO-3: Cy 5. These images were then analysed using the INCell Investigator protocol to determine three parameters: nuclear morphology (Hoechst), mitochondrial potential (TMRM) and membrane permeability (TOTO-3). Data were normalised to controls treated with a known toxicant (100%) or DMSO (0%) for each parameter individually to determine the percentage of dead cells.

Calculation of logP values

The calculated logP values of inhibitors were obtained using MarvinView 5.1.1.4 (ChemAxon Ltd) and are an equally-weighted average of three methods: the calculation method derived from Viswanadhan et al (Viswanadhan et al., 1989); a method using logP data from Klopman *et al* (Klopman et al., 1994);

a method using logP data from the PHYSPROP© database (Syracuse Research Corporation, SRC Environmental Science Center: Syracuse, NY, 1994).

The polar surface area (PSA) values were calculated using MarvinView 5.5.1.0.

Biology Experimental Procedures

Cell culture

Human umbilical vein endothelial cells (HUVECs) (Lonza, Ghent, Belgium) were cultured as described previously (Wang et al., 2013) using endothelial growth medium EGM containing endothelial cell basal medium, 2 % foetal bovine serum (FBS), hydrocortisone, bFGF, VEGF, hEGF, ascorbic acid, R3-IGF, heparin, and GA-100 (Lonza, Ghent, Belgium).

NIH3T3 cells were cultured in DMEM medium supplemented with 10 % (v/v) heat-inactivated FBS, 2 mM L-glutamine, MEM non-essential amino acids 100 U/ml of penicillin and 100 µg/ml of streptomycin. Cells were maintained at 37°C in a 5 % CO₂ humidified atmosphere (Wang et al., 2012).

Western blotting for the dansyl inhibitor interaction with TG1, TG3 and FXIII

To study the specificity of the inhibitors toward TG2, recombinant human TG1, TG3 and FXIIIa pre-treated with 10 mM Ca²⁺ or 10 mM EDTA were incubated with TG2 inhibitor **1h** and **3h** for 30 min at room temperature. The presence of dansyl was detected as described above following denaturing SDS-PAGE and Western Blotting.

Lentiviral transduction of wild type TG2 into NIH3T3 cells

Lentiviral particles were produced as described previously by Wang et al. (2013). NIH3T3 cells were transduced with wild type TG2 containing virus or the empty vector and used in subsequent studies.

Non-denaturing gel electrophoresis

RhTG2 was pre-incubated for 30 min on ice with either GTP (10mM, unless specified in the figure legend) or Calcium (10mM), followed by incubation with inhibitors **1h** or **3h** at the specified concentrations for further 30 min on ice. The enzyme conformation was analyzed by their mobility in a non-denaturing polyacrylamide gel electrophoresis system using Laemmli buffer without SDS and then stained with PageBlue. The gels were imaged using a Gel Doc system. 1µM of inhibitor R281 was used as the control treatment.

Cell toxicity assay

The toxicity of the TG2 inhibitors were studied using the XTT assay as described previously (Wang and Griffin, 2013). Briefly, 3,000 HUVEC cells/well were seeded into 96-well tissue culture plates in endothelial growth medium EGM containing endothelial cell basal medium, 2 % foetal bovine serum (FBS), hydrocortisone, bFGF, VEGF, hEGF, ascorbic acid, R3-IGF, heparin, and GA-100 (Lonza, Ghent, Belgium) and allowed to settle and spread overnight. The inhibitors dissolved in DMSO were diluted with complete endothelial growth medium EGM to the required concentration so that the final DMSO concentration in the medium was 0.01% and incubated for up to 72 h. Fresh medium was replaced every 24 h during the culture period. DMSO used at the same concentration as that used for delivery of the inhibitor was used as the vehicle control treatment. 30 µl of XTT reagent mixture (Roche, East Sussex, UK) was added to the cells after the indicated culture period and incubated for 4 h before measuring the absorbance at 490 nm. In order to rule out the possibility that TG2 or Factor XIIIa might be present in the media that might react with the inhibitor, toxicity for some of the inhibitors was repeated using culture medium without serum for endothelial cell lines (Sigma-Aldrich, Dorset, UK).

Caspase 3/7 assay

2×10⁴ cells/ well HUVEC cells were seeded into 96-well plates overnight and were treated with the apoptosis inducing agent Staurosporine (100 nM) for 3 h to induce apoptosis and activation of Caspase, in the presence or absence of 10 µM of the TG2 inhibitors **3h**, **1h**, **3e** and **1e** while Caspase inhibitor Z-VAD-FMK at the concentration of 25 µM (Promega, UK) and DMSO (the vehicle control) was used as the positive and negative control treatments, respectively. The TG inhibitor **R283** (250 µM) was used as a negative reference compound. Caspase activity was measured using the Caspase-Glo3/7 Assay (Promega, Southampton, UK). Briefly, the cultures were incubated with 100 µl of the caspase assay reagent for 45 min at room temperature after mixing at 300 rpm for 30 sec. The luminescence was recorded using an Orion II Microplate Luminometer (Berthod Technologies, UK).

Co-IP for detection of TG2 and syndecan-4 binding

To detect protein-protein interactions, co-IP was performed as described previously (Wang et al., 2010; Wang and Griffin, 2013). After the appropriate treatments, cells were washed twice with PBS pH 7.4,

then collected and lysed for 30 min on ice in lysis buffer (Tris-HCl 50mM pH 7.4 containing 1% Nonidet P-40, 0.5% sodium deoxycholate, 0.1% SDS, 1 mM NaF, 1 mM sodium orthovanadate, 0.1 mM PMSF and 1% protease inhibitor cocktail). Anti-syndecan-4 antibody was used to pull down the immune-complex and Western blotting was performed to detect the presence of TG2 in the immune-complex.

Biotinylation of cell surface proteins

Biotinylation of cell surface proteins was performed as previously described by Wang et al. (2012). Briefly, after specified treatments, cell monolayers were rinsed once with ice-cold PBS pH 8.0 and labelled with 450 μ M sulfo-NHS-SS-Biotin in PBS pH 8.0 at 4°C for 30 min. Cells were lysed in PBS pH 8.0 containing 1% SDS, 0.1 mM PMSF, 1% protease inhibitor cocktail and benzonase (1:1000 dilution, Merck). Biotinylated proteins were bound to NeutrAvidin-Agarose resin beads (Thermo Scientific) and extracted via heating at 100°C for 5 min in Laemmli sample Buffer. Western blotting was performed using anti-TG2 antibody Cub74002 to detect the presence of TG2.

Detection of TG2 and FN in the ECM and calculation of cell EC50 for fibronectin deposition using compound 3h

After the indicated treatments, cells were detached with 2 mM EDTA in PBS pH 7.4 and the ECM was extracted in 30 μ l of 2 \times Laemmli Buffer sample buffer. Proteins were then separated by denaturing SDS-PAGE and proteins detected by Western blotting (Wang et al., 2013).

For calculation of cell the EC50 for fibronectin deposition for compound **3h**, HUVEC cells or mouse endothelial cells were treated with different concentrations of **3h** (0.1, 0.5, 1, 2.5 and 5 μ M) for 72 h and the ECM fractions collected as described above and the presence of FN in the ECM detected after separation of proteins by denaturing SDS-PAGE and fibronectin detected by Western blotting (Wang et al., 2013). Band intensity was measured using densitometry. DMSO was used as the vehicle control treatment (0 μ M).

To detect the presence of FN via immunofluorescence staining, HUVECs were seeded into 8-well chambers at a density of 7×10^4 cells/well in the presence or absence of inhibitor 1 μ M **3h** for 72 h. Following incubation of the cells with anti-FN antibody in fresh medium for 2 h, the cells were fixed and stained as described previously by Wang et al (2013).

Measurement of Ca²⁺ dependence of inhibitor binding

Recombinant human TG2 was incubated for 30 min at 4°C with either Ca²⁺ (1 mM) or GTP (1 mM), and then for a further 30 min in presence of compounds **3h** (10 nM) or **1h** (1 μ M). Afterwards, samples were centrifuged in spin columns with a 30 kDa molecular weight cut off. To remove excess inhibitor, 3 washes were undertaken. The TG2 transamidating activity in the remaining filtrate was then measured via the biotin-cadaverine incorporation into immobilized FN. To evaluate the efficiency of the spin-columns, for inhibitor removal reaction mixes with inhibitor alone (either **3h** or **1h**) were prepared and filtered through the spin columns. The filtrate was then added to the TG2 assay reaction mixture and enzyme activity measured. To check the efficacy of GTP binding, enzyme was incubated with 250 μ M Ca²⁺ to show activation of rhTG2 in absence of GTP but to also show that 1 mM Ca²⁺ could still activate TG2 with 250 μ M GTP present. Samples with 1 mM GTP and 250 μ M calcium were prepared in duplicate and one processed through the spin-column and the other not to evaluate whether the spin column affects GTP binding. A positive control incubated without inhibitor was used as 100% reference.

References

- Gillie, D.J., Novick, S.J., Donovan, B.T., Payne, L.A., Townsend, C. (2013) Development of a high-throughput electrophysiological assay for the human ether-à-go-related potassium channel hERG. *J. Pharmacol. Toxicol. Methods.* 67, 33–44
- Humphrey, W., Dalke, A. and Schulten, K. (1996) VMD: visual molecular dynamics, *J. Mol. Graph.* 14, 33-38, 27-38.
- Viswanadhan, V.N., Ghose, A.K., Revankar, G.R., and Robins, R.K. (1989). Atomic physicochemical parameters for three dimensional structure directed quantitative structure-activity relationships. 4. Additional parameters for hydrophobic and dispersive interactions and their application for an automated superposition of certain naturally occurring nucleoside antibiotics. *Journal of Chemical Information and Computer Sciences* 29, 163-172.

Klopman, G., Li, J.-Y., Wang, S., and Dimayuga, M. (1994). Computer Automated log P Calculations Based on an Extended Group Contribution Approach. *Journal of Chemical Information and Computer Sciences* 34, 752-781.